MNRAS **000**, 1–47 (2016) Preprint 6 June 2017 Compiled using MNRAS LATEX style file v3.0

SONS: The JCMT legacy survey of debris discs in the submillimetre

Wayne S. Holland,[1,2⋆] Brenda C. Matthews,[3,4] Grant M. Kennedy,[5] Jane S. Greaves,[6†] Mark C. Wyatt,[5] Mark Booth,[7,8] Pierre Bastien,[9] Geoff Bryden,[10] Harold Butner,[11] Christine H. Chen,[12] Antonio Chrysostomou,[13‡] Claire L. Davies,[6§] William R. F. Dent,[14] James Di Francesco,[3,4] Gaspard Duchêne,[15,16] Andy G. Gibb,[17] Per Friberg,[18¶] Rob J. Ivison,[2,19] Tim Jenness,[18‖] JJ Kavelaars,[3,4] Samantha Lawler,[3,4] Jean-François Lestrade,[20] Jonathan P. Marshall,[21,22,23] Amaya Moro-Martin,[12,24] Olja Panić,[5⋆⋆] Neil Phillips,[14] Stephen Serjeant,[25] Gerald H. Schieven,[3,4] Bruce Sibthorpe,[26††] Laura Vican,[27] Derek Ward-Thompson,[28] Paul van der Werf,[29] Glenn J. White,[25,30] David Wilner,[31] Ben Zuckerman[27]

Affiliations are listed at the end of the paper.

Accepted XXX. Received YYY; in original form ZZZ

ABSTRACT

Debris discs are evidence of the ongoing destructive collisions between planetesimals, and their presence around stars also suggests that planets exist in these systems. In this paper, we present submillimetre images of the thermal emission from debris discs that formed the SCUBA-2 Observations of Nearby Stars (SONS) survey, one of seven legacy surveys undertaken on the James Clerk Maxwell telescope between 2012 and 2015. The overall results of the survey are presented in the form of 850 μm (and 450 μm, where possible) images and fluxes for the observed fields. Excess thermal emission, over that expected from the stellar photosphere, is detected around 49 stars out of the 100 observed fields. The discs are characterised in terms of their flux density, size (radial distribution of the dust) and derived dust properties from their spectral energy distributions. The results show discs over a range of sizes, typically 1–10 times the diameter of the Edgeworth-Kuiper Belt in our Solar System. The mass of a disc, for particles up to a few millimetres in size, is uniquely obtainable with submillimetre observations and this quantity is presented as a function of the host stars' age, showing a tentative decline in mass with age. Having doubled the number of imaged discs at submillimetre wavelengths from ground-based, single dish telescope observations, one of the key legacy products from the SONS survey is to provide a comprehensive target list to observe at high angular resolution using submillimetre/millimetre interferometers (e.g., ALMA, SMA).

Key words: circumstellar matter – submillimetre: stars

⋆ E-mail: wayne.holland@stfc.ac.uk
† Present address: School of Physics & Astronomy, Cardiff University, 5 The Parade, Cardiff, CF24 3AA, UK
‡ Present address: SKA Organisation, Jodrell Bank Observatory, Lower Withington, Macclesfield, Chesire, SK11 9DL, UK
§ Present address: School of Physics, University of Exeter, Physics Building, Stocker Road, Exeter, EX4 4QL, UK

¶ Present address: East Asian Observatory, 660 N. A'ohōkū Place, University Park, Hilo, HI 96720, USA
‖ Present address: LSST Project Office, 950 N. Cherry Avenue, Tucson, AZ 85719, USA
⋆⋆ Present address: School of Physics and Astronomy, E C Stoner Building, University of Leeds, Leeds, LS2 9JT, UK

1 INTRODUCTION

Debris discs represent the longest-lived phase in the lifetime of circumstellar discs. Following the decline of the gas-rich protoplanetary phase when agglomeration processes prevail, the remnant mass of circumstellar discs is dominated by planetesimals, which undergo collisional grinding down to smaller and smaller bodies, until particles reach the blow-out size determined by the radiation pressure from the host star (e.g. Wyatt 2008; Krivov 2010). The presence of these unseen planetesimals can be inferred through scattered light or thermal emission from micron to millimetre-sized dust grains. The dust must be continuously replenished, by ongoing collisions between the aforementioned planetesimals, since the timescales for dust grains to be removed from the system are significantly shorter than the ages of the stars around which they are observed (Backman & Paresce 1993). It appears to be the case that debris discs can persist over *all* stages following the pre-main-sequence phase of stellar evolution (e.g. Bonsor et al. 2013), even including white dwarfs (e.g. Farihi 2016).

Observations at submillimetre/millimetre wavelengths are immensely valuable to the study of debris discs in that they trace the Rayleigh-Jeans tail of the outer cold dust in a system (Matthews et al. 2014). For example, they probe substantially different (thermal) emission mechanisms than scattered light observations, and lower characteristic temperatures for the material than far-infrared (far-IR) data. These long wavelengths also provide an important anchor to the flux energy distribution (loosely referred to in this paper as the spectral energy distribution, or SED) in an otherwise poorly constrained wavelength range, and can indicate the presence of any (cold) disc components not detectable at shorter wavelengths. By probing the Rayleigh-Jeans tail of the spectrum, the effect of any possible bias introduced by modelling the dust temperatures from the observed data is minimised, thus allowing information to be derived on the radial distribution of the disc and the size distribution of the emitting grains (Ertel et al. 2012; Marshall et al. 2014b). The slope of the spectrum constrains the dust size distribution, providing a test of whether or not the solids in the disc are undergoing a steady-state collisional cascade. Critically, since the emission is optically thin, the dust mass for grain sizes up to $\sim$1 mm is uniquely determined from submillimetre data.

The disc component (in millimetre-sized grains) probed in the submillimetre is also unique from the perspective of understanding disc dynamics. These relatively large dust grains are less affected by the radiation or stellar wind pressure (Burns et al. 1979) and therefore trace the location of their parent planetesimal belts more reliably than smaller grains at shorter wavelengths. Debris discs act as important pointers to planetary systems (Kóspál et al. 2009) with features in the discs having the potential to highlight the presence of planets, even in cases where the planet is as yet undetected, or would be difficult to detect by any other method, including direct imaging (e.g. Wyatt 2003, 2006). For example, the planet around β Pictoris was predicted due to structure in the debris disc through scattered light imaging before the planet was found (Mouillet et al. 1997; Heap et al. 2000). Whilst scattered light observations are sensitive to the small grains around a given star, the bulk of the mass resides in the largest grains most detectable at submillimetre to centimetre wavelengths. These grains are most likely to be located in or near the planetesimal belts, and hence may show evidence of perturbed geometries due to resonances with long-period planets (Wyatt 2006).

The James Clerk Maxwell telescope (JCMT) has a long history of debris disc studies (e.g., Zuckerman & Becklin 1993), including some of the earliest imaging using the SCUBA camera (Holland et al. 1999). At the time of its decommissioning in 2005, half of the resolved images of debris discs (about a dozen in total) were due to submillimetre imaging with SCUBA (e.g., Holland et al. 1998; Greaves et al. 2005). Subsequent surveys in the mid-far IR (e.g. using *Spitzer*, *AKARI* and *Herschel*) identified a large sample of discs in the solar vicinity (to a distance of $\sim$100 pc). For example, the *Herschel* DEBRIS (Disk Emission via a Bias-Free Reconnaissance in the Infrared/Submillimetre) survey observed the nearest $\sim$90 stars in each of the spectral type groups A, F, G, K and M, obtaining a disc detection rate of 17 per cent based on 100 µm and 160 µm results, corresponding to 77 out of a total of 446 targets detected (Matthews et al. 2014). Similarly, the *Herschel* DUNES (DUst around NEarby Stars) survey detected an incidence of 20 per cent for nearby Sun-like stars, probing to the photospheric level (Eiroa et al. 2013; Montesinos et al. 2016). In terms of limits to the detectable flux, *Spitzer* and *Herschel* achieved average sensitivities, expressed as fractional dust luminosities (see Section 4.4) of $\sim 10^{-5}$ and $\sim 10^{-6}$, respectively. These levels compare to $\sim 10^{-7}$ for the Edgeworth-Kuiper belt in our Solar System. Crucially, the surveys by *Herschel* spatially resolved half of the detected discs, many for the first time. Other surveys, in the near-mid IR with *AKARI*, have probed "warmer" debris discs ($T \geqslant 150$ K), i.e. material to be found closer to the central star, with incidence rates typically 3 per cent, much lower than for the "cooler" discs detected at longer wavelengths (Fujiwara et al. 2013).

The SCUBA-2 Observations of Nearby Stars (SONS) survey was one of the seven original legacy surveys undertaken on the James Clerk Maxwell telescope between 2012 and 2015 (Chrysostomou 2010). The survey set out to target 115 known disc host stars (within 100 pc of the Sun) searching for debris signatures in the form of dust emission at 850 µm. The aim of the SONS survey was to characterise these discs to the fullest extent possible by: (1) providing direct dust masses that cannot be obtained from shorter wavelengths alone; (2) adding to the far-IR/submillimetre spectrum to constrain the dust size distribution; (3) using the power of a 15 m telescope to resolve disc structures around the nearest systems, and (4) looking for evidence of resonant clumps and other features in resolved structures that could be indicative of unseen perturbers, such as planets. This paper presents the first results from the full survey. Future work will concentrate on detailed modelling of the disc structures, further investigations into dust grain properties and size distributions, and their interpretation in terms of the relationship to possible planetary systems.

†† Present address: Astrium Airbus Defence and Space, Gunnels Wood Road, Stevenage, SG1 2AS, UK

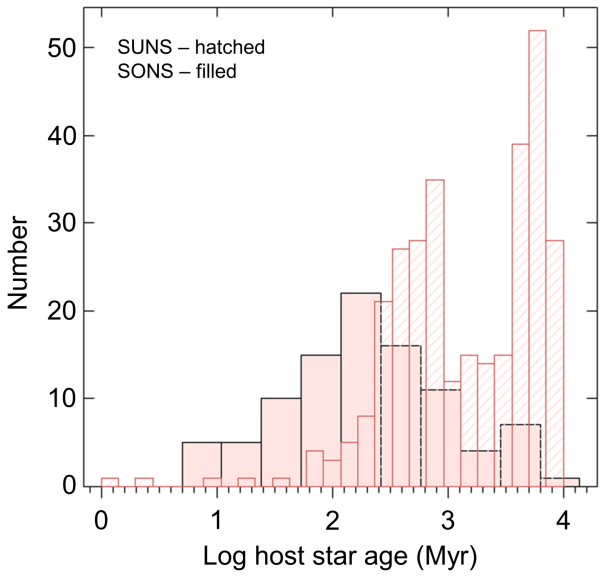

Figure 1. Histogram showing the difference in age distribution between the targets in the original SUNS (SCUBA-2 Unbiased Nearby Stars) survey of 500 stars, and the re-scoped SONS survey of 115 targets.

2 SURVEY HISTORY AND TARGET SELECTION

The original concept was for a volume-limited, unbiased survey of 500 stars, the 100 nearest in each of the spectral type groups A, F, G, K, and M (Matthews et al. 2007). First formulated in 2004, this was called the SCUBA-2 Unbiased Nearby Stars (SUNS) survey. The aforementioned extensive surveys by *Spitzer* and *Herschel* during the period 2004 – 2012, together with a shortfall in instrument sensitivity of approximately a factor of 2, however, meant that the greatest potential legacy lay in a revamped JCMT/SCUBA-2 survey to target a more modest number of known debris disc hosts. Discs would have to be very cold to be detectable with SCUBA-2 but below the detection threshold of, for example, the *Herschel* DEBRIS survey. Hence the SONS survey became targeted towards younger stars, and stars with known infrared excesses, with a higher expectation of detection at a wavelength of 850 µm over the original volume-limited survey. Fig. 1 shows the distribution of stars by age, emphasising the survey bias towards younger targets.

The revised target list was assembled in 2011 from *IRAS* and *Spitzer* published data (Low et al. 2005; Su et al. 2006; Beichman et al. 2006; Rhee et al. 2007; Trilling et al. 2007, 2008; Bryden et al. 2009; Plavchan et al. 2009; Koerner et al. 2010; Zuckerman et al. 2011; Morales et al. 2011), unpublished data from *Spitzer*, *Herschel* DEBRIS and DUNES, the *Herschel* Guaranteed Time discs programme, *Herschel* GASPS (GAS in Protoplanetary Systems; Dent et al. 2013), and several smaller programmes on planet/disc hosts. Flux densities at 850 µm were therefore predicted based on existing photometric data and a fit to the IR excess from the target. Simply assuming a standard blackbody spectrum would result in an over-estimate of the 850 µm flux by about a factor of four (Wyatt et al. 2007). Hence, particularly in the cases where few photometric points existed, predictions were based on modified blackbody spectra, $B_\nu(\lambda/\lambda_0)^{-\beta}$, assuming a critical wavelength, $\lambda_0 = 200$ µm and a dust emissivity index, $\beta = 1.0$ (Wyatt 2008; Phillips 2011). Targets were then classified according to the likelihood of a 3σ detection being achievable at 850 µm with a flux density of at least 3 mJy.

Those sources classified as having guaranteed, likely or hard to quantify fluxes (i.e., with an unconstrained dust temperature) were retained if they were within 100 pc, had declinations between −40 to +80° and predicted 850 µm fluxes of >1 mJy (or above −60° dec with predicted fluxes exceeding 15 mJy, to include several southern bright targets). It was accepted that there was still up a factor 3 uncertainty in the 850 µm flux predictions for some targets. This uncertainty arises because the grain properties and size distribution are generally unknown; characterising these was one of the key science goals of this survey. This method produced a candidate list of 115 targets (see Table 1) with 37 (i.e. one-third) of these in the guaranteed or likely detection categories. The selection criteria led to the expectation of a high detection rate, given the evidence of discs at multiple wavelengths for many targets. Fig. 2 shows the distribution of targets by host star spectral type and distance.

The survey was formally allocated 270 hrs of observing time on the JCMT, equally split between weather bands 2 and 3, equivalent to 225 GHz zenith optical depths in the range 0.05 – 0.08 for band 2 and 0.08 – 0.12 for band 3[1]. The time allocated was sufficient to reach a $1\,\sigma$ sensitivity limit of 1.4 mJy at 850 µm for each of the 115 fields. Furthermore, to maximise the chances of a disc detection a "quick-look" approach to the observing methodology was adopted, in which each star was initially targeted for a minimum 1 hr observation block, typically achieving a 1σ noise level of 1.5 − 2 mJy. Although SCUBA-2 operates simultaneously at wavelengths of 450 µm and 850 µm, the allocation of band 2 and 3 weather meant that it was unlikely any significant number of discs would be detected at 450 µm. Such detections, however, were never a goal of the survey as it was planned to follow up possible 450 µm detections with future observations, most likely requiring the best weather conditions ("band 1").

Any stars with detectable flux were immediately prioritised for more observing time (as needed, to boost the significance of the detection), with the possibility of returning to the others if and when time allowed. Although the time was scheduled as 3 – 4 night blocks on the telescope, roughly spaced every few months during the 3 yr survey period, the fact that the survey had targets all over the sky (as shown in Fig. 3) meant that SONS observations benefited from gaps in the schedules for the other legacy surveys. The broad sky distribution was the main reason that SONS became the first survey to be completed in terms of time in 2014 August. In addition to the 270 hr formal allocation the data presented in this paper also includes observations from the initial survey verification phase (2012 Jan) amounting to 26 hrs, 4.5 hrs from the SCUBA-2 Guaranteed Time allocation (PI: Holland) for observations of ϵ Eridani, a further 21 hrs from the

[1] Zenith optical depths at 225 GHz in the range 0.05 – 0.12 correspond to line-of-sight precipitable water vapour levels of approximately 1 – 2.5 mm.

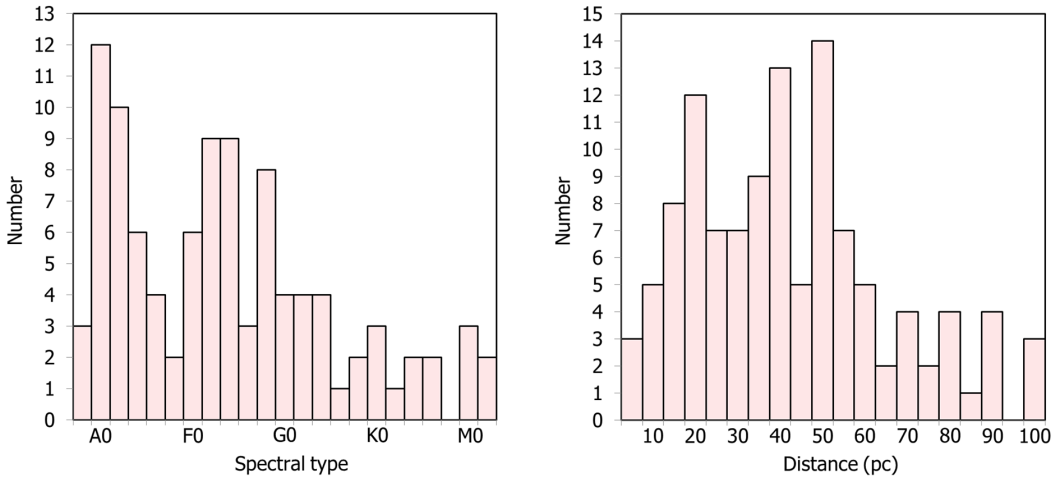

Figure 2. The distribution of SONS survey targets as a function of host star spectral type (left) and distance (right).

survey extension programme in late 2014/early 2015, and 2 hrs each from the PI programmes M12AC17 and M13AC19 (PIs: Brenda Matthews and Christine Chen, respectively). The total observing time for the survey data was therefore 325.5 hrs.

During the observing campaign, some observations were prioritised to confirm (or rule out) a previous marginal disc detection. Hence, more observing time was expended on a handful of disc candidates than was originally planned. Together with an over-allocation of sources and fields around 05 hrs RA from the entire Legacy Survey programme, it became necessary to remove 15 targets from the list of 115. These were mainly around 05 hrs RA (see Table 1), and included β Pictoris as it has been well-characterised in the past at 850 µm (e.g. Holland et al. 1998; Dent et al. 2014), and 14 further targets least likely to yield a disc detection based on the criteria outlined above.

3 OBSERVATIONS AND DATA REDUCTION

3.1 Observations

The SCUBA-2 camera (Holland et al. 2013) on the JCMT was used to take the survey data between 2012 Jan and 2015 Feb. The wavelengths of observation were 850 µm and 450 µm, where the primary beam sizes are 13.0″ and 7.9″ (measured Full-Width at Half Maximum; FWHM) (Dempsey et al. 2013). The data were taken exclusively using the constant speed DAISY observing mode, which maximises the observing time in the central 3 arcmin^2 region of a field (Bintley et al. 2014). This mode is appropriate for compact sources of less than a few arcminutes in diameter and so is well-suited to the observations of debris discs within the SONS survey. Each observation was taken as one continuous scan with a duration of approximately 30 min. The data is saved as 30 sec sub-scans, with each observation resulting in a total of 55 sub-scans, including a flat-field measurement at the start and end of each observation (Holland et al. 2013). The data were calibrated in flux density against the primary calibrators Uranus and Mars, and also secondary calibrators CRL 618 and CRL 2688 from the JCMT calibrator list (Dempsey et al. 2013), with estimated calibration uncertainties amounting to 20 and 7 per cent at 450 µm and 850 µm, respectively. Accurate telescope pointing was crucial to these observations and was regularly checked with reference to nearby bright sources (e.g. compact HII regions or blazars), with RMS pointing errors of less than 2″.

3.2 Data reduction

3.2.1 *Original approach: "Blank field"*

The data were reduced using the Dynamic Iterative Map-Maker within the Starlink SMURF package (Chapin et al. 2013) called from the ORAC-DR automated pipeline (Jenness & Economou 2015). The original data reduction approach, used in the "First Results" paper (Panić et al. 2013), saw the data heavily high-pass filtered at 1 Hz, corresponding to a gradual spatial cut-off centred at ∼150″ for a typical DAISY scanning speed of ∼150″ s^{-1}. The filtering was necessary to remove low-frequency noise originating from the detectors and readout electronics (Holland et al. 2013). To account for the attenuation of the signal, as a result of the time series filtering, the pipeline would re-make each map with a fake 10 Jy Gaussian added to the raw data, but offset from the nominal map centre by 30″ to avoid contamination with any detected source. The amplitude of the Gaussian in the output map gave the signal attenuation, and this correction was applied along with the flux conversion factor derived from the calibrator observations. This method produced satisfactory results for unresolved compact sources but residual noise artefacts often remained in the images.

3.2.2 *Revised approach: "Zero masking"*

The heavy high-pass filtering led not only to residual instrumental noise but also to an under-estimation of the flux density as a function of source-scale size. This effect is not surprising as when sources become larger, they contain more power at lower frequencies, meaning that a fixed-frequency, high-pass filter will remove more flux. Hence, SONS adopted

Table 1. The target list for the SONS survey. RA/Dec positions and spectral types are from the SIMBAD database (Wenger et al. 2000), and stellar distances from the *Hipparcos* catalogue (Perryman et al. 1997; van Leeuwen 2007). Stellar ages are referenced individually in Section 5.

HD number	Other names	RA (J2000)	Dec (J2000)	Spectral type	Distance (pc)	Age (Myr)	Association	Notes
377		00 08 25.75	+06 37 00.49	G2-V	39.1	170	Field	
	HIP 1368	00 17 06.38	+40 56 53.87	M0.5-V	14.7	500	Field	
3126		00 34 27.17	−06 30 14.05	F2-V	41.5	1500	Field	
3296	LTT 317	00 36 01.85	−05 34 14.59	F5-D	47.2	1700	Field	
6798		01 12 16.82	+79 40 26.27	A3-V	82.8	320	Field	
7590	V445 And	01 16 29.25	+42 56 21.90	G0-V	23.6	1820	Field	
8907		01 28 34.36	+42 16 03.68	F8-D	34.2	320	Field	
9672	49 Cet	01 34 37.78	−15 40 34.90	A1-V	59.4	40	Argus	
10647	q^1 Eri	01 42 29.32	−53 44 27.00	F9-V	17.4	1600	Field	Known planet host
10700	τ Cet	01 44 04.08	−15 56 14.93	G8.5-V	3.7	7650	Field	Possible planet host
10638		01 44 22.81	+32 30 57.16	A3-E	69.3	50	Field	
13161	β Tri	02 09 32.63	+34 59 14.27	A5-III	38.9	730	Field	Binary
14055	γ Tri	02 17 18.87	+33 50 49.90	A1-Vnn	34.4	230	Field	
15115		02 26 16.25	+06 17 33.19	F2-D	45.2	23	β Pic MG	
15257	12 Tri	02 28 09.98	+29 40 09.59	F0-III	49.8	1000	Field	
15745		02 32 55.81	+37 20 01.04	F2-V	63.5	23	β Pic MG	
17094	87 Cet	02 44 56.54	+10 06 50.91	F0-IV	25.8	1500	Field	Not observed
17093	38 Ari	02 44 57.58	+12 26 44.73	A7-III	36.3	580	Field	
17390		02 46 45.11	−21 38 22.28	F3-IV/V	48.0	600	Field	Not observed
19356	β Per; Algol	03 08 10.13	+40 57 20.33	B8-V	27.6	450	Field	Triple star system
21997		03 31 53.65	−25 36 50.94	A3-IV/V	71.9	30	Columba	
22049	ϵ Eri	03 32 55.85	−09 27 29.73	K2-V	3.22	850	Field	Possible planet host
22179	V* 898 Per	03 35 29.90	+31 13 37.44	G5-IV	16.0	16	Field	
25457		04 02 36.75	−00 16 08.12	F6-V	18.8	130	AB Doradus	
25570		04 03 56.60	+08 11 50.16	F2-V	34.9	600	Hyades	
28226		04 28 00.78	+21 37 11.66	A5-C	47.1	600	Hyades	
28355	79 Tau	04 28 50.16	+13 02 51.37	A7-V	48.9	600	Hyades	
30447		04 46 49.53	−26 18 08.85	F3-V	80.3	30	Columba	Not observed
30495	58 Eri	04 47 36.29	−16 56 04.04	G1.5-V	13.3	650	Field	
31392		04 54 04.21	−35 24 16.27	G9-V	25.7	3700	Field	Not observed
31295	7 Ori	04 54 53.73	+10 09 03.00	A0-V	37.0	125	Field	
33636		05 11 46.45	+04 24 12.73	G0-V	28.4	2500	Field	
34324		05 15 43.90	−22 53 39.70	A3-V	85.8	450	Field	Not observed
35650		05 24 30.17	−38 58 10.77	K6-V	18.0	?	Field	Not observed
35841		05 26 36.59	−22 29 23.72	F3-V	96.0	30	Columba	
36968		05 33 24.07	−39 27 04.64	F2-V	140.0	20	Octans	Not observed
37484		05 37 39.63	−28 37 34.66	F3-V	59.5	30	Columba	Not observed
37594		05 39 31.15	−03 33 52.93	A8-V	42.6	650	Field	
38206		05 43 21.67	−18 33 26.92	A0-V	69.2	30	Columba	Not observed
38678	ζ Lep	05 46 57.34	−14 49 19.02	A2-IV/Vn	21.6	23	β Pic MG	Not observed
39060	β Pic	05 47 17.09	−51 47 17.09	A6-V	19.3	23	β Pic MG	Not observed;
38858		05 48 34.94	−04 05 40.72	G4-V	15.2	4700	Field	Known planet host
40540		05 57 52.60	−34 28 34.01	A8-IVm	89.9	170	Field	Not observed
45184		06 24 43.88	−28 46 48.41	G1.5-V	21.9	4400	Field	Not observed
48682	56 Aur	06 46 44.34	+43 34 38.73	F9-V	16.7	6000	Field	
49601	GJ 249	06 51 32.39	+47 22 04.14	K6-V	18.6	?	Field	
57703		07 23 04.61	+18 16 24.27	F2 D	41.4	600	Field	
61005	"The Moth"	07 35 47.46	−32 12 14.04	G8-V	35.3	40	Argus?	
70313		08 23 48.50	+53 13 10.96	A3-V	50.4	200	Field	
73350	V401 Hya	08 37 50.29	−06 48 24.78	G5-V	24.0	300	Field	
72905		08 39 11.70	+65 01 15.27	G1.5-Vb	14.4	490	Ursa Major	Not observed
	GJ 322; HIP 43534	08 52 00.34	+66 07 53.37	K5 D	16.5	490	Ursa Major	
75616		08 53 06.10	+52 23 24.83	F5 D	35.4	1400	Field	
76543	62 Cnc	08 57 14.95	+15 19 21.95	A5-III	45.7	400	Field	
76582	63 Cnc	08 57 35.20	+15 34 52.61	F0-IV	46.1	540	Field	
82943		09 34 50.74	−12 07 46.37	F9-VFe	27.5	430	Field	Multiple planet host
84870		09 49 02.85	+34 05 07.40	A3	88.0	100	Field	
85301		09 52 16.77	+49 11 26.85	G5-V	32.8	600	Hyades	
91312		10 33 13.89	+40 25 32.02	A7-IV	34.6	410	Field	
91782		10 36 47.84	+47 43 12.47	G0+M9V	61.4	1580	Field	Binary?

Table 1 – *continued*

HD number	Other names	RA (J2000)	Dec (J2000)	Spectral type	Distance (pc)	Age (Myr)	Association	Notes
	TWA7; CE Ant	10 42 30.11	−33 40 16.21	M2-Ve	50	9	TW Hydrae	Distance is uncertain
92945		10 43 28.27	−29 03 51.43	K1-V	21.4	200	Field	
95418	β UMa	11 01 50.48	+56 22 56.73	A1-V	24.4	490	Ursa Major	
95698		11 02 24.45	−26 49 53.42	F1-V	56.1	1520	Field	
	TWA13	11 21 17.24	−34 46 45.5	M1-Ve	50.0	9	TW Hydrae	
98800		11 22 05.29	−24 46 39.76	K5-V	50.0	9	TW Hydrae	Pre-MS dwarf
102647	β Leo	11 49 03.58	+14 34 19.41	A3-V	11.0	45	IC 2391	Binary
102870	β Vir	11 50 41.72	+01 45 52.99	F9-V	10.9	2900	Field	
104860		12 04 33.73	+66 20 11.72	F8	45.5	200	Field	
107146		12 19 06.50	+16 32 53.86	G2-V	27.5	100	Field	
109085	η Crv	12 32 04.23	−16 11 45.62	F2-V	18.3	1380	Field	
109573	HR 4796; TWA 11	12 36 01.03	−39 52 10.23	A0-V	72.8	9	TW Hydrae	Binary
110411	ρ Vir	12 41 53.06	+10 14 08.25	A3-V	36.3	90	Field	
111631		12 50 43.57	−00 46 05.26	K7	10.6	600	Field	
113337		13 01 46.93	+63 36 36.81	F6-V	36.9	1450	Field	Binary; Planet host
115617	61 Vir	13 18 24.31	−18 18 40.30	G7-V	8.6	6300	Field	Multiple planet host
122652		14 02 31.64	+31 39 39.08	F8	39.3	300	Field	
125162	λ Boo	14 16 23.02	+46 05 17.90	A0p	30.4	2800	Field	
125473	ψ Cen	14 20 33.43	−37 53 07.06	A0-IV	79.4	300	Field	Binary
127821		14 30 46.07	+63 11 08.83	F4-IV	31.8	1020	Field	
127762	γ Boo	14 32 04.67	+38 18 29.70	A7-III	26.6	950	Field	Binary
128167	σ Boo	14 34 40.82	+29 44 42.46	F2-V	15.8	1000	Field	
131625		14 55 44.71	−33 51 20.82	A0-V	77.8	200	Field	
135502	χ Boo	15 14 29.16	+29 09 51.46	A2-V	77.4	200	Field	
135599		15 15 59.17	+00 47 46.89	KO-V	15.8	1300	Field	
	GJ 581; HIP 74995	15 19 26.82	−07 43 20.21	M3	6.2	5700	Field	Multiple planet host
139006	α CrB	15 34 41.27	+26 42 52.89	A1-IV	23.0	490	Ursa Major	Binary
139590		15 39 01.06	−00 18 41.38	G0-V	55.8	5000	Field	
141378		15 48 56.80	−03 49 06.64	A5-IV	54.0	150	Field	
143894	44 Ser	16 02 17.69	+22 48 16.03	A3-V	54.9	300	Field	
149630	σ Her	16 34 06.18	+42 26 13.35	B9-V	96.5	700	Field	Binary
150378	37 Her	16 40 38.69	+04 13 11.23	A1-V	90.0	200	Field	Binary
150682	39 Her	16 41 36.70	+26 55 00.77	F3-V	43.7	1700	Field	
151044		16 42 27.81	+49 56 11.19	F8-V	29.3	3900	Field	
157728	73 Tau	17 24 06.59	+22 57 37.01	F0-IV	42.7	530	Field	
158633		17 25 00.10	+67 18 24.15	K0-V	12.8	5900	Field	
158352		17 28 49.66	+00 19 50.25	A8-V	59.6	750	Field	
161868	γ Oph	17 47 53.56	+02 42 26.20	A0-V	31.5	185	Field	
170773		18 33 00.92	−39 53 31.28	F5-V	37.0	200	Field	
172167	α Lyr; Vega	18 36 56.34	+38 47 01.28	A0-V	7.7	700	Field	
181327		19 22 58.94	−54 32 16.97	F5-V	51.8	23	β Pic MG	
182681		19 26 56.48	−29 44 35.62	B8-V	69.9	145	Field	
191089		20 09 05.22	−26 13 26.53	F5-V	52.2	23	β Pic MG	
192425	ρ Aql	20 14 16.62	+15 11 51.39	A2-V	47.1	410	Field	
197481	AU Mic	20 45 09.53	−31 20 27.24	M1-Ve	9.9	23	β Pic MG	
202560		21 15 15.27	−38 52 02.50	M0-Ve	3.9	?	Field	Not observed
205674		21 37 21.11	−18 26 28.25	F4-IV	51.8	130	AB Doradus?	
206893		21 45 21.91	−12 47 00.07	F5-V	38.3	860	Field	
207129		21 48 15.75	−47 18 13.02	G2-V	16.0	3800	Field	Binary
209253		22 02 32.96	−32 08 01.48	F6.5-V	30.1	950	Field	
212695		22 26 14.44	−02 47 20.32	F5	46.5	2300	Field	
213617	39 Peg	22 32 35.48	+20 13 48.06	F1-V	50.3	1200	Field	
216956	α PsA; Fomalhaut	22 57 39.05	−29 37 20.05	A4-V	7.7	440	Field	Triple star; planet host
218396	HR 8799	23 07 28.72	+21 08 03.31	A5-V	39.4	30	Columba	Multiple planet host
221853		23 35 36.15	+08 22 57.43	F0	68.4	100	Local	

a revised map-maker configuration optimised for known position, compact and moderately-extended sources. It used the technique of "zero masking" in which the map is constrained to a mean value of zero in all cases outside a radius of 60″ from the centre of the field, for all but the final iteration of the map-maker (Chapin et al. 2013). The technique not only helped convergence in the iterative part of the map-making process but suppressed the large-scale ripples that can produce ringing artefacts. The results were more uniform, lower noise (by an average of ∼20 per cent) final images, largely devoid of gradients and artefacts (Chapin et al. 2013). Each output map was regridded with 1″ pixels

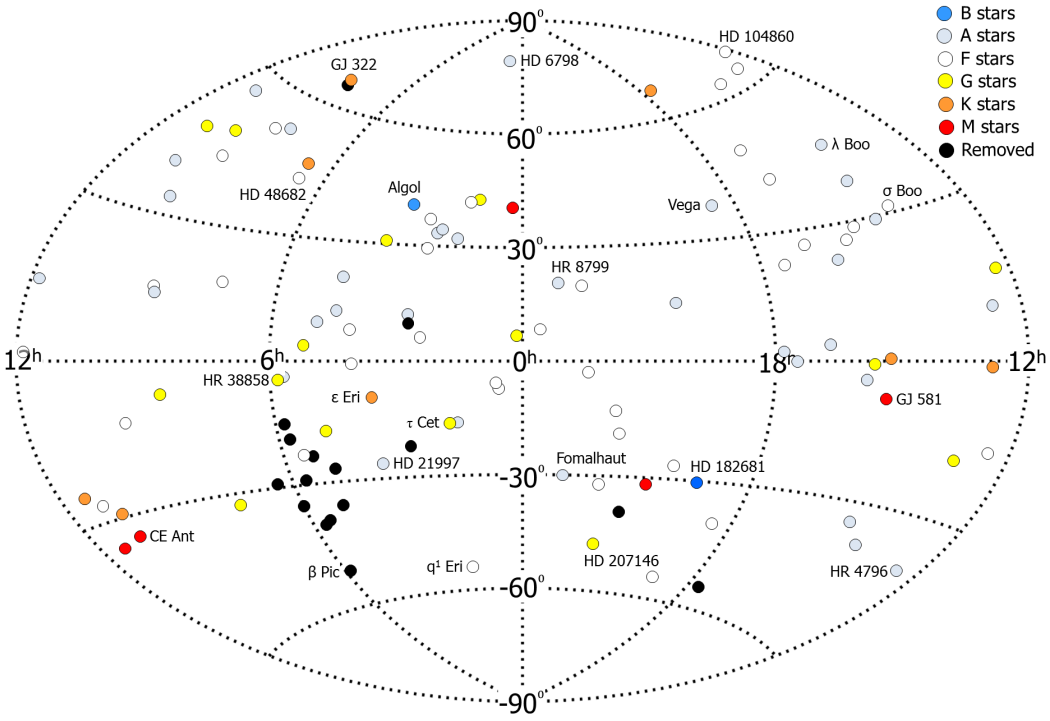

Figure 3. The distribution of SONS survey targets on the sky by spectral type. The spectral type for the stars is indicated by the colour table. Filled black circles are stars that were removed from the original 115 target list. For information, names for some of the stars are also labelled.

at both wavelengths, and then smoothed with a 7″ Gaussian using the Starlink package KAPPA recipe GAUSMOOTH (Currie & Berry 2013). Flux conversion factors (FCFs) were derived from the calibrator observations taken on the same night as the observations, reduced in exactly the same way as the source data, and applied to calibrate each map in flux density. FCFs were calculated based on the diameter of the observed disc. For unresolved discs the FCF was measured in a beam-sized aperture from the calibrator observation (often referred to as "per beam" fluxes), whereas for resolved discs the conversion factor was based on an aperture diameter appropriate for the disc size (often referred to as "integrated" or "aperture" fluxes). The final images were made by coadding two or more maps using inverse-variance weighting implemented by the Starlink package PICARD recipe MOSAIC JCMT IMAGES (Gibb et al. 2013).

3.2.3 Noise analysis

Output data files from the map-maker were written in Starlink *N*-Dimensional Data Format (Jenness et al. 2015) and contain the rebinned image ("DATA" array) in terms of signal per output map pixel, together with a variance array representing the spread in values falling in a map pixel ("VARIANCE" array). Signal-to-noise maps were produced (Starlink package KAPPA recipe MAKESNR) creating a new NDF file by dividing the DATA component by the square root of the VARIANCE array. This method, however, provides a noise estimate that is only representative of the true noise in an image if there are no residual features on a scale larger than approximately half a beam diameter. For unresolved discs the noise in an image was also obtained directly from the DATA array by taking integrated flux measurements within multiple beam-sized areas, spaced by 4″, from the central few arcminutes of the image. Similarly, for resolved discs the noise was estimated from apertures appropriate for the diameter of the disc, spaced by the one-third of the aperture diameter. In both cases the resulting flux distribution was fitted by a Gaussian (IDL HISTOGAUSS) with the noise level corresponding to the standard deviation of the fit. For the vast majority of the SONS survey measurements, both methods gave very similar results. This similarity was expected since the "zero masking" technique is very effective at ensuring the final image is devoid of instrumental artefacts. The noise estimates reported in this paper are based on the measurements directly from the rebinned image (DATA array), and cases of residual instrumental artefacts in the images are discussed in Section 5 for individual targets. The errors reported for integrated fluxes (aperture photometry) are similarly derived from overlapping apertures of the same diameter used to determine the source flux.

3.3 The Fomalhaut debris disc: A test case

As discussed in Section 3.2, due to the excess low-frequency noise, one of the major challenges for the SONS survey was the reduction and calibration of moderately extended disc structures. The recovery of large-scale structure is a common issue for all observations undertaken with SCUBA-2. To test the robustness of the "zero mask" data reduction method an extended, well-characterised debris disc was adopted as a test case. HD 216956 (Fomalhaut; α PsA) has been well-

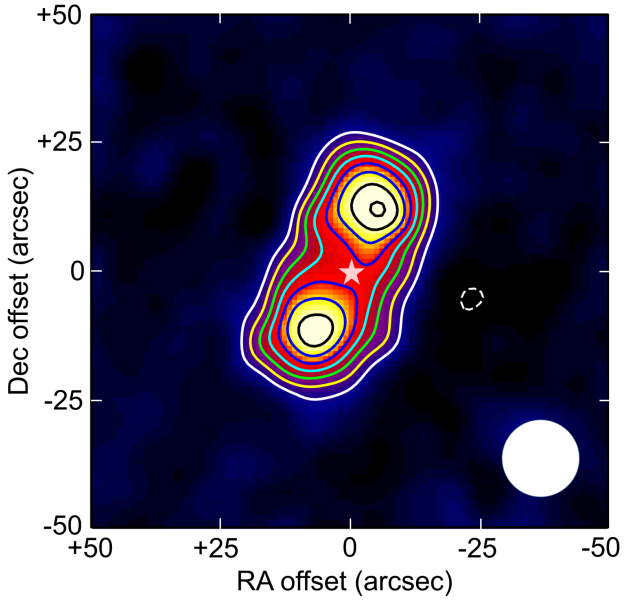

Figure 4. The Fomalhaut debris disc imaged by SCUBA-2 at 850 µm. This signal-to-noise image is colour scaled from -5σ (black) to the maximum S/N in the image at 26σ (white). The dashed contour is at -5σ and the solid contours start at 5σ and increase in 3σ steps. The star symbol shows the position of Fomalhaut with respect to the disc (after proper motion corrections). The white circle represents the approximate FWHM beam size at 850 µm after smoothing.

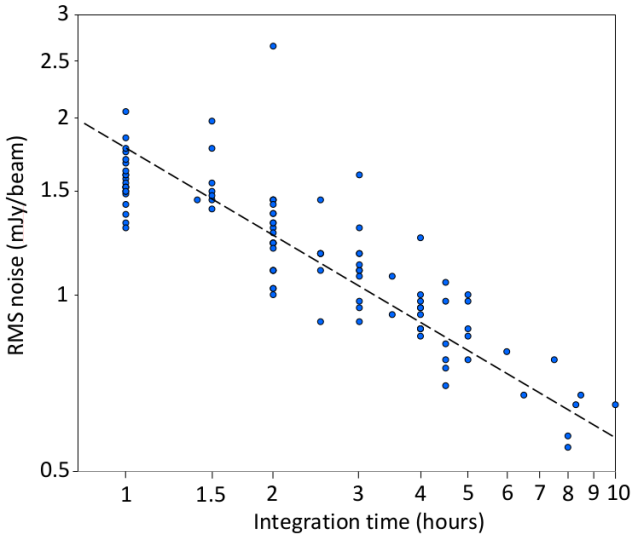

Figure 5. The measured RMS noise (mJy/beam) at 850 µm as a function of integration time (t_{obs}) for all 100 target fields in the SONS survey sample. The trend line indicates a noise decrease as $t_{obs}^{-0.5}$.

studied at all wavelengths from the optical to the millimetre, and the associated debris disc has a well-sampled spectral energy distribution. The disc is also one of the most extended so far discovered. The SCUBA-2 signal-to-noise (S/N) image of the Fomalhaut debris disc at 850 µm (Fig. 4) shows an identical structure to previous submillimetre observations (Holland et al. 2003). Furthermore, the measured integrated flux within a 60″ diameter aperture is 91 ± 3 mJy, compared to the 97 ± 5 mJy measured from the SCUBA observations (Holland et al. 2003), consistent within the measured errors. Hence, the "zero mask" data reduction method works well for discs extending to at least 1′ in diameter, although there remains some uncertainty for targets such as Vega (see Section 5.44).

4 SURVEY OUTPUTS AND INTERPRETATION

4.1 Survey outputs

The outputs of the survey are a catalogue of images and fluxes (including errors) for the 100 observed fields at 850 µm[2]. Table 2 lists the measured flux densities for all 100 stars and indicates whether the discs are resolved or unresolved by these observations. Signal-to-noise images for the detected fields are presented in Appendix A. Integration times ranged from a minimum of 1 hr to a maximum of 10 hrs. (The 5 hrs or longer observations were largely undertaken during the survey verification programme time, prior to the formal start of the SONS survey.) The results for each star are described in Section 5. As shown in Fig. 5, the RMS noise (determined from beam-sized apertures in all cases) within the inner 3′ diameter region of each image decreases as $t_{obs}^{-0.5}$, where t_{obs} is the integration time. The spread in RMS values is due to the relatively wide range of sky transmissions during the observations (i.e., the zenith sky opacity as defined by the allocated weather band combined with the airmass of the source at the time of the observation). Table 2 also lists five targets for which the peak is offset from the star by more than half a beam diameter (∼7.5″ for the smoothed 850 µm beam). In each of these cases the peak is interpreted as more likely to be a background object rather than a disc about the star (see Section 5).

Although the primary wavelength of observation for the survey was 850 µm, reflected by the allocation of weather bands 2 and 3 at the JCMT, a significant number of the targets showed flux excesses at 450 µm. Experience has shown that in band 2 and 3 weather conditions, which is far from optimal for 450 µm observations, the chances of a false detection are minimised by adopting a detection threshold of 5σ. Hence, whilst a level of 3σ has been used when reporting 850 µm results in this paper, a level of 5σ has been adopted at 450 µm. A total of 14 targets in the sample reached this threshold, all of which were also detected at 850 µm. The 450 µm photometry has been used to constrain further the fitting of the SED (Section 4.2) and offers improved angular resolution for extended structures (i.e., ∼10″ when the image is smoothed with a 7″ FWHM Gaussian). The results from the 450 µm observations, where applicable, are noted in Table 2, and discussed in the individual source descriptions in Section 5.

[2] The complete catalogue of images and spectral energy distributions for the entire sample of targets in the SONS survey, including the non-detections, is available online (doi:10.11570/17.0005).

Table 2. Integration times and measured fluxes for the SONS survey sample. The column "Disc" refers to whether the observed structure is unresolved ("P" - point-like) or resolved ("E" - extended compared to the beam diameter) at 850 µm. Fluxes are presented at both wavelengths with $3\,\sigma$ and $5\,\sigma$ upper limits quoted at 850 µm and 450 µm, respectively, in the case of a non-detected excess. Calibration uncertainties, as described in Section 3.1, are not included in the listed fluxes. For resolved (extended) structures the flux quoted is from aperture photometry (see Section 3.2.2) with the diameter of the aperture given in the individual source descriptions in Section 5.

HD number	Other names	Time (hrs)	Disc	850 µm flux (mJy)	450 µm flux (mJy)	Notes
377		4.0	P	5.3 ± 1.0	<90	
	HIP 1368	1.0	–	<4.2	<105	
3126		1.0	–	<4.5	<95	
3296	LTT 317	2.0	–	<3.0	<100	
6798		4.5	P	7.2 ± 1.0	<65	
7590	V445 And	3.5	–	<3.3	<110	
8907		2.0	P	7.8 ± 1.2	51 ± 10	
9672	49 Cet	2.5	P	13.5 ± 1.5	125 ± 18	Detected and resolved at 450 µm
10647	q[1] Eri	2.0	P	20.1 ± 2.7	<2800	Background galaxy contamination to east of star
10700	τ Ceti	8.0	P	4.4 ± 0.6	25 ± 4.5	
10638		4.0	P	5.1 ± 0.9	<105	
13161	β Tri	4.0	P	5.1 ± 0.9	<85	
14055	γ Tri	4.0	P	7.2 ± 1.0	<70	
15115		3.0	P	8.2 ± 1.1	<150	Peak is 5″ offset from the star
15257	12 Tri	2.0	P	10.3 ± 1.2	56 ± 11	
15745		3.0	E	12.0 ± 1.4	<110	Marginally resolved at 850 µm
17093	38 Ari	5.0	–	(8.8 ± 0.9)	<110	Peak is 10″ offset; likely a background object
19356	β Per; Algol	4.0	P	6.4 ± 0.9	<35	Is the emission from a debris disc?
21997		4.5	E	10.7 ± 1.5	<125	Marginally resolved at 850 µm
22049	ϵ Eri	4.5	E	31.3 ± 1.9	181 ± 15	Detected at 450 µm, but poor S/N in clumps
22179	V* 898 Per	2.0	–	(7.0 ± 1.3)	<100	Peak is 18″ offset; likely a background object
25457		2.0	P	6.2 ± 1.4	<145	
25570		3.0	–	<3.6	<120	
28226		1.0	–	<4.5	<100	
28355	79 Tau	1.0	–	<3.9	<150	
30495	58 Eri	1.0	–	<4.8	<150	
31295	7 Ori	2.0	–	<4.5	<165	
33636		3.0	–	<3.3	<37	
35841		4.5	P	3.5 ± 0.8	<35	Peak is 5″ offset from the star
37594		3.0	–	<3.6	<200	
38858		10.0	E	7.5 ± 1.4	<55	Extended structure with background source?
48682	56 Aur	8.0	E	3.9 ± 0.8	<25	Possibly resolved. Peak is 6.5″ offset from star
49601	GJ 249	1.0	–	<4.5	<100	
57703		2.0	–	<3.9	<150	
61005	"The Moth"	1.5	P	13.5 ± 2.0	<200	
70313		1.0	–	<4.5	<135	
73350	V401 Hya	1.5	–	<4.5	<115	
	GJ 322	2.0	P	7.3 ± 1.4	57 ± 11	
75616		2.0	–	<3.3	<45	
76543	62 Cnc	2.5	–	<3.6	<100	
76582	63 Cnc	5.0	P	5.7 ± 1.0	89 ± 17	
82943		1.0	–	<4.5	<225	
84870		4.0	P	6.2 ± 1.0	<50	
85301		2.0	–	<4.5	<75	
91312		3.0	–	<3.3	<110	
91782		1.5	–	<4.8	<350	
	TWA7; CE Ant	4.0	P	7.2 ± 1.3	<300	Peak is 6″ offset from the star
92945		3.0	P	8.6 ± 1.1	<90	Background source contamination to south of star
95418	β UMa	1.0	–	<4.8	<100	
95698		1.0	–	<5.4	<500	
	TWA13	2.0	–	<3.0	<70	
98800	LTT 317	1.5	P	93.6 ± 1.5	242 ± 14	
102647	β Leo	1.0	–	<4.5	<75	
102870	β Vir	1.0	–	<4.2	<145	
104860		5.0	P	6.5 ± 1.0	<135	
107146		1.0	P	20.6 ± 2.1	<375	Peak is 4″ offset from the star
109085	η Crv	8.3	E	15.4 ± 1.1	54 ± 12	Detected and resolved at 450 µm, but poor S/N
109573	HR 4796; TWA 11	1.0	P	14.4 ± 1.9	117 ± 21	
110411	ρ Vir	1.5	–	<4.5	<165	
111631		3.5	–	<0.9	<110	

Table 2 – *continued*

HD number	Other names	Time (hrs)	Disc	850 μm flux (mJy)	450 μm flux (mJy)	Notes
113337		2.0	–	<3.6	<75	
115617	61 Vir	7.5	E	5.8 ± 1.0	<70	Marginally resolved at 850 μm
122652	12 Tri	1.0	–	<5.1	<200	
125162	λ Boo	4.5	P	3.9 ± 0.8	<30	
125473	ψ Cen	2.0	–	<3.9	<65	
127821		8.5	P	5.8 ± 0.7	<60	Interpreted as a single dust peak
127762	γ Boo	2.0	–	<3.6	<105	
128167	σ Boo	5.0	–	(4.1 ± 0.9)	<80	Peak is 11″ offset; likely a background object
131625		2.0	–	<4.5	<180	
135502	χ Boo	2.0	–	<4.2	<115	
135599		2.0	–	<3.6	<120	
	GJ 581; HIP 74995	3.0	–	<4.8	<115	
139006	α CrB	1.0	–	<5.1	<170	
139590		1.0	–	<3.9	<60	
141378		1.0	–	(8.5 ± 1.8)	<165	Peak is 13″ offset; likely a background object
143894	44 Ser	4.0	E	10.1 ± 1.2	<80	Peak is 4″ offset from the star
149630	σ Her	1.4	–	<4.5	<75	
150378	37 Her	2.0	–	(10.2 ± 1.1)	<54	Peak is 17″ offset; likely a background object
150682	39 Her	4.0	P	5.5 ± 0.9	<60	
151044		3.0	–	<2.7	<35	
157728	73 Tau	1.0	–	<4.5	<155	
158633		1.0	–	<4.8	<85	
158352		4.0	P	5.3 ± 1.0	<100	
161868	γ Oph	4.5	E	7.1 ± 1.0	<90	Marginally resolved at 850 μm
170773		1.5	E	26.0 ± 2.3	<225	
172167	α Lyr; Vega	6.0	E	34.4 ± 1.4	229 ± 14	Also resolved at 450 μm
181327		1.0	P	23.6 ± 3.4	<7500	
182681		2.5	P	6.8 ± 1.2	<65	Could be more than one clump?
191089		2.5	P	4.9 ± 0.9	<70	
192425	ρ Aql	1.5	–	<4.2	<85	
197481	AU Mic	5.0	P	12.6 ± 0.8	57 ± 9	Also resolved at 450 μm
205674		5.0	P	4.0 ± 0.7	<40	Peak is 6″ offset. Two point sources?
206893		2.0	P	4.5 ± 1.1	<75	Peak is 4″ offset from the star
207129		2.5	E	10.8 ± 1.8	<210	Marginally resolved at 850 μm
209253		1.0	–	<4.8	<200	
212695		2.5	P	5.7 ± 1.1	<85	
213617	39 Peg	3.0	P	4.6 ± 1.3	<215	Peak is 4″ offset from the star
216956	α PsA; Fomalhaut	2.0	E	91 ± 2.5	475 ± 21	Also resolved at 450 μm
218396	HR 8799	3.0	E	17.4 ± 1.5	346 ± 34	Likely background cloud contamination at 450 μm
221853		2.0	–	<3.9	<100	

4.2 Dust temperature and emissivity

Photometry for the target stars has been compiled from the optical to the millimetre from a wide variety of sources, including all-sky surveys such as *IRAS* (Moshir et al. 1990), *Hipparcos* (Perryman et al. 1997), 2MASS Point Source Catalog (Cultri et al. 2003), *AKARI* (Ishihara et al. 2010) and *WISE* (Wright et al. 2010), as outlined in Section 2. Further data are also provided by the surveys undertaken by *Spitzer* (including IRS data from the CASSIS database) (e.g., Lebouteiller et al. 2011) and *Herschel* (e.g., Booth et al. 2013). Specific references to the photometric points provided for each target are given in the individual source descriptions in Section 5. The photometric data allow a spectral energy distribution to be assembled for each of the target stars, and these are shown in the figures presented in Appendix A, together with the 850 μm S/N images.

The SED modelling adopted in this paper (Kennedy et al. 2012) has been successfully implemented for other surveys of debris discs, including the *Herschel* DEBRIS survey (e.g. Booth et al. 2013; Thureau et al. 2014). Photometry shortward of about 10 μm was first used to model the stellar photospheric emission, and the estimated contributions to the remaining infrared and submillimetre/millimetre photometric fluxes were then subtracted. These photometric points were then fitted by one or two component Planck functions in which a pure blackbody spectrum is modified beyond a critical wavelength, λ_0, as described in Section 2. The best fitting model was found by a least-squares minimisation method. The model therefore accounts for inefficient emission by grains that are small relative to the wavelength of emission. The factor λ_0 is therefore representative of the grain size that dominates the emission spectrum, whilst the parameter β is an index that describes the emissivity of the dust grains as well as being indicative of the size distribution of the dust.

In many cases, even with the 850 μm photometry provided by the SONS survey, the sparse data coverage at submillimetre and millimetre wavelengths means that both λ_0 and β are poorly constrained by the modelling. Moreover,

in cases of only a single measurement beyond 160 µm, λ_0 and β become strongly degenerate and no unique solution is possible. For some targets, a well-defined second component fit to the SED may possibly indicate the presence of multiple planetesimal belts (e.g., Morales et al. 2011; Chen et al. 2014; Kennedy & Wyatt 2014). The main output parameters from the SED fitting (for one or more components), relevant to the interpretation of the IR/submm flux excess, are the dust temperature ($T_{\rm d}$), critical wavelength (λ_0) and the dust emissivity index (β). These values are listed in Table 3 for the SONS survey sample, in which the derived β's are presented as a range of values (i.e., all values within the quoted range are possible).

4.3 Disc radius and orientation

The disc radius can also be estimated from derived parameters from the SED fit, assuming that the dust grains behave as a blackbody, and are uniformly distributed in a disc at a distance $R_{\rm BB}$ from the star (Wyatt 2008). In the cases where the emission is optically thin, the dust temperature can be used as a proxy for the radial separation from the star, which is given by:

$$R_{\rm BB} = \left(\frac{278.3}{T_{\rm d}}\right)^2 L_*^{0.5} \quad (1)$$

where, if the dust temperature ($T_{\rm d}$) is measured in Kelvins, and the stellar luminosity (L_*) in Solar luminosities, then $R_{\rm BB}$ is in astronomical units. The disc radii estimated from this method are presented in Table 3.

As already discussed in Section 4.2, the far-IR/submillimetre emission from discs is typically modelled using a modified blackbody spectrum. Therefore, the true radius of the disc is expected to be significantly larger in most cases (Rodriguez & Zuckerman 2012; Booth et al. 2013; Pawellek et al. 2014), as is further discussed in Section 6.2. Hence, whilst modelling the SED provides a wealth of information about the disc properties, measuring the radius, directly from an image, allows better constraints to be placed on other physical properties such as the particle size distribution (Wyatt & Dent 2002). For the cases in which discs are spatially resolved the 850 µm (or 450 µm, as available) images are fitted using a 2-D Gaussian function (IDL routine MPFIT2DFUN; Markwardt 2009) to estimate the radial extent of the disc. The fitted disc major and minor axes are deconvolved with the beam size (including the broadening effect of the smoothing factor), and the major axis multiplied by the distance of the star to give an estimate of the true disc radius according to:

$$R_{\rm fit} = \frac{d}{2}\sqrt{{\rm FWHM}_{\rm fit}^2 - ({\rm FWHM}_{\rm beam}^2 + {\rm FWHM}_{\rm smo}^2)} \quad (2)$$

where d is the distance of the star, ${\rm FWHM}_{\rm fit}$ is the measured major axis of the Gaussian fit, ${\rm FWHM}_{\rm beam}$ is the beam diameter (assumed circular and with a measurement variation of $\pm$ 0.2″), and ${\rm FWHM}_{\rm smo}$ is the Gaussian smoothing component (by default 7″)[3].

[3] If the distance of the star is measured in parsecs and the FWHM beam in arcseconds, then the disc radius as specified in Equation 2 will be in astronomical units.

There are a few cases where the emission is not well-approximated by a Gaussian profile. An example of this is Fomalhaut (HD 216956) where there are two equidistant lobes offset from the star position, and so the emission is not centrally concentrated. As discussed in Section 5.54, *Herschel* and ALMA observations show that the emission is confined to a thin belt with the mid-point at a radius of ∼20″ from the star. Fig. 6 presents the results of the radial fit transposed into a model image and compared to the observed result. The model-subtracted map shows a residual peak at the star position (and to a lesser extent in the south-east lobe) but the fit, for the purposes of this paper, is a reasonable representation of the overall disc size. The Fomalhaut case is somewhat of an extreme example, and for the vast majority of stars in the sample the fitting is well-suited to the disc morphology.

The inclination angle of the disc to the plane of the sky is derived from the axial ratio of the deconvolved major and minor axes fits (noting a 90° angle degeneracy). Finally, the position angle (PA) of the major axis of the disc is measured north through east (also noting an angle degeneracy of 180°). The estimated disc radius, including upper limits for the cases in which the disc is unresolved, are given in Table 3. Full details of the measured major and minor axes radii, as well as the inclination and position angles, are presented in Table 4 for the 16 resolved discs in the SONS survey sample.

4.4 Fractional luminosities

The amount of dust in debris discs is often quantified in terms of the fractional luminosity, and can be determined from the SED fits to both the stellar photospheric and excess thermal emission. This quantity is defined as the ratio of the IR luminosity from the dust to that of the star, $f = L_{\rm IR}/L_\star$ (e.g. Wyatt 2008), and can be estimated from the wavelength and flux of the maximum in the emission spectra of the star and the disc, according to:

$$f = \frac{F_{\rm d(max)}}{F_{\star(\rm max)}}\frac{\lambda_{\star(\rm max)}}{\lambda_{\rm d(max)}}. \quad (3)$$

As Equation 3 represents only an approximation to the fractional luminosity, f is determined for the targets in this paper by the ratio of the integrated areas under the star and disc SED component fits. When there are two temperature components of the SED fit to the IR excess, then the fractional luminosity is derived from the sum of both. A defining property of a debris disc is that, in general, it has a fractional luminosity of $f < 10^{-2}$ (Lagrange et al. 2000) in contrast to protoplanetary discs, which have higher fractional luminosities. This criterion is certainly met by cool Edgeworth-Kuiper belt analogues, but falls down for stars at an earlier evolutionary phase where planet formation is believed to be ongoing, and where the flux excess tends to peak at mid-IR wavelengths (e.g. Melis et al. 2010; Fujiwara et al. 2012; Vican et al. 2016). The fractional luminosities for the SONS surveys discs are given in Table 3, and all but

Table 3. The derived parameters from the SED fitting, measurements (and upper limits) from the radial profile fitting, and dust mass calculations for the SONS survey sample. Note that this list does not include the five "extreme" offset cases, in which the flux peak is observed to be equal to, or greater than 10″ from the star (as indicated in Table 2). In the cases where the disc is unresolved the parameter R_{fit} represents the upper limit to disc radius, corresponding to the beam radius at the distance of the star (see also the scale bars in the figures of Appendix A).

HD number	Other names	$L_\star^{(1)}$ ($L_\odot$)	$L_{\rm disc}/L_\star$ ($\times 10^{-4}$)	λ_0 (μm)	β	$T_{\rm d}$ (K)	$R_{\rm BB}^{(1)}$ (au)	$R_{\rm fit}$ (au)	$M_{\rm dust}$ ($\times 0.01\,{\rm M}_\oplus$)
377		1.2 ± 0.03	3.8 ± 1.4	–	0.0 – 1.4	56 ± 6	27 ± 4	<290	3.6 ± 0.8
6798		35.2 ± 0.6	1.7 ± 1.1	<142	0.2 – 0.9	48 ± 8	200 ± 48	<615	25.4 ± 5.5
8907		2.2 ± 0.03	2.5 ± 0.2	<655	0.4 – 2.1	51 ± 5	44 ± 5	<175	4.4 ± 0.8
9672	49 Cet	16.9 ± 0.3	8.5 ± 0.6	79 – 129	0.9 – 1.1	59 ± 2	92 ± 5	421 ± 16$^{(2)}$	20.0 ± 2.2
10647	q^1 Eri	1.6 ± 0.04	3.2 ± 0.8	<75	0.6 – 0.8	44 ± 2	49 ± 6	<125	3.3 ± 0.5
10700	τ Cet	0.49 ± 0.02	0.08 ± 0.02	–	0.0 – 1.1	71 ± 23	11 ± 5	<18	0.021 ± 0.007
10638		7.8 ± 0.1	5.0 ± 1.5	<357	>0.6	34 ± 15	187 ± 114	<515	17.9 ± 8.4
13161	β Tri	73.5 ± 1.4	0.29 ± 0.02	113 – 204	0.6 – 1.7	84 ± 5	94 ± 8	<290	2.2 ± 0.4
14055	γ Tri	25.3 ± 0.5	0.89 ± 0.03	155 – 250	0.7 – 1.5	77 ± 2	66 ± 3	<260	2.8 ± 0.4
15115		3.3 ± 0.1	5.5 ± 1.0	<149	0.5 – 0.9	57 ± 4	44 ± 5	<340	7.3 ± 1.1
15257	12 Tri	14.7 ± 0.3	1.1 ± 0.4	–	0.0 – 1.9	53 ± 10	106 ± 27	<240	10.8 ± 2.3
15745		3.3 ± 0.1	20.1 ± 0.9	–	0.0 – 0.9	89 ± 2	18 ± 1	514 ± 111	13.3 ± 1.6
19356	β Per	101 ± 2.5	0.09 ± 2.34	–	0.0 – 2.0	27 ± 17	1106 ± 976	<210	4.5 ± 2.9
21997		11.7 ± 0.2	5.5 ± 0.2	86 – 371	0.4 – 1.4	64 ± 1	66 ± 3	813 ± 69	21.5 ± 3.0
22049	ϵ Eri	0.34 ± 0.01	1.2 ± 0.5	<200	0.6 – 1.0	44 ± 8	23 ± 6	67 ± 2	0.16 ± 0.03
25457		2.1 ± 0.03	1.1 ± 1.6	<786	>0.1	50 ± 12	44 ± 15	<280	1.1 ± 0.4
35841		2.4 ± 0.3	14.3 ± 2.3	–	0.0 – 2.7	71 ± 3	24 ± 5	<725	11.4 ± 2.7
38858		0.83 ± 0.02	0.82 ± 0.13	–	∼0.0	50 ± 10	28 ± 8	192 ± 18	0.86 ± 0.24
48682	56 Aur	1.9 ± 0.1	0.67 ± 0.10	<182	0.7 – 1.8	43 ± 12	57 ± 22	184 ± 33	0.62 ± 0.21
61005	"The Moth"	0.58 ± 0.01	27.1 ± 0.7	109 – 217	0.4 – 0.7	61 ± 1	16 ± 1	<265	6.9 ± 1.0
	GJ 322	0.10 ± 0.01	3.2 ± 0.7	–	>0.1	24 ± 10	43 ± 27	<85	2.1 ± 1.0
76582	63 Cnc	8.9 ± 0.2	2.3 ± 0.3	185 – 547	>1.1	52 ± 2	85 ± 5	<230	5.7 ± 1.0
84870		7.6 ± 0.1	5.0 ± 2.1	<324	0.3 – 1.2	50 ± 6	85 ± 14	<660	23.5 ± 4.5
	CE Ant	0.05 ± 0.01	16.9 ± 1.7	–	0.0 – 2.5	19 ± 8	49 ± 30	<380	24.1 ± 11.8
92945		0.37 ± 0.01	6.5 ± 0.5	<270	0.4 – 1.1	42 ± 7	27 ± 7	<160	2.4 ± 0.5
98800	LTT 317	0.98 ± 0.03	1090 ± 39	–	0.0 – 0.1	156 ± 3	3.1 ± 0.2	<255	36.9 ± 0.9
104860		1.2 ± 0.01	6.2 ± 0.4	138 – 296	0.4 – 1.2	47 ± 3	39 ± 4	<340	7.1 ± 1.2
107146		0.99 ± 0.01	10.8 ± 3.2	276 – 425	0.8 – 1.0	41 ± 2	46 ± 5	<210	9.3 ± 1.1
109085	η Crv	5.2 ± 0.1	1.4 ± 0.3	<806	0.2 – 1.0	41 ± 7	87 ± 18	190 ± 7	3.1 ± 0.6
109573	HR 4796	24.1 ± 0.8	56.5 ± 4.7	<72	0.7 – 1.0	99 ± 3	38 ± 3	<370	18.9 ± 2.5
115617	61 Vir	0.83 ± 0.02	0.28 ± 0.04	–	0.0 – 1.5	65 ± 11	17 ± 4	40 ± 13	0.16 ± 0.04
125162	λ Boo	17.1 ± 0.3	0.30 ± 0.03	<216	0.3 – 1.8	87 ± 6	43 ± 4	<230	1.0 ± 0.2
127821		3.1 ± 0.1	1.9 ± 0.2	94 – 199	0.9 – 1.9	47 ± 3	61 ± 12	<235	3.1 ± 0.6
143894	44 Ser	29.1 ± 0.5	0.32 ± 0.04	–	0.0 – 1.1	53 ± 9	148 ± 37	561 ± 69	14.1 ± 3.0
150682	39 Her	6.8 ± 0.1	0.13 ± 0.03	–	0.0 – 2.2	32 ± 14	201 ± 130	<330	8.1 ± 3.8
158352		18.9 ± 0.3	0.78 ± 0.04	<797	0.1 – 2.2	62 ± 7	88 ± 13	<450	7.5 ± 1.6
161868	γ Oph	26.2 ± 0.6	1.1 ± 0.2	109 – 217	0.8 – 1.4	68 ± 3	85 ± 6	246 ± 35	2.5 ± 0.4
170773		3.6 ± 0.1	5.2 ± 0.3	101 – 343	0.5 – 1.4	46 ± 2	70 ± 4	252 ± 26	19.1 ± 1.9
172167	α Lyr; Vega	48.4 ± 0.9	0.17 ± 0.12	<80	1.2 – 1.6	46 ± 7	260 ± 58	73 ± 3$^{(2)}$	1.1 ± 0.2
181327		3.3 ± 0.1	26.5 ± 5.2	<90	0.5 – 0.6	63 ± 3	47 ± 4	<390	24.8 ± 3.7
182681		25.7 ± 0.3	2.7 ± 0.2	<331	0.2 – 1.0	80 ± 7	62 ± 8	<525	10.4 ± 1.0
191089		3.0 ± 0.1	14.2 ± 0.5	<672	0.3 – 2.3	89 ± 5	17 ± 2	<395	3.7 ± 0.7
197481	AU Mic	0.09 ± 0.01	3.9 ± 0.3	–	0.0 – 0.3	50 ± 8	9 ± 2	70 ± 10$^{(2)}$	0.60 ± 0.10
205674		2.9 ± 0.1	3.8 ± 0.2	<752	0.1 – 1.1	60 ± 2	37 ± 2	<390	4.4 ± 0.7
206893		2.5 ± 0.1	2.4 ± 0.1	94 – 423	0.5 – 2.7	54 ± 2	43 ± 4	<290	3.0 ± 0.8
207129		1.3 ± 0.03	1.1 ± 0.2	<156	0.4 – 1.1	46 ± 8	41 ± 10	159 ± 23	1.5 ± 0.4
212695		3.0 ± 0.05	0.49 ± 0.13	–	0.0 – 2.7	35 ± 19	108 ± 83	<350	8.6 ± 5.0
213617		5.5 ± 0.3	1.0 ± 0.1	–	0.0 – 2.1	59 ± 6	52 ± 8	<380	4.9 ± 1.5
216956	Fomalhaut	16.5 ± 0.3	0.58 ± 0.16	<87	1.0 – 1.3	41 ± 3	185 ± 22	151 ± 8	3.2 ± 0.3
218396	HR 8799	5.4 ± 0.1	3.1 ± 0.3	<449	0.6 – 1.9	43 ± 5	98 ± 18	395 ± 42	15.6 ± 2.4

(1)The error quoted for L_* and R_{BB} includes the uncertainty in the distance of the star from the *Hipparcos* catalogue (Perryman et al. 1997; van Leeuwen 2007). This is typically less than 5 percent of the total error, which is dominated by errors in the fitting.
(2)Based on the fitted radius from the 450 μm image.

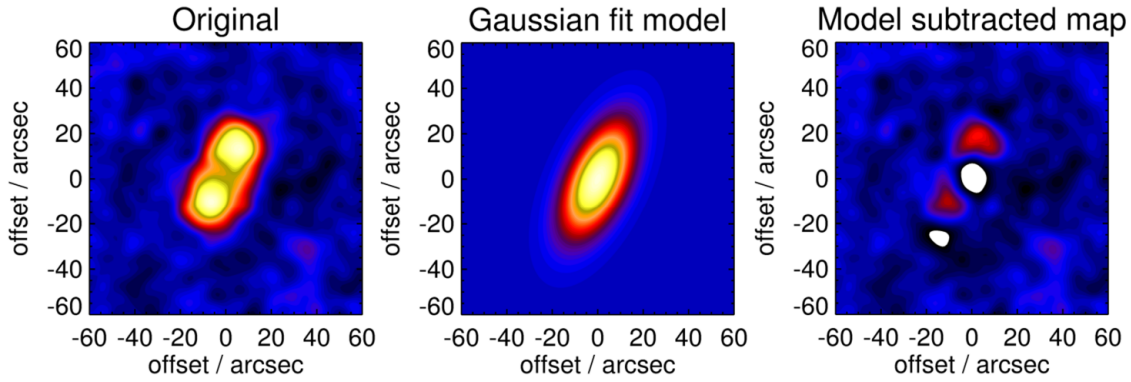

Figure 6. (left) The original 850 µm observed image for HD 216956 (Fomalhaut); (centre) The Gaussian model is based on the fit to the radial extent; (right) The result of subtracting the observed image from the model map. Note that the residual emission at the star is not due to the star, but is due to over-subtraction, as the Gaussian model used is centrally peaked but the real flux distribution is not.

Table 4. Derived parameters from the radial extent fitting for resolved sources in the SONS survey sample. The waveband indicates the wavelength from which the measurements were made.

HD number	Other names	Waveband (µm)	Measured disc FWHM major (″)	minor (″)	Decconvolved disc radius (″)	Disc radius $R_{\rm fit}$ (au)	Inclination (°)	Position angle (° E of N)
9672	49 Cet	450	17.5 ± 0.5	11.0 ± 0.7	7.1 ± 0.5	420 ± 16	74 ± 13	130 ± 10
15745		850	21.9 ± 3.5	<15	8.1 ± 3.5	514 ± 111	⩾22	164 ± 21
21997		850	27.0 ± 1.9	<15	11.3 ± 1.9	813 ± 69	⩾48	27 ± 12
22049	ϵ Eri	850	44.1 ± 1.2	40.2 ± 1.3	20.8 ± 1.2	67 ± 4	26 ± 2	61 ± 3
38858		850	29.3 ± 2.4	18.2 ± 2.9	12.7 ± 2.4	192 ± 18	65 ± 18	75 ± 11
48682		850	26.5 ± 3.9	<15	11.0 ± 3.9	184 ± 33	⩾47	94 ± 19
109085	η Crv	850	25.5 ± 1.2	21.8 ± 1.2	10.4 ± 1.2	190 ± 7	44 ± 4	132 ± 5
115617	61 Vir	850	17.5 ± 3.0	<15	4.7 ± 3.0	40 ± 13	⩾0	66 ± 25
143894	44 Ser	850	25.2 ± 2.5	16.8 ± 2.7	10.2 ± 2.5	561 ± 69	67 ± 24	70 ± 15
161868	γ Oph	850	21.5 ± 2.2	<15	7.8 ± 2.2	246 ± 35	⩾16	75 ± 17
170773		850	20.1 ± 1.4	16.0 ± 1.6	6.8 ± 1.4	252 ± 26	63 ± 17	140 ± 13
172167	α Lyr; Vega	450	21.6 ± 0.7	18.1 ± 0.8	9.5 ± 0.7	73 ± 3	34 ± 2	40 ± 17
		850	38.1 ± 0.8	32.3 ± 0.9	17.5 ± 0.8	135 ± 3	35	45 ± 19
197481	AU Mic	450	17.5 ± 2.1	13.5 ± 2.3	7.1 ± 2.1	70 ± 10	52 ± 16	127 ± 15
207129		850	24.8 ± 2.9	15.2 ± 3.1	10.0 ± 2.9	159 ± 23	80 ± 69	115 ± 13
216956	Fomalhaut	850	42.0 ± 1.8	21.1 ± 2.7	19.7 ± 0.5	151 ± 8	68 ± 5	156 ± 3
218396	HR 8799	850	24.9 ± 2.1	18.8 ± 2.8	10.1 ± 2.1	395 ± 42	55 ± 6	71 ± 16

one (the exception being HD 98800) of the discs detected fall into this "debris" classification.

4.5 Dust masses

Although the fractional luminosity can be converted into an estimate of dust mass by assuming all dust grains have the same diameter and density, dust masses are usually derived directly from the 850 µm flux density measurement. Since the emission from debris discs is optically thin at these wavelengths, their mass is directly proportional to the emission, according to,

$$M_{\rm d} = \frac{F_\nu d^2}{\kappa_\nu B_\nu(T_{\rm d})} \quad (4)$$

where F_ν is the measured flux density, d is the distance of the target, κ_ν is the dust opacity which is assumed to be 1.7 cm^2 g^{-1} at 850 µm in accordance with similar studies (Pollack et al. 1994; Dent et al. 2000), and $T_{\rm d}$ is the dust temperature derived from the SED fit. In the Rayleigh-Jeans limit, the mass becomes a linear function of temperature and so equation 4 reduces to,

$$M_{\rm d}[M_\oplus] = 5.8 \times 10^{-10} \frac{F_\nu[{\rm mJy}]{\rm d}[{\rm pc}]^2 \lambda[\mu{\rm m}]^2}{\kappa_\nu[{\rm cm^2 g^{-1}}] T_{\rm d}[{\rm K}]} \quad (5)$$

The calculated dust masses are summarised in Table 3 for the SONS survey sample, with quoted uncertainties based on the errors in the 850 µm flux and fitted dust temperature only.

5 INDIVIDUAL TARGETS DISCUSSION

This section of the paper provides a discussion of each of the targets for which emission was detected in the vicinity of the star. Each sub-section summarises the new SONS survey results at 850 µm (and 450 µm, if available) within the context of previous observations, as well as the results of the modelling of the SED and the estimation of the dust mass from the 850 µm flux. Full details, including estimated er-

rors on the modelled and calculated parameters such as $T_{\rm d}$, $R_{\rm BB}$, $R_{\rm fit}$, β and $M_{\rm d}$, are given in Tables 3 and 4.

5.1 HD 377

HD 377 is a Solar-type star (G2V) at a distance of 39.1 pc with an estimated age of around 170 Myr (Chen et al. 2014), but could be as young as 32 Myr (Hillenbrand et al. 2008) or as old as 250 Myr (Choquet et al. 2016). The SONS survey image, as shown in Fig. A1a, reveals emission centred on the stellar position with flux density of 5.3 ± 1.0 mJy at 850 μm. (This value is revised slightly higher from the result reported in Panić et al. 2013.) Interpreting this peak as an unresolved disc about the star gives an upper limit to the radius of 290 au.

HST/NICMOS imaging of HD 377 shows an edge-on disc at a position angle of 47° with a radius of 2.2″ (∼86 au) (Choquet et al. 2016). The disc has also been resolved using the SMA (Steele et al. 2016) with a 850 μm flux of 3.5 ± 1 mJy, just consistent with the SONS result, and a deconvolved disc radius of 47 au at a PA of 30°. Although the mid-far IR region is reasonably well characterised by *Spitzer* (Chen et al. 2014), there are few constraining points in the submillimetre/millimetre. Previous SED modelling suggested a two-component fit deriving "warm" and "cold" elements with dust temperatures of 240 K and 57 K (Chen et al. 2014). Using photometry at 1.2 mm from the IRAM 30 m telescope a dust mass of 0.058 $M_\oplus$ was derived (Roccatagliata et al. 2009). Modelling of the SED with the new 850 μm flux density measurement included gives a cold component dust temperature of 56 K, but the poorly sampled long-wavelength slope means that β is only constrained to be less than a value of 1.4. The estimated dust mass for the cold component of 0.036 $M_\oplus$ is lower than the IRAM result, but is just consistent within the measurement errors.

5.2 HD 6798

HD 6798 is a luminous A3 star in Cepheus lying at a distance of 83 pc and an estimated age of around 320 Myr but with an uncertainty spanning the range from 260 to 400 Myr (Moór et al. 2006). An emission peak is seen at 850 μm with a flux density of 7.2 ± 1.0 mJy (Fig. A1b). As an unresolved disc the upper limit to the radius is 615 au.

The SED contains flux measurements from *IRAS* and *Herschel*/PACS (archival data) in the range 25 – 160 μm but no other long wavelength points. Modelling suggests, as in the case of HD 377, that there are both warm and cold disc components with the former having a dust temperature of 203 K. The fit to the far-IR/submillimetre detected cold disc component gives a dust temperature of 48 K and constrains β to be between 0.2 and 0.9. The dust mass is estimated to be 0.25 $M_\oplus$.

5.3 HD 8907

HD 8907 is an F8 star in Andromeda at a distance of 35 pc and with an estimated age of around 320 Myr (Hillenbrand et al. 2008), although there is significant uncertainty with lower and upper limits put at 110 Myr and 870 Myr, respectively (Moór et al. 2006). The peak in emission is coincident with the star position, and is detected at a flux density of 7.8 ± 1.2 mJy at 850 μm (Fig. A1c), somewhat higher than the previous SCUBA measurement of 4.8 ± 1.2 mJy (Najita & Williams 2005). Emission was also detected (and unresolved) at 450 μm with a flux density of 51 ± 10 mJy. The 450 μm image with 850 μm contours overlaid is shown in Fig. 7, showing both peaks to be coincident. Based on the 450 μm image, and interpreting the peak as a disc about the star, gives an upper limit to the radius of 175 au.

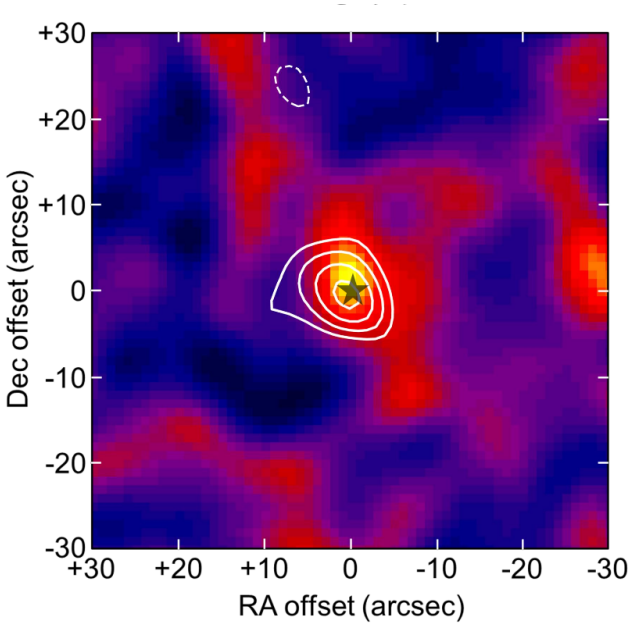

Figure 7. The 450 μm S/N image from observations of HD 8907 with contours from the 850 μm image overlaid. The colours are scaled from $-3\,\sigma$ to the maximum S/N in the image (∼$6\,\sigma$). The contours start at $-3\,\sigma$ (dashed white) and then solid colours from $3\,\sigma$ to the maximum in 1σ steps. The star symbol represents the position of the star with respect to the flux peak.

The SED is well characterised in the IR and submillimetre/millimetre, and observations at 1.2 mm using the SMA (Steele et al. 2016) resolve the disc with a measured radius of 54 au at a PA of 55°. The SONS measurements help to constrain the SED fit, with a dust temperature of 51 K, and a β value in the range 0.4 – 2.1. The dust mass is estimated to be 0.044 $M_\oplus$.

5.4 49 Ceti (HD 9672)

HD 9672 (49 Ceti) is a young A1 star in Cetus and a member of the Argus Association, at a distance of 59 pc with an estimated age of 40 Myr (Torres et al. 2008) but could be as young as 20 Myr (Chen et al. 2014). At 850 μm the detected emission at the stellar position appears to be unresolved (Fig. A1d) with a flux density of 13.5 ± 1.5 mJy. At 450 μm, however, the emission morphology is elongated at a PA of 130° with a flux density of 125 ± 18 mJy, as shown in Fig. 8 (Greaves et al. 2016). The measured disc FWHM of 17.5″ (deconvolved radius of 7.1″, corresponding to ∼420 au) at 450 μm, indicates that the structure is likely a disc about the star, that could also be marginally resolved at 850 μm.

Herschel/PACS observations at 70 μm reveal a resolved

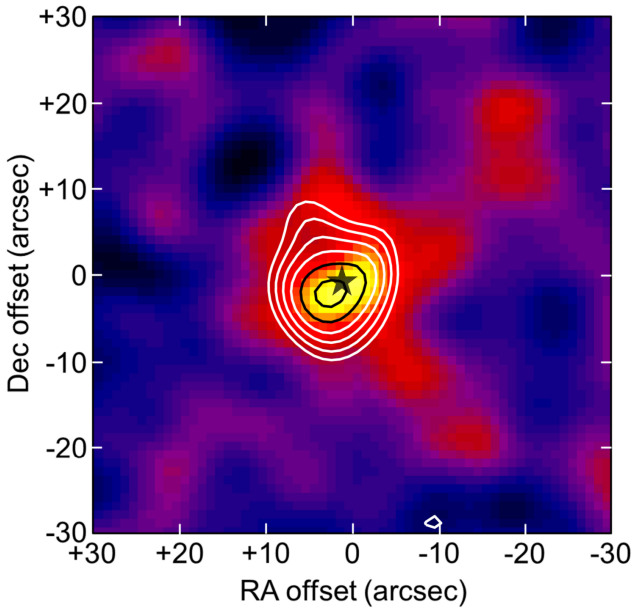

Figure 8. The 450 μm image from observations of 49 Ceti (HD 9672) with contours from the 850 μm image overlaid. The contours and symbols are as described in Fig. 7.

disc of radius 250 au with a PA of 105° (Roberge et al. 2013). Recent ALMA observations also resolve the disc with a PA of 107° identifying dust that extends from just a few to around 300 au from the star (Hughes et al. 2017). The fact that this is significantly less in extent than implied by the SONS result at 450 μm remains an open issue. The observed structure has been modelled as having two components: an inner disc extending to a radius of 60 au (and depleted at less than 30 au) (Wahhaj et al. 2007), and an outer disc of radius up to 400 au (Greaves et al. 2016). Scattered light images, from *HST*/NICMOS and coronograhic H-band images using VLT/SPHERE, show the outer disc extending from 1.1 to 4.6″ (∼65 – 250 au) with an inclination angle of 73°and a PA of 106 – 110° (Choquet et al. 2017). In addition, the system has a well-known molecular and atomic gas reservoir, which was originally purported to be consistent with the properties of a low-mass protoplanetary disc (Zuckerman et al. 1995). The age estimate for the system (likely to be 40 Myr), however, suggested it was more likely the gas had a secondary origin, perhaps involving a high rate of comet destruction given the large observed dust mass (Zuckerman & Song 2012; Hughes et al. 2017).

The disc is well-characterised in the far-IR, with observations from *Spitzer* and *Herschel* contributing to points in the SED. In the millimetre the measured flux from IRAM at 1.3 mm of 13.9 ± 2.5 mJy (Walker & Butner 1995) is significantly higher than expected based on the SED fit to the far-IR and submillimetre points. The reason for this is unknown. The SED, including 9 mm photometry from the VLA (MacGregor et al. 2016a) but not using the IRAM 1.3 mm photometry, is modelled with a two-component fit. The "warm" (inner) element has a characteristic temperature of 165 K. The dominant "cold" (outer) component has a dust temperature of 59 K, a β value of between 0.9 and 1.1, and a calculated dust mass of 0.20 $M_\oplus$.

5.5 q^1 Eridani (HD 10647)

q^1 Eridani is a nearby F9 star at a distance of 17 pc and with an estimated age of 1600 Myr (Chen et al. 2014). There is, however, considerable uncertainty in the age with estimates ranging from 300 Myr to 7000 Myr (Moór et al. 2006). Even though the southerly declination of HD 10647 was quite a challenge for observing with the JCMT, a structure, peaking in emission at the star and extending eastwards, was detected at 850 μm (Fig. A2a). The measured integrated flux of 30.3 ± 3.9 mJy, measured in a 50″ diameter aperture centred on the star, is just consistent with the APEX/LABOCA result of 39.4 ± 4.1 mJy at 850 μm (Liseau et al. 2008), the data for which also show a roughly eastward extension to the disc. The structure is resolved within the 15″ beam, and interpreted as a disc with a deconvolved radius of 9.0″ (∼155 au) at a PA of 72°, dominated by the eastward extension.

The infrared excess was first detected by *IRAS* (Stencel & Backman 1991). The system has one known Jupiter-mass planet (HD 10647 b; Butler et al. 2006) orbiting at a semimajor axis of 2 au, so is unlikely to have any significant influence on a dust disc of radius >100 au. *HST*/ACS coronography revealed an 7.0 – 8.2″ (∼120 – 140 au) radius disc in scattered light with a PA of 56° (Stapelfeldt et al. 2007). *Herschel*/PACS also resolved the disc with a PA of 54° and a beam-deconvolved radius of 6.7 × 3.8″ at 160 μm (∼115 × 65 au; Liseau et al. 2010). In the 850 μm SONS image, the disc appears moderately extended compared to the beam in a roughly easterly direction with most of the flux concentrated at the position of the star. Within the 4σ contour the PA of the disc in the 850 μm SONS image is ∼65°, agreeing reasonably well with both the *HST* and *Herschel* observations, and on a similar scale (∼15″) at least in the north-east direction. (There is also a hint of an extension to the south-west.)

A more plausible explanation is that the eastward extension seen in the SCUBA-2 and LABOCA images is caused by a background object. This extra flux would explain why both 850 μm values are slightly high based on the SED model fit to the far-IR photometric points, and why there is not a symmetric disc seen about the star, as in the *HST* and *Herschel* images. In the *Herschel*/PACS 70 μm image there is evidence of a isolated source 20″ to the east of the main flux peak (Liseau et al. 2010), which aligns well with the eastward extension seen at 850 μm. A similar extension is also seen in the *Herschel*/PACS 160 μm. Hence, in this paper, the infrared excess flux surrounding q^1 Eri has been re-interpreted as an unresolved disc with a flux density of 20.1 ± 2.7 mJy at 850 μm. (This being the flux measured in a beam-sized aperture, centred on the star position.) The SED is well-constrained by *Spitzer*, *Herschel*, the long submillimetre points (including SCUBA-2 at 850 μm) and 6.8 mm photometry from ACTA (Ricci et al. 2015b), to give a dominant temperature component at 44 K, a well-constrained β between 0.6 and 0.8, and an estimated dust mass of 0.033 $M_\oplus$. An upper limit to the disc radius from the 850 μm image, assuming an unresolved source, is 125 au.

5.6 τ Ceti (HD 10700)

HD 10700 (τ Ceti) is a nearby G-type star, believed to be very similar to our Sun, at a distance of 3.7 pc with an estimated age of 7650 Myr, but with an uncertainty in the range 6130 to 8500 Myr (Pagano et al. 2015). The SONS 850 μm image shows a peak in emission at the stellar position with a flux density of 4.4 ± 0.6 mJy (Fig. A2b) of which an estimated 1 mJy is emission from the photosphere. Interpreting the emission morphology as a disc gives an upper limit to the radius from the 850 μm image of 27 au.

The infrared excess has been known since the early days of *IRAS* and was later confirmed by *ISO* (Habing et al. 2001). τ Ceti was first imaged by SCUBA (Greaves et al. 2004) which suggested a disc extending some 55 au from the star, and identified the structure as possibly being a massive Edgeworth-Kuiper Belt analogue. The disc was subsequently resolved by *Herschel* at 70 μm and 160 μm (possibly also at 250 μm) with the peak emission occurring at a radius of 5″ (∼20 au) in the photosphere-subtracted image at 70 μm (Figure 3 of Lawler et al. 2014), and modelled as a wide annulus with an inner edge between 1 and 10 au and an outer edge at ∼55 au inclined from a face-on orientation by 35 ± 10° (Lawler et al. 2014). More recently 1.3 mm interferometric observations with ALMA have revealed a nearly face-on belt of cold dust at a radius of 44 au with a PA of 90° surrounding an unresolved central source at the stellar position (MacGregor et al. 2016a). Modelling of the belt suggests an inner edge of 6 au, consistent with *Herschel* observations. There are also 5 candidate planets orbiting τ Ceti, all of which are believed to lie within a radius of 1.35 au of the star (Tuomi et al. 2013). Whilst the outermost planet may have some influence on the disc inner edge, the majority of the disc extending from a few au to over 50 au will be largely unaffected by the planetary system. The existence of the planetary system, however, remains unconfirmed, following recent work in which periodic signals were not detected from Doppler measurements obtained in the California Planet Survey (Howard & Fulton 2016).

The disc is also detected at 450 μm within the SONS survey with a flux density of 25.2 ± 4.5 mJy (Fig. 9) including an estimated 5 mJy from the photosphere. The separation of the 450 and 850 μm peaks is ∼5″, consistent within the expected statistical uncertainties (see Section 6.4), with the star positioned equidistant between the two peaks. The upper limit to the radius from the 450 μm image of 18 au. Lawler et al. (2014) suggested that since no SED model can adequately fit both the *Herschel*/PACS and SCUBA/SCUBA-2 points, a separate, cooler disc component, may be required to explain the submillimetre observations. The SED shown in Fig. A2b is the best single fit to all the points beyond 70 μm, and results in a single-temperature component of 71 K (but with large errors of ± 23 K), a β constrained between 0 and 1.1, and implying a dust mass of 2.1 × 10^{-4} $M_\oplus$ surrounding the star, only approximately 20 times that of the Edgeworth-Kuiper belt (Greaves et al. 2004).

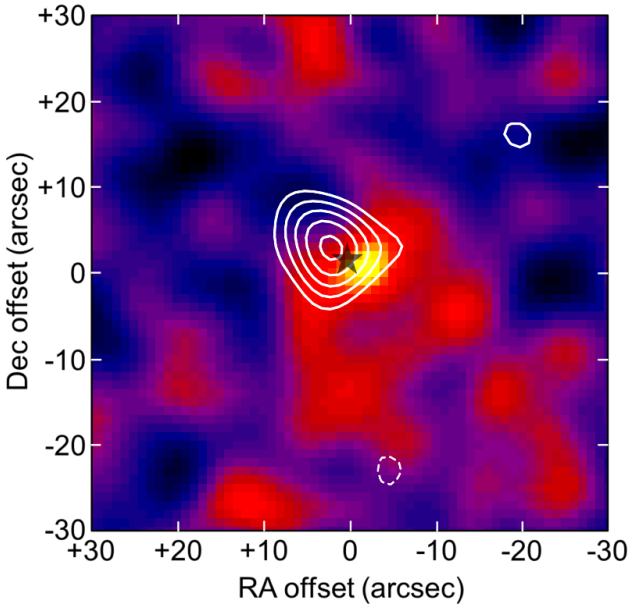

Figure 9. The 450 μm image from observations of τ Ceti (HD 10700) with contours from the 850 μm image overlaid. The contours and symbols are as described in Fig. 7.

5.7 HD 10638

HD 10638 is a luminous A3 star at a distance of 69 pc with an estimated age of 50 Myr, with lower and upper limits of 20 and 150 Myr Moór et al. (2006). Although the SONS survey image is somewhat uneven (i.e., there is a prominent gradient in the background towards the west), an emission peak is detected at 850 μm with a flux density of 5.1 ± 0.9 mJy (Fig. A2c) that is centred on the stellar position. As an unresolved disc about the star the upper limit to the radius is 515 au.

IRAS detected excess far-IR emission from the star (Silverstone 2000), but no other far-IR photometric measurements have been made. The SED is therefore loosely constrained by only the IRAS 60 μm and SONS 850 μm photometry, but the fit suggests a dominant cold component at 34 K but with a large uncertainty, a β value of >0.6, and an estimated dust mass of 0.18 $M_\oplus$. Modelling of the near-mid IR photometric points of the SED also hints at the presence of a warmer, inner component at 138 K.

5.8 β Trianguli (HD 13161)

HD 13161 (β Tri) is a spectroscopic binary (primary of spectral type A5-IV) at a distance of 39 pc, with a period of 31 days. It has an estimated age of 730 Myr with an uncertainty of ± 300 Myr (Vican 2012). The 850 μm image shows a peak in emission at the stellar position with a flux density of 5.1 ± 0.9 mJy (Fig. A2d). Interpreting this unresolved peak to be a disc about the star, gives an upper limit to the radius of 290 au.

The disc is well-characterised in the far-IR, particularly with *Herschel* contributing to points in the SED. *Herschel*/PACS observations at 70 μm reveal a deconvolved radius of 102 au at a PA of 66° (Booth et al. 2013). Modelling

of the *Herschel* images concluded that the disc is consistent with being aligned with the binary orbital plane (Kennedy et al. 2012). The SED is modelled as a single modified blackbody with a characteristic dust temperature of 84 K and a β in the range 0.6 to 1.7. The estimated dust mass is 0.022 $M_\oplus$.

5.9 γ Trianguli (HD 14055)

HD 14055 (γ Tri) has a spectral type A1 and is at a distance of 34 pc. It has an estimated age of 230 Myr with a lower and upper limits of 160 Myr (Thureau et al. 2014) and 300 Myr (Chen et al. 2014), respectively. The 850 µm image shows an emission morphology which peaks at an offset of 3″ from the star, and appears to be slightly elongated in the north-south direction. The peak flux is 7.2 ± 1.0 mJy/beam (Fig. A3a), a value slightly higher than previously reported (Panić et al. 2013). The integrated flux density, determined over a 40″ diameter aperture, however, reveals no significant evidence of extended emission compared to the beam. The flux is also consistent with that measured using SCUBA of 5.5 ± 1.8 mJy (Williams & Andrews 2006). There is no SCUBA-2 detection at 450 µm with the 5σ upper limit of 70 mJy being close to the predicted flux from the SED. Interpreting this structure as a disc about the star gives an upper limit to the disc radius from the 850 µm image of 260 au.

The disc has been resolved by *Herschel*/PACS observations at 70, 100 and 160 µm and interpreted as a fairly broad disc extending from a radius of 3.7 to 5″ (∼125 – 170 au), at a PA of 163° from the 160 µm image (Booth et al. 2013). Based on the *Herschel* results the north-south extension hinted at in the SONS 850 µm image could be real, although, as previously mentioned, the integrated flux measurement indicates that it is not statistically significant. The 850 µm SONS survey photometry helps to anchor the long-wavelength side of the SED, allowing a single blackbody fit with a dust temperature of 77 K, a β emissivity value of between 0.7 and 1.5, and an estimated dust mass of 0.028 $M_\oplus$.

5.10 HD 15115

HD 15115 is a young F2 star within the β Pictoris Moving Group at a distance of 45 pc, with an estimated age of 23 ± 3 Myr (Mamajek & Bell 2014). The 850 µm image shows a structure with a slightly elongated morphology (PA of ∼150°), with a peak in emission 5″ offset to the north from the star position (Fig. A3b). The flux density of 8.2 ± 1.1 mJy is marginally lower than that previously reported (Panić et al. 2013). The elongation is not significant compared to the beam size, and so interpreting the structure as an unresolved disc at the star gives an upper limit to the radius of 340 au.

HD 15115 has been observed in optical scattered light with images showing a remarkable asymmetry between the eastern and western sides of the disc (Kalas et al. 2007), with the western side reaching a radius of 12″ (∼550 au) from the star. The PA of the major axis of the disc from the scattered light image is 98.5°. Observations with the SMA at 1.3 mm resolved the HD 15115 disc into an asymmetric structure extending to the west of the star with a measured radius of 6″ (MacGregor et al. 2015). Modelling of the image suggests a well-defined emission belt at a radius of 110 au from the star, and a ∼3 σ feature aligned with the asymmetric western extension of the scattered light disc (MacGregor et al. 2015). A fit to the *Herschel*/PACS, 850 µm and 6.8 mm photometry from ACTA (MacGregor et al. 2016a) suggests a dominant cold disc of characteristic temperature 57 K, a β in the range 0.5 to 0.9, and an estimated dust mass of 0.073 $M_\oplus$.

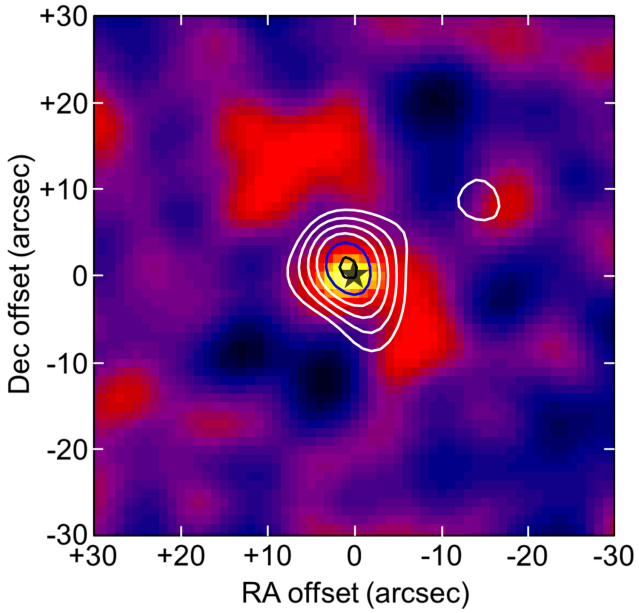

Figure 10. The 450 µm image from observations of HD 15257 with contours from the 850 µm image overlaid. The contours and symbols are as described in Fig. 7.

5.11 12 Trianguli (HD 15257)

HD 15257 (12 Tri) is an F0 star at a distance of 50 pc, with an estimated age of 1000 Myr (Chen et al. 2014). The 850 µm image reveals a well-detected emission peak with a flux density of 10.3 ± 1.2 mJy (Fig. A3c) well-centred on the star position. Emission is also detected at 450 µm in the SONS survey with a flux of 56 ± 11 mJy (∼ 5.1σ) as shown in Fig. 10. The emission is unresolved at both wavelengths, and interpreting the results as being a disc about the star gives an upper limit to the disc radius from the 450 µm image of 240 au.

IRAS detected excess far-IR emission from the star at 60 µm, but no other far-IR photometric measurements have been made. The SED is therefore sparsely sampled by only the *IRAS* and SONS 450 and 850 µm photometry leading to a poorly constrained value of β in the range 0 to 1.9. The SED is modelled by a two-component fit, the warm element of which has a dust temperature 161 K, based on a fit to the near/mid-IR photometric points from *AKARI* (Ishihara et al. 2010), *Spitzer* (Chen et al. 2014), and *WISE* (Wright et al. 2010). The dominant cold component is at 53 K, and the disc has an estimated dust mass of 0.11 $M_\oplus$.

5.12 HD 15745

HD 15745 is a young F2 star also in the β Pictoris Moving Group, lying at a distance of 64 pc with an estimated age

of 23 Myr (Mamajek & Bell 2014). The 850 μm image shows a well-detected, elongated structure with a peak flux of 8.4 ± 1.0 mJy/beam (Fig. A3d). The peak is offset to the south from the stellar position by ∼3″. Even though the star is at 64 pc, the structure appears to be marginally resolved with an integrated flux, as measured in a 50″ diameter aperture centred on the star, of 12.0 ± 1.4 mJy. The fitted radial extent of the structure gives a deconvolved radius of 8.1″ (∼510 au), suggesting the existence of a very large disc about the star at a PA of 164°.

In optical scattered light observations using the *HST*/ACS coronograph, the disc appears asymmetric about the star at a PA of ∼22.5°, with fan-shaped emission extending to 480 au in the region between position angles of 190 and 10° (Kalas et al. 2007b; Schneider et al. 2014). The scattered light emission seems to extend to a radius close to that seen in the SONS 850 μm image (∼8″; ∼510 au) but the orientation of the disc in the submillimetre does not show the same asymmetry as in scattered light. *Herschel*/PACS images at 70 and 160 μm show that the disc appears to be well-centred on the stellar position but there is little evidence of the extension seen in the 850 μm image (as shown in Fig. 11).

The SED is reasonably well-sampled in the mid-far IR from *IRAS* (Rhee et al. 2007), *Spitzer*/MIPS at 70 μm (Moór et al. 2011b), and *Herschel*/PACS (archival data) leading to a constraint on β between 0 and 0.9. The model fit through the photometric points yields a dust temperature of 89 K, leading to an estimated dust mass of 0.13 $M_\oplus$. The relatively high derived dust temperature means that the modelled disc radius, assuming that the grains behave as blackbodies, lies close to the star at only 18 au. Hence, there is a large discrepancy (factor of 28) in the modelled disc radius and that measured from the resolved image. This is further discussed in Section 6.2.

5.13 38 Arietis (HD 17093)

HD 17093 (38 Ari) is a luminous A7 star at a distance of 36 pc with an estimated age of 580 Myr (Vican 2012). The SONS survey 850 μm image was first reported by Panić et al. (2013) and shows a well-detected peak of flux density 8.8 ± 0.9 mJy, which is offset from the stellar position by 10″ (Fig. A4a). This offset is far in excess of what would be expected for a disc about the star, allowing for positional and statistical uncertainties in the measurement (see Section 6.4). It is therefore likely that the peak is due to a separate source, perhaps a background galaxy. This hypothesis is further supported by *Herschel*/PACS archival images showing significant 100 μm and 160 μm emission at the same offset position to the SCUBA-2 850 μm map (Panić et al. 2013). A fit to the far-IR photometric and submillimetre points (Fig. A4a) suggests an object with a very cold (∼14 K) dust temperature. The conclusion is that there is no current evidence for a debris disc surrounding HD 17093.

5.14 Algol (HD 19356, β Persei)

HD 19356 (Algol) is a triple-star system with the primary of spectral type B8-V, lying at a distance of 28 pc with an age estimated at 450 Myr, although it could be as young as 300 Myr (Rhee et al. 2007) or as old as 570 Myr (Söderhjelm et al. 1980). The bright primary (Algol/β Per Aa1) is eclipsed by the fainter secondary (Aa2; separation of 0.062 au) on a period of 2.9 days. The third star in the system (Ab) lies at a distance of 2.7 au from the primary. The SONS survey 850 μm image shows well-detected emission with a peak flux 6.4 ± 0.9 mJy/beam, centred on the stellar position (Fig. A4b). Although the morphology of the emission looks somewhat extended at 850 μm, the integrated flux, determined in a 30″ diameter aperture, is in good agreement to the peak value, suggesting the structure is unresolved. Given that all three stars lie within an area subtended by the telescope beam, it is impossible to ascertain which star is responsible for the excess flux at submillimetre wavelengths.

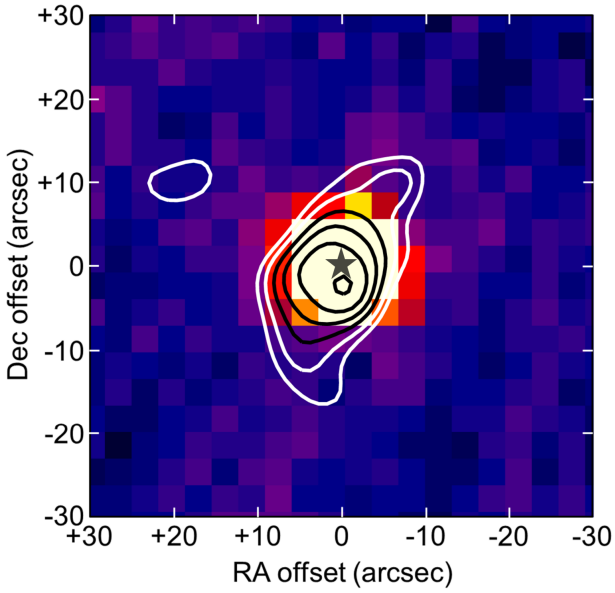

Figure 11. *Herschel*/PACS 160 μm image of HD 15745 with contours from the SONS survey 850 μm image overlaid. The contours are 3 and 4σ (white) and then 5 to 8σ (black). The star symbol represents the position of the star with respect to the flux peak. The *Herschel* image is taken from the *Herschel* Science Archive.

Although *Spitzer*/MIPS detected emission from Algol at 24 and 70 μm (Su et al. 2006), a modified blackbody fit to these points and the new SONS survey 850 μm flux is not possible. Multiple discs may be present, with an ultra-cold component dominating the emission at 850 μm. The SED model fit through the 850 μm point (Fig. A4b) is only indicative, as there are no other constraining points. Indeed, a cold disc component with a temperature of around 27 K could exist (noting a large uncertainty of ± 17 K in this temperature estimation). The estimated dust mass based on the 850 μm flux density is 0.045 $M_\oplus$. Algol Aa1 is ∼100 times more luminous than the Sun. Combined with a relatively low derived dust temperature, this high luminosity suggests the radius of a disc (assuming the grains behave as blackbodies) could be as large as ∼1100 au (again, with large uncertainties). This value compares to only 210 au based on the upper limit to the disc radius from the 850 μm image.

The emission from the Algol system is known to be

highly variable and of very high brightness temperature ($\sim 10^9$ K) (Lestrade et al. 1988). More specifically, it has been identified as gyro-synchrotron emission from mildly relativistic electrons accelerated by magnetic reconnections in its stellar chromosphere (as also known for the Sun and other stars). The spectrum of such emission peaks at a few centimetres, and may extend into the millimetre wavelength domain (Dulk 1985). The flux observed at 850 µm therefore might be such a tail, rather than thermal emission from a debris disc. The recently measured variability of the millimetre flux density observed at the SMA strengthens this interpretation (Wyatt/Wilner, *priv. comm.*).

There are, however, also a number of possible scenarios to explain the presence of cool debris around the star. First, a dust ring may surround at least one of the stars but companion perturbations in the system may cause it to be disrupted, hampering the formation of planets but allowing for the formation of enough planetesimals to generate significant debris material (e.g. Thebault & Haghighipour 2016). Second, a significant part of the emission may be related to mass loss from the secondary (and/or tertiary) to the primary, resulting in the presence of circumstellar material (Miller et al. 2006). Finally, there could be a mass outflow from the mass-gaining star, so the system loses angular momentum (the "non-conservative" problem) with the outflow, which then forms a shock as it encounters the interstellar medium (Deschamps et al. 2015). High angular resolution observations are needed to resolve the proposed structures and give further insight on the true nature of any "debris" surrounding Algol. Hence, although it may be possible for a debris disc to exist around Algol, evidence from longer wavelengths points to the emission at 850 µm being due to radio variability rather than a debris disc.

5.15 HD 21997

HD 21997 is a young A3 star in the Columba Moving Group, at a distance of 72 pc and an estimated age of 30 Myr (Torres et al. 2008) with an uncertainty for the group in the range 20 to 50 Myr (Marois et al. 2010). At 850 µm, the emission appears slightly elongated to the south at a PA of 25° with a peak flux of 7.9 ± 1.1 mJy/beam at the stellar position (Fig. A4c). The peak flux is also consistent with that measured using SCUBA photometry of 8.3 ± 2.3 mJy (Williams & Andrews 2006). The integrated flux density, measured over a 40″ diameter aperture, is 10.7 ± 1.5 mJy, suggesting that, even at a distance of 72 pc, the structure is marginally resolved. This extent, however, depends largely on the significance of the feature to the south within the 3σ contour. The fitted radial extent taking in this extension suggests that HD 21997 could be surrounded by an enormous disc of radius 810 au at a PA of 27°.

Herschel/PACS and SPIRE observations resolved the disc, identifying a structure with a radius of at least 2.8″(∼200 au) at a PA of ∼25° (Moór et al. 2015). The disc has also been resolved by ALMA at 886 µm revealing an inclined ring-like structure of radius ∼2.1″ (∼150 au) at a PA of 22.5° (Moór et al. 2013). Modelling of the morphology of the ring suggests inner and outer radii of ∼55 and ∼150 au, respectively. The measured flux from the ALMA image is 2.7 ± 0.3 mJy, considerably lower than previously measured at 850 µm, suggesting that some of the emission has been resolved out by the interferometric observations, and leading to a significant underestimate of the amount of dust present in the system. Such a hypothesis would be consistent with detectable emission extending beyond the outer radius of ∼150 au derived from ALMA, as indicated in the *Herschel* and 850 µm SONS observations (perhaps extending to ∼500 au or more).

HD 21997 is also one of the few systems with an age greater than 10 Myr that contains a detectable amount of cold CO gas (Moór et al. 2011a). The SED contains photometric points in the mid-far IR from *Spitzer*/MIPS and *Herschel*/PACS and SPIRE. The well-constrained fit through the photometric points, gives a dust temperature of 64 K, and a β of between 0.4 to 1.4. The estimated dust mass of 0.22 $M_\oplus$ is considerably higher than the value of 0.09 $M_\oplus$ reported based on the ALMA observations, due to the aforementioned larger flux.

5.16 ϵ Eridani (HD 22049)

ϵ Eridani (HD 22049) is a nearby K2 star at a distance of 3.2 pc with an estimated age of 850 Myr within a range spanning 800 Myr (Di Folco et al. 2004; Mamajek & Hillenband 2008) and 1.4 Gyr (Bonfanti et al. 2015). The SONS image at 850 µm reveals a well-resolved, largely circularly-symmetric, ring structure with considerably less emission at the stellar position (Fig. A4d). There appears to be significant sub-structure in the ring with the brightest clump to the south-east having a flux of 5.3 ± 0.7 mJy/beam. The integrated flux, measured within a 70″ diameter aperture centred on the star, is 31.3 ± 1.9 mJy. Both the peak clump flux and the total integrated flux agree well with the previous SCUBA observations (Greaves et al. 1998, 2005), although the latter is some 15% lower, but within the measured uncertainties. Interpreting the structure as a dust ring about the star, gives a deconvolved radius, based on the Gaussian fit to the 850 µm image, of 20.8″ (∼67 au). The inclination angle to the plane of the sky is estimated to be 26° also consistent with the SCUBA results. The image at 450 µm only shows clumps with low S/N (∼3–5σ), but nevertheless suggests a ring structure that is not inconsistent with the results at 850 µm (Fig. 12). The integrated flux, within a 70″ diameter aperture, is 181 ± 15 mJy, which compares to 250 ± 20 mJy determined by Greaves et al. (2005). Significantly more integration time is ideally needed to improve upon the 450 µm results.

Given its age and close proximity to the Sun in both distance and spectral type, the ϵ Eridani dust ring has been widely studied at multiple wavelengths. The original 850 µm SCUBA image from 1998 first revealed the ring-like structure, peaking at a radius of 60 au from the star and with an estimated dust mass of at least 0.01 $M_\oplus$ (Greaves et al. 1998). It was concluded that the ring structure was probably akin to the Edgeworth-Kuiper belt in our Solar System with a central region partially cleared of dust by forming planetesimals. Further deep imaging with SCUBA over the period 1999 – 2004 confirmed the dust ring morphology as well as producing the first image of the structure at 450 µm (Greaves et al. 2005). The latter work also presented tentative evidence that two clumps in the ring were following the

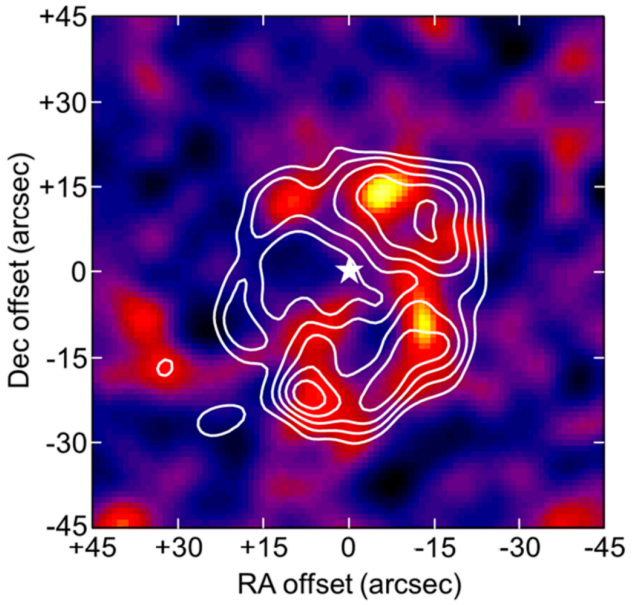

Figure 12. The 450 µm image from observations of ϵ Eridani (HD 22049) with contours from the 850 µm image overlaid. The contours and symbols are as described in Fig. 7.

stellar motion (i.e. were not background objects) and furthermore showed evidence of counter-clockwise rotation. It was suggested that the structure in the ring could be caused by perturbations of a planet orbiting the star at a few tens of AU, and led to the speculation that the ϵ Eridani system could resemble an early version of our Solar System.

Far-infrared observations with *Spitzer* indicated the likely presence of two unresolved warm, inner dust rings, in addition to a wider, icy outer belt (Backman et al. 2009). The inner belt lies at a radius of around 3 au, very similar to the distance of the Asteroid belt in the Solar System. There is also at least one candidate Jupiter-mass planet (ϵ Eri b) in the system believed to lie just outside of this belt at a orbital radius of 3.5 au, discovered using the radial-velocity (RV) technique (Hatzes et al. 2000). Astrometric observations also provide evidence for the existence of a planet and allow its inclination to be determined (Benedict et al. 2006; Reffert & Quirrenbach 2011). Although the planet's orbit appears to be inclined at a similar angle (∼30°) to the disc, the inclination is in a very different direction, meaning the disc and planetary orbit are not likely coplanar. The planet has also proven somewhat controversial as extensive followup RV observations have so far failed to confirm its existence (Zechmeister et al. 2011). *Herschel* observations at 160 µm to 350 µm resolved two belts of debris emission. The inner belt has a radius of 12 – 16 au, whilst the outer cold belt orbited the star at a radius of 54 – 68 au Greaves et al. (2014). There has also been considerable speculation about the existence of a planet orbiting at a distance close to the outer dust belt. The brightness asymmetry between the north and south ends of the belt from the *Herschel* observations indicates a pericentre glow that could be attributable to such a planet.

The clumpy structure of the observed disc was presented as evidence that dynamical interaction between an unseen planetary companion and the debris belt (Quillen & Thorndike 2002). Millimetre-wave observations with MAMBO-2 on the IRAM 30 m telescope at 1.2 mm also confirmed the clumpy structure seen in the submillimetre images (Lestrade & Thilliez 2015). However, other observations, most notably millimetre-wave observations using the bolometer array SIMBA on SEST (Schütz et al. 2004) and the SMA interferometer (MacGregor et al. 2015) did not confirm the presence of significant substructure within the ring. More recently, the AzTEC camera on the 50 m Large Millimeter Telescope imaged the ϵ Eridani dust belt reaching an RMS noise level of 0.12 mJy at 1.1 mm (Chavez-Dagostino et al. 2016). The measured radius for the outer belt of 64 au agrees well with other measurements, and although there are some inhomogeneities, the observed structure indicates a morphology that is essentially smooth. The deep LMT image also highlights the presence of numerous point-like sources, with the likelihood, based on the near 20 years of observations (and noting the large stellar proper motion of $1''\mathrm{yr}^{-1}$), that at least one of the original submillimetre clumps within the ring is likely to be a background source. The northern arc of the ring has also been imaged by ALMA at a wavelength of 1.3 mm, revealing tentative evidence of the presence of a clumpy structure in the ring (Booth et al. 2017). The ring is very narrow at just 11 – 13 au, making the fractional disc width comparable with the Edgeworth-Kuiper belt in our Solar System.

The SED is well-sampled in the far-IR through to the millimetre. There is somewhat of a discrepancy in the total disc flux between the recent millimetre-wave observations (IRAM/MAMBO-2 and the LMT/AzTec) and a fit to the *Spitzer*, *Herschel*, SCUBA, SCUBA-2 and the original IRAM photometry as shown in the SED in Fig. A4d. The reason for this is unclear, but may be very dependent on the precision of the aperture photometry with respect to the ring and the presence of background sources. Modelling of the SED suggests a two component fit to the overall IR excess consistent with the results from *Spitzer* and the resolved imaging from *Herschel*. The fit to the warmer, inner component suggests the existence of an "asteroid belt" at an orbital radius of ∼14 au with a characteristic temperature of 133 K. The colder component is the more familiar outer ring from the submillimetre observations at a radius of ∼ 60 au, modelled as a disc/belt with a dust temperature 44 K, and a β value in the range of 0.6 to 1.0, with an estimated dust mass of only 0.002 $\mathrm{M}_{\oplus}$ calculated from the 850 µm flux. The derived dust temperature for the cold disc is also in good agreement with previous estimates (Greaves et al. 1998, 2005). The equivalent disc radius, assuming blackbody emission, is 23 au, this being significantly lower than the value measured from the 850 µm image of 67 au.

5.17 HD 22179

HD 22179 is a young G5 star, at a distance of 16 pc and an estimated age of only 16 Myr (Carpenter et al. 2009). At 850 µm, there is a bright emission peak with a flux density of 7.0 ± 1.3 mJy, located 18″ from the stellar position to the south west (Fig. A5a). Given the large offset it is unlikely that the peak is associated with a putative disc around the

star, and is probably a background object. At far-IR wavelengths *Spitzer* detected excess flux from the star at 70 μm (just over 3σ), but no detection was made in the longer wavelength 160 μm channel (Hillenbrand et al. 2008). Photometry shortward of 24 μm indicated clear evidence of a flux excess, but it is also possible that *Spitzer* detected the same offset peak seen in the SONS 850 μm image. Hence, there is some uncertainty as to whether a debris disc does exist around HD 22179.

5.18 HD 25457

HD 25457 is a F6 star in the AB Doradus Moving Group, at a distance of 19 pc with a somewhat controversial age but generally accepted to be very similar to the Pleiades at 130 +/- 20 Myr (Barrado y Navascués et al. 2004). The SONS image at 850 μm shows an unresolved peak of flux density 6.4 ± 1.4 mJy, offset from the stellar position by 2″(Fig. A5b). Interpreting the peak as an unresolved disc associated with the star, gives an upper limit for the disc radius of 140 au. The 850 μm image shows some unevenness, with ridges of excess flux towards the east and corresponding negative features in the west.

Spitzer detected excess flux from the star at wavelengths between 3.6 μm and 160 μm (Hillenbrand et al. 2008). Although there have been several observations of the star in the submillimetre and millimetre, the SONS 850 μm image is the only clear detection of a disc at such long wavelengths. Modelling of the SED suggests a two component fit to the overall IR excess consistent with the results from *Spitzer* and the imaging from SONS. The fit to the warmer component, dominated by the near-mid IR photometry, gives a characteristic temperature of 124 K. The colder component has a dust temperature of 50 K, a β value only loosely defined as >0.1, and an estimated dust mass of 0.011 $M_\oplus$ derived from the 850 μm flux.

5.19 HD 35841

HD 35841 is a young F3 star, also in the Columba Moving Group, at a distance of 96 pc with an estimated age of 30 Myr. The SONS survey image at 850 μm reveals several peaks in the vicinity of the star, including a faint 4σ peak offset from the star by ∼5″ to the south, with a flux density of 3.5 ± 0.8 mJy (Fig. A5c). To the south-west, some 23″ offset, is another peak with a flux of 3.1 ± 0.8 mJy and a low-level (∼2.5σ) ridge running between the two that extends to the north-east of the star. If the peak just to the south is an unresolved disc associated with the star, then the upper limit for the disc radius is 725 au.

The disc has been detected in scattered light via *HST*/NICMOS observations that show a very compact, nearly edge-on disc with a radius of 1.5″ (∼144 au) from the star (Soummer et al. 2014). The two lobes are not diametrically aligned with position angles of ∼180 and ∼335°. Only *Spitzer*/MIPS photometry at 24 and 70 μm (Chen et al. 2014) contributes to an otherwise poorly constrained SED. A fit to the SED, assuming the peak detected at 850 μm is representative of a disc about the star, gives a dust temperature of 71 K, a β value very loosely constrained in the range 0 to 2.7, and an estimated dust mass of 0.11 $M_\oplus$.

5.20 HD 38858

HD 38858 is a nearby (15 pc) Sun-like star of spectral type G4, hosting a super-Earth planet within 1 AU, with a highly uncertain stellar age usually adopted as being 4700 Myr (Beichman et al. 2006), but likely to be in the range of 3200 Myr (Chen et al. 2014) to 6200 Myr (Vican 2012). The SONS observation at 850 μm (Fig. A5d) reveals a large extended structure with an integrated flux density, measured in a 60″ diameter aperture, of 11.5 ± 1.3 mJy (Kennedy et al. 2015). In terms of the interpretation of the image, the peak is clearly offset from the star position by 9″ to the east, although there is still significant emission at the star position itself (∼5 mJy/beam). One possibility is that the extended structure to the south-east is a separate background source.

Herschel/PACS observations at 70 μm reveal a disc of radius 7.5″ (∼110 au) at a PA of 67°, which is well-centred at the stellar position (Kennedy et al. 2015), and similar to the results reported by *Spitzer*/MIPS (Krist et al. 2012). Observations at 160 μm, however, reveal a separate source to the south, coincident with the peak flux of the 850 μm extension. Hence, there is a strong likelihood that this source is a background object (perhaps a high redshift galaxy given the absence of such a source at 70 μm), and therefore the remainder of the discussion on this target assumes this to be the case. Finally, the image is also likely "contaminated" at some level by the Orion Complex background emission to the east of the star (Kennedy et al. 2015).

By constructing models of the HD 38858 disc it is possible to estimate the likely contribution to the true disc flux at 7.5 ± 1.5 mJy, taking into account the background contamination and assuming the southern peak is not associated with a disc (Kennedy et al. 2015). This interpretation still assumes that the flux peak is at a distance of 9″ from the star. With this single long wavelength point, the disc spectrum is now close to a pure blackbody with β around zero. A fit to the SED gives a characteristic dust temperature of 50 K and an estimated dust mass of 0.0086 $M_\oplus$.

The radius of the disc, derived from the SED fit and assuming blackbody grain properties, is only 28 au. This value is significantly smaller than the measured deconvolved radius of the disc of 12.7″ (∼190 au) at a PA of 75°(determined after subtracting a point-source at the location of the southern peak). Such a result is surprising given the requirement of a nearly pure blackbody spectrum fit to the SED (as described above), which would imply that the blackbody and resolved disc sizes should be in agreement, i.e., the disc material should lie at a single radius from the star. Blackbody spectra have been seen for other discs at larger radii than their blackbody temperatures would suggest. An example is AU Mic (Matthews et al. 2015) where it is likely that the submillimetre observations trace the parent-body distribution (which may have blackbody properties), whilst the far-IR data sample a halo of smaller grains from highly eccentric orbits due to radiation pressure. In summary, the SONS 850 μm image of HD 38858 is interpreted as a resolved disc, with a peak flux offset from the star position by 9″ and with the presence of a background object contaminating the observed structure to the south.

5.21 56 Aurigae (HD 48682)

HD 48682 (56 Aur) is an old F9 star, at a distance of 17 pc with an estimated age of around 6000 Myr (Barry 1988), though could be as young as 3200 Myr (Holmberg et al. 2009) or as old as 8900 Myr (Beichman et al. 2006). The field at 850 μm shows faint multiple peaks, of which the nearest to the star has a flux of 2.7 ± 0.6 mJy/beam (Fig. A6a). The peak is offset by 6.5″ from the star, significantly greater than the maximum offset of 3.7″ expected due to statistical and positional uncertainties (Section 6.4). The structure near the star could also be marginally extended compared to the beam, mainly in the east-west direction, and has an integrated flux density (in a 30″ diameter aperture) of 3.9 ± 0.8 mJy. Interpreting the structure nearest the star to be a disc, the radial fitting gives a deconvolved disc radius of 11″ (∼184 au) at a PA of 94°, which is larger than the estimated radius of 57 au based on the assumption of pure blackbody emission from grains (see discussion in Section 6.3).

Observations with *Herschel*/PACS at 100 μm reveal an elongated disc with a measured deconvolved radius 16.4″ (∼280 au) at a PA of 107° (Eiroa et al. 2013; Pawellek et al. 2014) approximately 50% larger than the estimate from the SONS 850 μm image. The peak to the SW is not considered to be associated with this main disc. A fit to the SED, mainly sampled by *Herschel* photometry, and including the 850 μm SONS flux, gives a dust temperature of 43 K and a β in the range 0.7 to 1.8, leading to an estimated dust mass of 0.0062 $M_\oplus$.

5.22 HD 61005 ("The Moth")

HD 61005 is a G8 star and a possible member of the Argus Association, at a distance of 35 pc with an estimated age of 40 Myr (Desidera et al. 2011), although other estimates include 100 Myr (Hillenbrand et al. 2008) and in the range of range of 72 Myr to 186 Myr (Desidera et al. 2011). The 850 μm image shows emission peaking just offset from the stellar position and extending somewhat to the south-east, with a flux density of 13.5 ± 2.0 mJy (Fig. A6b). The elongation is not significant compared to the beam size, however, and interpreting the structure as a disc about the star gives an upper limit to the disc radius of 265 au.

The disc has been studied in detail at many wavelengths and results include the fan-like scattered light observation that led to the nickname of "The Moth" (Hines et al. 2007). Observations with the SMA first resolved the disc at millimetre wavelengths, revealing a double-peaked structure, viewed close to edge-on, with a measured major axis radius of 2.2″ (∼80 au) at a PA of 71° (Ricarte et al. 2013). ALMA observations at 1.3 mm also resolve the disc into a highly-inclined ($i \sim 85°$) structure with the emission peaking at a radius of 1.5″ (∼55 au) from the star, with the disc having a PA of 71° (Olofsson et al. 2016). Although the disc was not detected at 450 μm in the SONS survey, the SED is further well-constrained in the mid-far IR with photometry from both *Spitzer*/MIPS (Chen et al. 2014) and *Herschel*/PACS (Morales et al. 2016), and in the millimetre by photometry at 9 mm from the VLA (MacGregor et al. 2016a). The fit to the SED gives a characteristic dust temperature of 61 K, and a β value tightly constrained within the range 0.4 – 0.7. The calculated dust mass from the 850 μm flux is 0.069 $M_\oplus$.

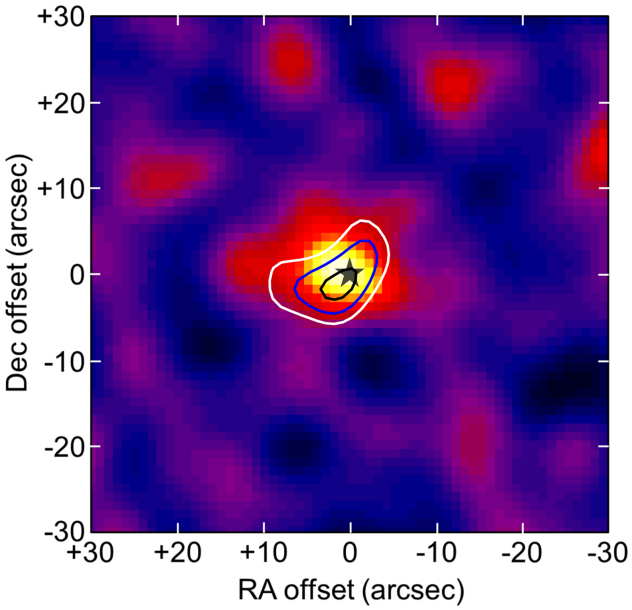

Figure 13. The 450 μm image from observations of GJ 322 with contours from the 850 μm image overlaid. The contours and symbols are as described in Fig. 7.

5.23 GJ 322

GJ 322 is a K5 star in the Ursa Major Moving Group, at a distance of 16.5 pc with an estimated age of 490 ± 100 Myr (Jones et al. 2015). The SONS survey results show an unresolved peak, well-centred on the stellar position, at both 450 μm and 850 μm with flux densities of 57 ± 11 mJy and 7.3 ± 1.4 mJy, respectively (Fig. A6c and Fig. 13). Interpreting the peak to be a disc about the star gives an upper limit to disc radius of 85 au based on the 450 μm image. The SED, however, is poorly constrained in the mid-far IR with only *Spitzer*/MIPS photometry at 70 μm (Chen et al. 2014), which together with the steep spectral slope between 450 and 850 μm leads to unconstrained values of both λ_0 and β. A fit to the SED gives a characteristic dust temperature of 24 K (but with a large error of ± 10 K), and a derived dust mass of 0.021 $M_\oplus$. The disc radius from the SED fit is also poorly estimated at 43 ± 24 au, assuming emission from pure blackbody grains.

5.24 63 Cancri (HD 76582)

HD 76582 (63 Cnc) is a moderately old F0 star, at a distance of 46 pc with an estimated age of 540 Myr (Moór et al. 2006) and a likely age in the range 300 Myr to 2130 Myr (Zorec & Royer 2002). The SONS survey observations show unresolved emission at both 450 and 850 μm at the stellar position, with peak fluxes of 89 ± 17 and 5.7 ± 1.0 mJy/beam, respectively (Fig. A6d and Fig. 14). The 450 μm flux estimate is based on a re-analyis of the data, and is slightly lower than previously published (Marshall et al. 2016). The 450 μm image looks slightly extended in a roughly east-west direction, but aperture photometry reveals an integrated flux density that is not significant higher than the peak value. Based on the 450 μm image, and interpreting

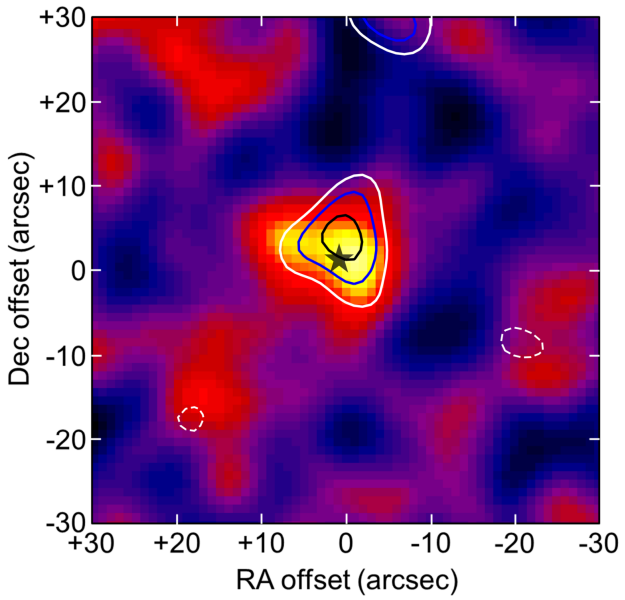

Figure 14. The 450 μm image from observations of HD 76582 (63 Cnc) with contours from the 850 μm image overlaid. The contours and symbols are as described in Fig. 7.

the structure as a disc about the star, gives an upper limit to the radius of the disc of 230 au.

The disc was originally detected by *IRAS* and has been well-characterised in the mid-far infrared (Zuckerman & Song 2004; Moór et al. 2006). The disc has also been resolved by *Herschel*/PACS, giving a radius of 5.9″ (∼ 271 au) at a PA of 103° for the 100 μm image, and 8.5″ (∼ 390 au) at a PA of 115°at 160 μm (Marshall et al. 2016). The disc is inclined at 64° to the plane of the sky (Marshall et al. 2016). Based on these measurements, it is possible that the disc might be marginally resolved at 450 μm (even though the integrated flux suggests otherwise). At least a two-component, modified, blackbody model is needed to fit the photometric points from the near-IR to the submillimetre in the SED. The inner component, based on a fit to the near-mid IR photometry, has an estimated dust temperature of 157 ± 31 K. The relative sparse coverage at far-IR and submillimetre wavelengths, coupled with the steep spectral slope between 450 and 850 μm, means that both λ_0 and β are poorly constrained by the modelling. A fit to the long wavelength photometric points gives a characteristic dust temperature of 52 K, and a lower limit on β of 1.1. The estimated dust mass from the 850 μm flux is 0.057 $M_\oplus$. Marshall et al. 2016 also suggest that there could actually be three distinct components to the disc, a warm inner element that fits the near-mid IR photometry (radius of ∼20 au) and two annuli for the far-IR and submillimetre points (with radii of ∼80 au and ∼270 au).

5.25 HD 84870

HD 84870 is a luminous A3 star at a distance of 88 pc with an estimated age of 100 Myr (Rhee et al. 2007). At 850 μm, the emission peaks on the stellar position with a flux density of 6.2 ± 1.0 mJy (Fig. A7a). There are a couple of lower S/N peaks also in the vicinity which are most likely background sources. Interpreting the emission as a disc about the star gives an upper limit to the disc radius from the 850 μm image of 660 au.

The infrared excess was originally detected by *IRAS* (Rhee et al. 2007). The disc has recently been resolved by *Herschel*/PACS revealing a ring-like structure in the star-subtracted 100 μm image (Vican et al. 2016). Modelling of the disc indicates that the dust extends to a radius of 252 au from the star at a PA of 147°. The disc was not detected at 450 μm but a fit to the other SED points gives a dust temperature of 50 K, and constrains β in the range of 0.3 to 1.2. The estimated dust mass is 0.24 $M_\oplus$. There is also evidence for a warmer disc component at 146 K, based on a fit to the near-mid IR data from *AKARI* (Ishihara et al. 2010), *Spitzer* (Chen et al. 2014), and *WISE* (Wright et al. 2010).

5.26 CE Antliae (TWA 7, 2MASS J10423011−3340162)

CE Ant (TWA 7) is an M2 dwarf star in the TW Hydrae Association, with an estimated age of 9 Myr in a range spanning 3 Myr to 20 Myr (Barrado y Navascués 2006). The distance of the star is uncertain but is likely to be similar to other members of the association (∼50 pc). The 850 μm image shows a clear, unresolved dust emission peak that is offset by approximately 6″ to the east of the star (Fig. A7b). The offset is greater than the 3.3″ expected due to statistical and positional uncertainties (see Section 6.4). The peak has a flux density of 7.2 ± 1.3 mJy, consistent with the measurement made by SCUBA at 850 μm, of 9.7 ± 1.6 mJy (Matthews et al. 2007). The SCUBA measurement was carried out using photometry mode (Holland et al. 1999), and hence it is not possible to ascertain whether there was also an offset associated with that particular observation. Interpreting the structure as a disc about the star gives an upper limit to the radius from the 850 μm image of 380 au.

HST/NICMOS imaging of the scattered light reveals an inclined disc extending to a radius of 1″ (∼35 au) at a PA of 53° (Choquet et al. 2016). Modelling suggests the observed structure is more likely to be a ring rather than a continuous disc. *Herschel*/PACS observations at 70 μm resolve the disc with a deconvolved radius of 6.2″ (∼210 au) (Cieza et al. 2013). The *Herschel*/PACS image shows that the disc is reasonably well-aligned to the the stellar position, unlike the case for the SONS 850 μm result (see Fig. 15). It is therefore possible that the peak seen at 850 μm could be a background object, rather than a debris disc associated with CE Ant, although there is no evidence from *Herschel* observations that such an object exists at this position.

The SED contains both *Spitzer*/MIPS (Low et al. 2005) and *Herschel* photometry (Cieza et al. 2013) and is best fitted with two modified blackbodies, consistent with a previous analysis (Riviere-Marichalar et al. 2013). The first blackbody fits the photometric points shortward of ∼100 μm with a dust temperature of 81 K and suggests an inner disc at a radius of 2.5 au. Assuming the observed structure at 850 μm is a real disc associated with CE Ant, a second blackbody fit to the long-wavelength submillimetre photometry indicates

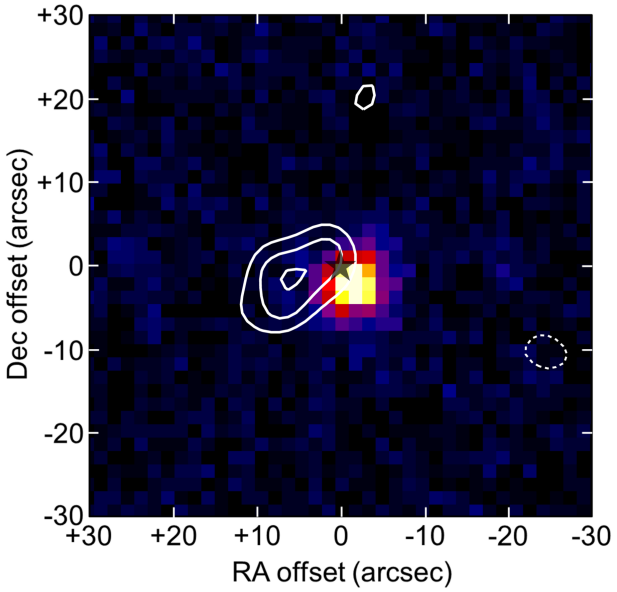

Figure 15. *Herschel*/PACS 70 µm image of CE Ant (TWA 7) with the SONS survey 850 µm contours overlaid. The contours start at 3σ and increase in 1σ steps. The *Herschel* image is taken from the *Herschel* Science Archive.

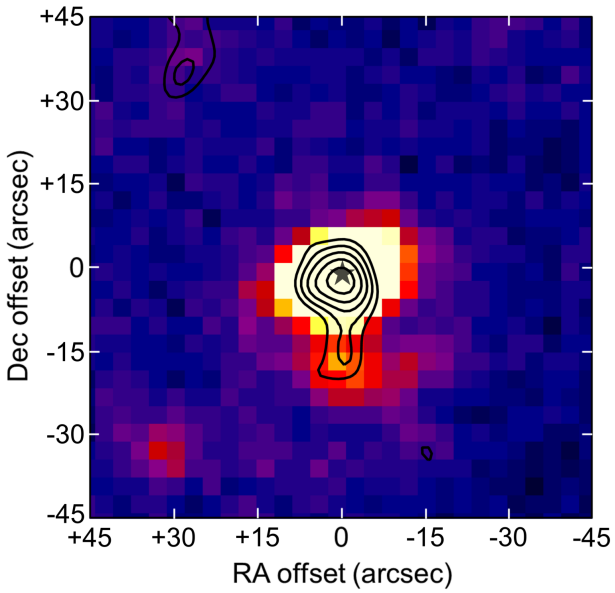

Figure 16. *Herschel*/PACS 160 µm image of HD 92945 with the SONS survey 850 µm contours overlaid. The contours start at 3σ and increase in 1σ steps. The *Herschel* image is taken from the *Herschel* Science Archive.

the presence of a very cold structure, with a dust temperature of 19 K, orbiting at a mean radius of 49 au, assuming the dust grains have pure blackbody emission (both of which have large uncertainties, as indicated in Table 3). The value of β is unconstrained due to the sparse photometric coverage, and lies in the range of 0 to 2.5, whilst the estimated dust mass is 0.24 $M_\oplus$.

5.27 HD 92945 (V419 Hya)

HD 92945 is a K1 dwarf star at a distance of 21 pc with an estimated age of 200 Myr, lying between the lower and upper estimates of 100 Myr and 300 Myr (Song et al. 2004; Chen et al. 2014), respectively. The 850 µm SONS survey image shows a structure where the emission peaks at the stellar position, but with an apparent asymmetric extension to the south (Fig. A7c). The peak flux is 8.6 ± 1.1 mJy/beam, that being consistent with the previously published result (Panić et al. 2013). The integrated flux, measured over an aperture of 40″ diameter, is 12.6 ± 1.5 mJy confirming that the structure is resolved, if the extension to the south is really associated with a disc about the star. From the 850 µm image, the measured deconvolved disc radius from the 2D Gaussian fitting is 11″ (∼210 au) in the major axis at a PA of 178°, i.e. dominated by the north-south extension.

The disc has been imaged in scattered light using *HST*/ACS, revealing an inclined, axisymmetric structure with an inner ring of radius 2 −3″ (∼43 − 65 au) from the star and an outer disc declining in brightness to 5″ (∼110 au) roughly oriented east-west (Golimowski et al. 2011). *Herschel*/PACS imaging at 70 and 160 µm reveal an extension (or possible second source) to the south, coincident with that seen in the 850 µm image (Fig. 16). Given the asymmetric nature of the extension, it is more likely that this feature is caused by a background object, and is not part of a disc (see Section 6.5). In this scenario, the peak flux of 8.6 ± 1.1 mJy/beam, and an upper limit to the disc radius of 160 au, are better estimates to be adopted for a disc about the star. The SED contains both *Spitzer*/MIPS (Golimowski et al. 2011) and *Herschel*/PACS photometry (archival data), and using the 850 µm peak flux, is well-fitted by a single temperature modified blackbody with a dust temperature of 42 K, a β in the range 0.4 to 1.1, and a dust mass of 0.024 $M_\oplus$.

5.28 HD 98800

HD 98800 is a pre-main-sequence K5 dwarf star in the TW Hydrae association, at a distance of 50 pc with an estimated age of 9 Myr (Barrado y Navascués 2006). HD 98800 is actually a quadruple star system, containing a pair of spectroscopic binary stars (HD 98800A and B, separated by ∼36 au) and in which only HD 98800B harbours a circumstellar disc (Torres et al. 1995; Koerner et al. 2000). Together with Fomalhaut Section 3.3, the 850 µm image represents by far the brightest disc in the SONS survey with a flux density of 94 ± 1.5 mJy (Fig. A7d). The disc is also well-detected at 450 µm, revealing an unresolved disc with a flux density of 242 ± 14 mJy. The upper limit to the disc radius from the 450 µm image is 255 au.

The HD 98800B disc has been resolved by the SMA revealing that it is closely aligned with the orbit of the spectroscopic binary (HD 98800A), and extends to a radius of only 10–15 au from HD 98800B at a PA of 158° (Andrews et al. 2010). The disc has a fractional luminosity of ∼0.1 and so is outside the generally accepted range for a debris disc

(see Section 4.4). Indeed, it is commonly referred to as a "transitional disc", i.e., a disc evolving between the younger protoplanetary and the older debris phases. The SED in the infrared is well-characterised by *WISE* (Wright et al. 2010), *AKARI* (Ishihara et al. 2010) and *Spitzer*/MIPS photometry (Chen et al. 2014). In the submillimetre, the photometry has considerable more scatter, with seemingly low flux estimates at 870 µm from APEX/LABOCA (a 4σ detection; Nilsson et al. 2010) and 1.3 mm from JCMT/UKT14 (also a 4σ detection; Sylvester et al. 1996), compared to the SED fit. The near blackbody fit suggests a dust temperature of 156 K, a well-constrained value of β in the range 0.0 to 0.1, and an estimated dust mass of 0.37 $M_\oplus$.

5.29 HD 104860

HD 104860 is a F8 star located at a distance of 46 pc with an estimated age of 200 Myr (Morales et al. 2013). The 850 µm image (Fig. A8a) shows a structure in which the peak emission is well-centred on the stellar position. The peak flux density is 6.5 ± 1.0 mJy/beam, in good agreement with previous SCUBA flux estimates (Najita & Williams 2005). The integrated flux, measured in a 50″ diameter aperture centred on the star, is 8.7 ± 1.4 mJy, indicating the overall structure could be marginally resolved. Another possibility, however, given the asymmetry of the structure, is that the 4σ peak to the east may be a background object. Interpreting the emission as that from a disc gives an upper limit to the radius from the 850 µm image of 340 au (assuming an unresolved structure).

The disc has been resolved by *Herschel*/PACS, with the modelled image at 160 µm suggesting a slightly elongated disc of radius 3.5″ (∼166 au) from the star at a PA of 12° (Morales et al. 2013). There is also a hint of a slight eastward extension to the image at 160 µm, which is coincident with the second peak seen in the 850 µm image, perhaps supporting the hypothesis that this is a background object. The disc also been resolved by the SMA at 1.3 mm, revealing a disc with a peak in emission at a radius of 2.5″ (∼110 au) and elongated at a PA roughly in a north-south direction (Steele et al. 2016). The SMA images, however, show no signs of a second source to the east. The SED in the infrared is well characterised by *Spitzer*/MIPS (Hillenbrand et al. 2008), in the far-IR by *Herschel*/PACS (Morales et al. 2013), CSO and IRAM (Roccatagliata et al. 2009) in the submillimetre/near-millimetre, and the VLA at 9 mm (MacGregor et al. 2016a). In fitting the SED it has been assumed that the flux at 850 µm is best represented by the peak value, giving a dust temperature of 47 K, a β index in the range of 0.4 to 1.2, and an estimated dust mass of 0.071 $M_\oplus$.

5.30 HD 107146

HD 107146 is a young solar analogue star (G2V) located at a distance of 28.5 pc with an estimated age of 100 Myr (Chen et al. 2014), although it could be as young as 30 Myr (Williams et al. 2004). The 850 µm image (Fig. A8b) reveals a bright structure, with a peak flux of 20.6 ± 2.1 mJy/beam slightly offset by ∼4″ from the star. The structure appears slightly extended to the south-west, although the integrated flux, measured over a 40″ diameter aperture, indicates that this feature is not significant compared to the peak flux value. Interpreted as a disc the upper limit to the radius from the 850 µm image is 210 au. The measurement is in excellent agreement with the previous SCUBA measurement of 20 ± 4 mJy, and the disc was also resolved by SCUBA at 450 µm with a deconvolved radius of 150 au from the star at a PA of 155° (Williams et al. 2004).

The disc was first detected in scattered light using *HST*/ACS, showing a circularly-symmetric structure with maximum opacity occurring at 130 au, with a PA of ∼160° and inclined at 25° to the plane of the sky (Ardila et al. 2004). The scattered light images also reveal an object ∼7″ south-west of the star, which was identified as a spiral galaxy. In the nine years between the *HST* and SCUBA-2 observations, the proper motion of the star means that the separation to the galaxy is now 5″. Hence, it is possible that the SONS survey image at 850 µm is contaminated by the presence of a background galaxy causing the apparent extension to the disc.

SMA observations at 880 µm show that the emission is distributed in a ring of radius 3.5″ from the star, and this emission is modelled with inner and outer radii of 50 and 170 au with a disc PA of 148° (Hughes et al. 2011). The total flux measured by the SMA was 36 ± 1 mJy, significantly higher than the SONS result at 850 µm. Given the 5″ separation between the star and the galaxy, it is possible that the total SMA emission also contains flux from the background source. Similarly, with ALMA at 1.3 mm the disc is seen extending from 30 to 150 au at a PA of 144°, whilst models suggest a clear decrease in the dust emission at a radius of ∼80 au extending over a width of 9 au (Ricci et al. 2015a). The total flux density for the disc of 12.5 ± 1.3 mJy from the ALMA observations may also be contaminated by flux from the nearby galaxy. Given that the star is a young Solar analogue, the disc could be a larger version of the Edgeworth-Kuiper belt in our Solar System (Ricci et al. 2015a).

The emission from the disc is well-sampled in the infrared through millimetre region, including measurements from *Spitzer*/MIPS (Chen et al. 2014), *Herschel*/PACS (Morales et al. 2016), CSO (Corder et al. 2009), OVRO (Carpenter et al. 2005) and ACTA (Ricci et al. 2015b). The fit to the SED, using the peak flux at 850 µm, tightly constrains β to a value of between 0.8 and 1.0 and gives a dust temperature of 41 K, leading to an estimated dust mass of 0.093 $M_\oplus$. The fit to the SED at near-mid IR wavelengths also suggests an inner, "warm" component radiating at 81 K.

5.31 η Corvi (HD 109085)

η Crv (HD 109085) is a nearby F2 star located at a distance of 18 pc with an estimated age of 1380 Myr (Chen et al. 2014) in a range of 1000 Myr to 2000 Myr (Vican 2012). The images and fluxes presented in this paper are slightly updated versions of those first published by Duchêne et al. (2014) following a re-analysis of the data. The 850 µm image (Fig. A8c) shows emission peaking with a flux of 7.2 ± 0.7 mJy/beam. The integrated flux density of 15.4 ± 1.1 mJy, measured in a 40″ diameter aperture centred on the star, in good agreement with previous SCUBA flux estimates (Wyatt et al. 2005). Interpreting the emission as a disc about the star gives

deconvolved major and minor axis radii of 10.4 and 7.5″ (190 and 135 au), respectively, at a PA of 132° and inclined to the plane of the sky by 44°. The SONS survey image at 450 μm is low S/N due to the relatively poor weather conditions at the time of the observations, but shows the disc is resolved into the two prominent clumps seen previously (Wyatt et al. 2005) albeit only at the ∼4σ significance level (Fig. 17).

The first infrared excess flux measurements of η Crv were made by *IRAS* (Stencel & Backman 1991), and the disc has been observed at many wavelengths over the past two decades. SCUBA observations at 450 μm resolved the disc for the first time revealing a ring-like structure oriented at PA of 130° with model fits indicating a disc inclination of 45° and radius of 150 au (Wyatt et al. 2005). *Herschel*/PACS images at 70 μm show a central flux peak on the star surrounded by an inclined ring at ∼47° to the plane of the sky (Duchêne et al. 2014), the latter being the same emission seen in the submillimetre. Modelling of the disc suggests that there are both warm and cold dust belts in the system, the cold component peaking in emission at 164 au with a estimated width of ∼9 au, at a PA of 116° (Duchêne et al. 2014).

More recently, ALMA observations at 880 μm reveal an asymmetric belt of emission of mean radius of 8.4″ (∼152 au) with a width of 2.6″ (∼46 au), at a PA of 117° and an inclination of 35° (Marino et al. 2017). The total flux emission measured from the ALMA image of 10.1 ± 0.4 mJy is 2–3σ lower than would be expected compared to the SCUBA-2 850 μm flux if extrapolated to 880 μm, assuming a spectral index of 3. As pointed out by Marino et al. (2017) the difference could be due either to extended emission being missed by ALMA as a result of having an insufficient number of short baselines, or to the image reconstruction method adopted for the ALMA data.

The photometric data from the SED is fitted by a two-component model. The fit to the near-mid IR data suggests an inner belt at a radius of ∼3 au composed of warm dust radiating at 254 K, whilst the fit to far-IR/submillimetre data indicates the presence of a cold belt with a characteristic dust temperature of 45 K, and a β in the range of 0 to 0.7, leading to an estimated dust mass of 0.028 $M_\oplus$.

5.32 HR 4796 (TWA11, HD 109573)

HR 4796 (HD 109573) is a binary star system in the constellation of Centaurus, at a distance of 73 pc and is part of the TW Hydrae Moving Group with an age of 9 Myr (Barrado y Navascués 2006). The two stars of the system are separated by 7.7″, with the primary having a spectral type A0, whilst the smaller companion is a red dwarf of type M2.5. Emission is detected at both 850 and 450 μm with flux densities of 14.4 ± 1.9 and 117 ± 21 mJy, respectively (Fig. A8d and Fig. 18). Interpreting the emission as a disc structure about the star gives an upper limit to the radius from the 450 μm image is 370 au.

The disc around HR 4796 was first resolved in the mid-IR (Koerner et al. 1998; Jayawardhana et al. 1998) at 12.5 and 20 μm revealing an elongated structure with the dust peaking at a radius of 70 au surrounding the central primary star. The PA of the disc was measured at 30°, consistent with the binary companion, and suggesting that the disk-

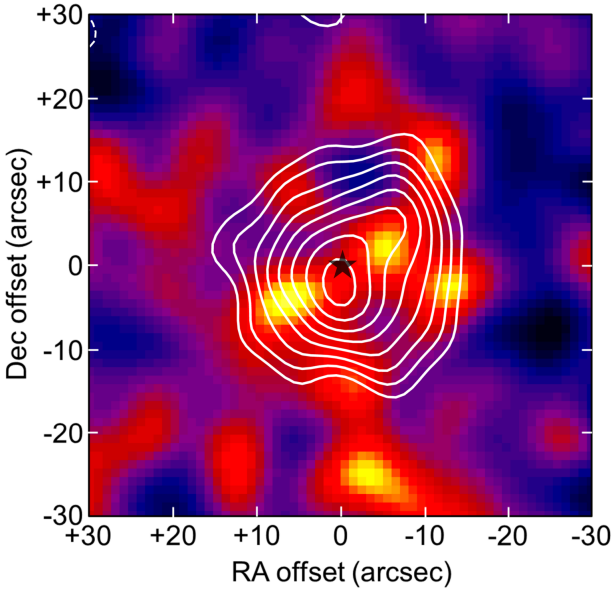

Figure 17. The 450 μm image from observations of HD 109085 (η Crv) with contours from the 850 μm image overlaid. The contours and symbols are as described in Fig. 7.

binary system is being seen nearly along the orbital plane. The disc was interpreted as a ring-like structure, having two lobes similar to HD 216956 (Fomalhaut), with an inner hole devoid of dust extending to a radius of 55 au. The disc has also been imaged in scattered light using *HST*/NICMOS and STIS which show a distinctive ring-like symmetrical structure, consistent with the mid-IR observations (Schneider et al. 1999, 2009). The images revealed that the ring has a peak intensity at 70 au, with a resolved width of 17 au, and a major axis lying at a PA of 27°. The observed brightness variation in across the disc in thermal emission has been attributed to pericentre glow, in which the asymmetry is caused by the gravitational perturbations from an unseen planetary system (Wyatt et al. 2000).

The SED is well-sampled from the near-IR to the millimetre and includes photometric points from both *Spitzer* (Chen et al. 2014) and *WISE* (Wright et al. 2010). Fitting the SED suggests a very well-defined, single temperature disc of 99 K, and a β value of 0.7 to 1.0, and an estimated dust mass of 0.19 $M_\oplus$ from the 850 μm flux.

5.33 61 Virginis (HD 115617)

HD 115617 (61 Vir) is a nearby main sequence star (G7-V) hosting a system of at least two known planets, both of which are sub-Saturn mass and have orbits of less than 0.5 AU. The star lies at a distance 8.6 pc with an estimated age of 6300 Myr, within a range of 6100 to 6600 Myr (Mamajek & Bell 2014). The SONS survey image at 850 μm reveals a main emission peak a few arcseconds offset from the star together with a second isolated 3.5σ peak 12″ to the north (Fig. A9a). The peak flux for the main structure is 3.9 ± 0.8 mJy and is possibly marginally resolved with an integrated flux of 5.8 ± 1.0 mJy measured in a 40″ diameter aperture centred on

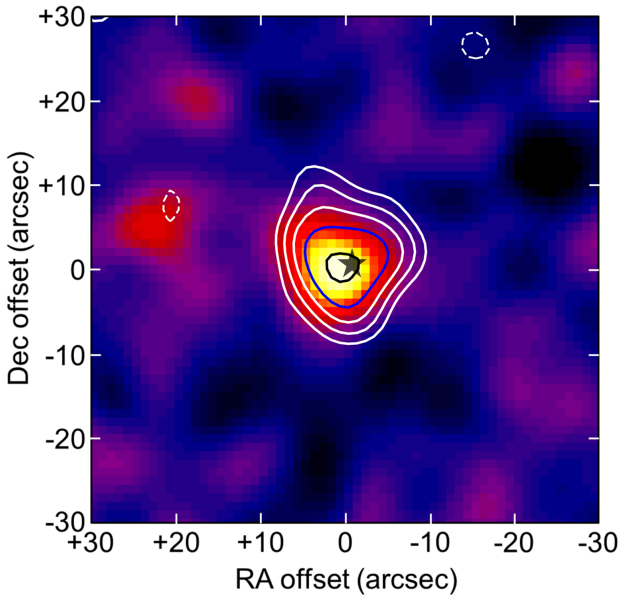

Figure 18. The 450 μm image from observations of HR 4796 (TWA 11; HD 109573) with contours from the 850 μm image overlaid. The contours and symbols are as described in Fig. 7.

the star, but not including the peak to the north. The image reported here benefits from further integration time than the image published by Panić et al. (2013). The structure has a PA of ∼66° and interpreting as a disc about the star gives a deconvolved radius of 4.7″ (∼40 au). The updated SONS results are reported in Marino et al. (2017b).

61 Vir was also included in a survey of FGK stars by *Spitzer* that detected the disc at 24 and 70 μm (Tanner et al. 2009). *Herschel* has provided the most definitive study of the HD 115617 debris disc so far with images from 70 to 500 μm as part of the DEBRIS survey. The images show a nearly edge-on configuration extending out to at least 100 au from the star at a PA of ∼65°, with the dust population peaking in density in a belt between 30 and 100 au (Wyatt et al. 2012). Thus, there is expected to be very little interaction between the disc and the known planets, although theory suggests that planetesimal belts such as this one might hold the key to understanding super-Earth systems such as HD 115617. The northern source, seen in the SONS 850 μm image, is most likely a background object based on the interpretation of the *Herschel*/PACS 160 μm image (Wyatt et al. 2012). Observations with ALMA at 870 μm resolve 3 compact sources Marino et al. (2017b), one of which seems coincident with the northern source seen in both SONS 850 μm and *Herschel*/PACS 160 μm images. By combining SCUBA-2 and ALMA observations it is inferred that the disc is likely very extended covering radius range of 30 au to at least 150 au, implying the existence of a broad parent planetesimal belt.

The SCUBA-2 850 μm result seems to indicate a rapid fall off in flux towards the millimetre region ($\lambda_0 > 650$ μm), although this sharp decrease is not totally consistent with the *Herschel*/SPIRE photometry. Hence the fit to the SED is not convincing with a characteristic dust temperature of 65 K, and only constrains β in the range between 0 and 1.5. The dust mass is estimated to be 1.6×10^{-3} $M_\oplus$. The radius of the disc, derived from the SED fit and assuming blackbody grain properties, is only 17 au, significantly smaller than the value of 40 au obtained from the marginally resolved 850 μm image.

5.34 λ Boötis (HD 125162)

HD 125162 (λ Boo) is a luminous A0 star at a distance 30 pc with an estimated age of 2800 Myr, but with a large uncertainly stretching from 2000 Myr to 3900 Myr (Montesinos et al. 2009). At 850 μm, unresolved emission is detected, well-centred on the stellar position, with a flux density of 3.9 ± 0.8 mJy (Fig. A9b). If interpreted as a disc about the star, the upper limit to the radius from the 850 μm image is 230 au.

The HD 125612 debris disc has been resolved by *Herschel*/PACS at 70 μm revealing a slightly elongated structure of radius 40 au at a PA of 42° (Booth et al. 2013). Photometry from *Spitzer* (Chen et al. 2014) also helps to define the mid-IR section of the SED. The 850 μm photometric point helps to anchor the SED fit to give a characteristic dust temperature of 87 K, but still a poorly constrained β value in the range of 0.3 to 1.8. The dust mass is estimated to be 0.010 $M_\oplus$.

5.35 HD 127821

HD 127821 is an F4 star at a distance of 32 pc with an estimated age of 1020 Myr (Chen et al. 2014), although it could be as old as 3400 Myr (Moór et al. 2006). The SONS image at 850 μm appears to show a predominantly double-peaked structure with one peak reasonably-well centred on the stellar position, and the other offset by ∼13″ to the south-east (Fig. A9c). The peak nearest to the star has a flux of 5.8 ± 0.7 mJy/beam. The integrated flux in a 40″ diameter aperture, centred between the two peaks, is 10.5 ± 1.4 mJy. This flux is just consistent with previous SCUBA photometry of 13.2 ± 3.7 mJy/beam (Williams & Andrews 2006), noting also the slightly larger FWHM beam for SCUBA. In addition, given that the two peaks are approximately the same brightness, and that the integrated flux is equal to their combined levels, it is most likely these are two separate sources. There is also other structure seen to the north, offset from the star by ∼18″.

Herschel imaging with PACS and SPIRE at 160 μm and 250 μm reveals a single source, well-aligned with the central peak in the SONS 850 μm image. Fig. 19 shows the *Herschel*/PACS 160 μm image with the SONS survey 850 μm contours overlaid. Based on these observations, it is therefore possible that the peak to the south-east (as well as the one to the north) are indeed background objects, although these are not seen in the *Herschel* images. It is therefore likely that only the central peak is representative of a disc, and under this assumption (i.e., only using the flux of the central peak at 850 μm) the SED can be fitted with a single-temperature 47 K modified blackbody and a β value in the range 0.9 – 1.9. The estimated dust mass is 0.031 $M_\oplus$, whilst the upper limit to the disc radius from the 850 μm image is 235 au.

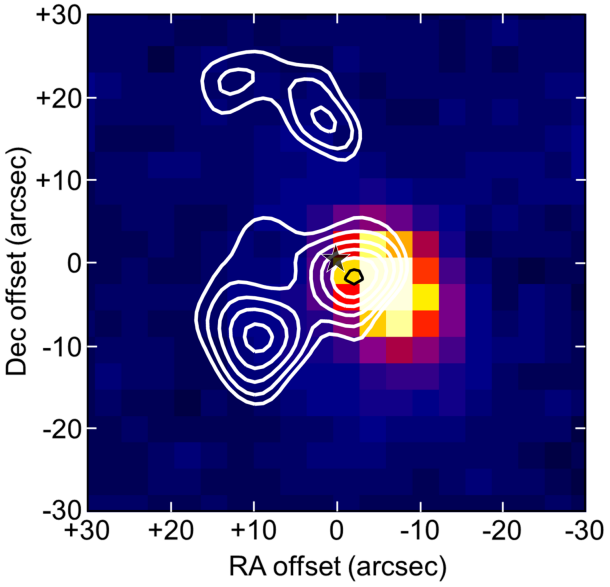

Figure 19. *Herschel*/PACS 160 µm image of HD 127821 with the SONS survey 850 µm contours overlaid. The *Herschel* image is taken from the *Herschel* Science Archive.

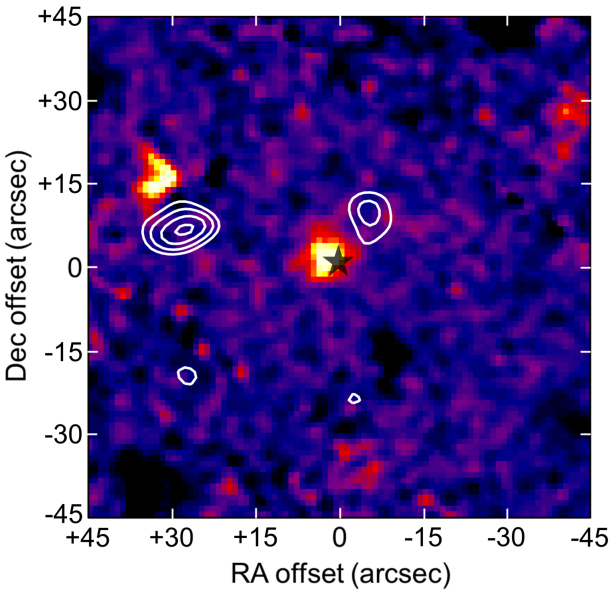

Figure 20. *Herschel*/PACS 160 µm image of HD 128167 (σ Boo) with the SONS survey 850 µm contours overlaid. The *Herschel* image is taken from the *Herschel* Science Archive.

5.36 σ Boötis (HD 128167)

HD 128167 (σ Boo) is an F2 star at a distance of 16 pc with an estimated age of 1000 Myr but it could be as old as 4780 Myr (Rhee et al. 2007). The SONS survey image at 850 µm shows emission, offset from the star by ∼11″ to the north-west, with a flux density of 4.1 ± 0.9 mJy (Fig. A9d). Given the large offset it is unlikely that this peak is associated with the star and is probably a separate source. Observations of HD 128167 with SCUBA at 850 µm reported a flux of 6.2 ± 1.7 mJy (Sheret et al. 2004). These observations used the technique of "extended photometry", in which a 9–point map was made around the source with a spacing of 5″. Such a map would have detected flux from the offset position shown in the SCUBA-2 image. Unpublished imaging observations with SCUBA also seem to indicate an offset peak in the same direction (Wyatt, *priv comm.*).

Herschel/PACS observations at 160 µm reveal a peak at 17.5 ± 3.5 mJy from a position coincident with the star (Fig. 20). A second peak detected in the PACS image to the north-east is ∼8.5″ offset from the brighter peak in the 850 µm SONS image. If a rotational shift of ∼25° was applied in either image then there would be close alignment between the peak near the centre of the field and that to the east. Given the accuracy of pointing and image reconstruction for both telescope facilities, such problems would be unlikely explanations for the discrepancies reported here. It is therefore concluded that the σ Boo disc was not detected by SCUBA-2 and the peak seen to the north-west is a likely background object. The SED (Fig. A9a) only includes photometric points from the position at the star (i.e., the SCUBA-2 850 µm point is presented as an upper flux limit). If the fit is truly representative of the SED at long wavelengths, then the disc would have a flux density of significantly less than 1 mJy at 850 µm (i.e., below the sensitivity threshold of this observation).

5.37 HD 141378

HD 141378 is a luminous A5 star at a distance of 54 pc with an estimated age of 150 Myr (Rieke et al. 2005). The SONS survey 850 µm image reveals a number of features, all of which are offset from the star to the south (Fig. A10a). The nearest peak is 13″ offset and has a flux density 8.5 ± 1.8 mJy. This offset is far in excess of what would be expected for a disc about the star, allowing for positional and statistical uncertainties in the measurement (see Section 6.4). It is therefore likely that this peak is due to a separate source, perhaps a background galaxy.

Herschel/PACS imaging at 100 and 160 µm reveals an emission peak that is well-centred on the star position, and does not show any evidence of the multiple peaks seen at 850 µm to the south (see Fig. 21). Furthermore, the SED fit to the *Herschel* photometry suggests that the disc would not have been detected by SCUBA-2 at the sensitivity levels reached in the observation. Hence, it is probable that a debris disc does exist around HD 141378, but would be very faint at 850 µm (∼2 mJy).

5.38 44 Serpentis (HD 143894)

HD 143894 (44 Ser) is a luminous A3 star at a distance of 55 pc and has an estimated age of 300 Myr (Rhee et al. 2007) although it could be as old as 530 Myr (Chen et al. 2014). The SONS 850 µm image clearly shows emission with a peak flux density of 5.6 ± 0.9 mJy/beam (Fig. A10b), but offset from the stellar position by ∼4″ (slightly above the level of 3.1″ expected due to positional and statistical uncertainties;

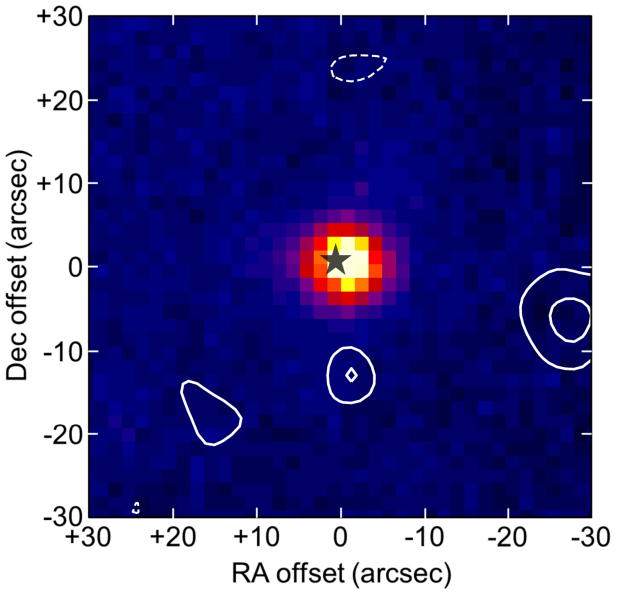

Figure 21. *Herschel*/PACS 100 µm image of HD 141378 with the SONS survey 850 µm contours overlaid. The contours start at 3σ and increase in 1σ steps. The *Herschel* image is taken from the *Herschel* Science Archive.

Section 6.4). The integrated flux in a 40″ diameter aperture, centred on the stellar position, is 10.1 ± 1.2 mJy, indicating that, even at a distance of 55 pc, the emission is resolved. Fitting the radial extent of the emission gives a deconvolved radius of 10.2″ (∼560 au) at a PA of 70°, almost four times the radius of 150 au derived assuming the dust grains have pure blackbody emission. If the emission is indeed indicative of a disc, it represents a very large structure about the star (i.e., 10× the size of the Edgeworth-Kuiper belt in our Solar System). Given the offset between the star and flux peak, one possibility is that the morphology could be somewhat distorted by a background object, resulting in an artificially enlarged structure. Further observations are needed to resolve this issue.

This target was placed in the "hard to quantify" flux category, having a very poorly constrained dust temperature due to lack of far-IR photometry. Hence, the SED is sparsely defined with only photometry from *Spitzer*/MIPS at 24 µm (Chen et al. 2014) and *IRAS* at 60 µm contributing to the disc model SED fit. The 850 µm flux helps to constrain β to a value in the range 0 to 1.1. A temperature of 53 K and a dust mass of 0.14 $M_\oplus$ are derived from the fit and 850 µm flux, respectively.

5.39 37 Herculis (HD 150378)

HD 150378 (37 Her) is a luminous A1 star at a distance of 90 pc with an estimated age of 200 Myr (Chen et al. 2014). The SONS survey image at 850 µm shows a bright peak, offset from the stellar position by 17″ with a flux density of 10.2 ± 1.1 mJy (Fig. A10c). This emission is highly unlikely to be associated with the star and is probably another object, although no identification has been possible from standard catalogues. There is also an *IRAS* detection of excess far-IR radiation at 60 µm, but the large *IRAS* beamsize means it is impossible to ascertain whether this is the same object as detected by SCUBA-2 (the most likely scenario) or a true debris disc associated with the star. The SED contains *Spitzer*/IRS photometry that suggests the possibility of a warm, inner disc component. The fit to the two long wavelength photometric points in the SED (Fig. A10c) suggests an object with a dust temperature of 32 K. Given the large offset in the 850 µm image, it is concluded that there is no strong evidence for a cold debris disc surrounding HD 150378 based on the far-IR and submillimetre data.

5.40 39 Herculis (HD 150682)

HD 150682 (39 Her) is an F3 star at a distance of 44 pc with an estimated age of 1700 Myr (Chen et al. 2014). The SONS survey image at 850 µm shows an unresolved peak, well-centred on the star with a flux density of 5.5 ± 0.9 mJy (Fig. A10d). The upper limit to the disc radius from the 850 µm image is 330 au. The only other far-IR photometry detection is from *Spitzer*/MIPS at 70 µm (Trilling et al. 2007). The fit to the poorly-sampled SED suggests a cold component disc with a dust temperature of 32 K (but with large error of ± 14 K), β in the range from 0.0 to 2.2, and an estimated dust mass of 0.081 $M_\oplus$.

5.41 HD 158352

HD 158352 is a luminous A8 star at a distance of 60 pc with an estimated age of 750 Myr, with an uncertainty of around ± 150 Myr (Moór et al. 2006). The SONS image at 850 µm shows an unresolved peak, well-centred on the star, with a flux density of 5.3 ± 1.0 mJy (Fig. A11a). Interpreting the emission as being representative of a disc about the star gives an upper limit to the disc radius from the 850 µm image of 450 au. There is another peak some 25″ to the north-west that is slightly brighter. The only other far-IR photometry detection is from *Spitzer*/MIPS at 24 and 70 µm (Chen et al. 2014) and so λ_0 and β are not well constrained. The fit to the SED suggests a single component disc with a dust temperature of 62 K, and an estimated dust mass of 0.075 $M_\oplus$.

5.42 γ Ophiuchi (HD 161868)

HD 161868 (γ Oph) is a luminous A0 star at a distance of 32 pc with an estimated age of 185 Myr with lower and upper limits of 50 Myr and 277 Myr, respectively (Song et al. 2001). There are, however, other studies that suggest the star could be as old as 450 Myr (Moór et al. 2015). The 850 µm observations reported in this paper are deeper than those previously published (Panić et al. 2013), and show a marginally extended structure, with the peak emission having a flux density of 4.8 ± 0.8 mJy/beam (Fig. A11b). The integrated flux, measured in an aperture of 50″ in diameter and centred on the peak of the emission is 7.1 ± 1.0 mJy, indicating that the structure is resolved. Interpreted as a disc about the star, the radial extent gives a deconvolved radius of 7.8″ (∼250 au) at a PA of 75°, compared to ∼85 au assuming pure blackbody emission from the dust grains (see Table 3).

Spitzer/MIPS observations first resolved the disc showing dust extending out to a large radius of 18″ (∼520 au) at 70 μm, with an inclination angle to the plane of the sky of ∼50° and a PA of 55° (Su et al. 2008). These data suggest a disc almost twice as large as the SCUBA-2 observations indicate. *Herschel*/PACS observations showed a disc of radius 4.3 to 5.5″ (∼135 – 172 au) over the observed wavelength range of 70 to 160 μm (Moór et al. 2015), inclined at 58° to the plane of the sky and at a PA of 61° (Moór et al. 2015). Subsequent modelling of the *Herschel*/PACS results suggested inner and outer radii for the disc of 49 and 278 au, respectively (Moór et al. 2015). A background object has also been identified at a position 21″ to the east of the star (Moór et al. 2015), and hence it is possible that the low-level emission (which is less than 3σ significance) seen in the 850 μm image at this position is due to this.

The far-IR SED is well constrained by measurements from *Spitzer*/MIPS (Su et al. 2008; Chen et al. 2014) and *Herschel* observations from PACS and SPIRE (Pawellek et al. 2014; Moór et al. 2015). The fit to the SED suggests a dual-component disc with the cold component having a characteristic dust temperature of 68 K, a β value in the range of 0.8 to 1.4, and an estimated dust mass of 0.025 $M_\oplus$. The warmer component, fitting to the near-mid IR photometric points, has a dust temperature of 174 K at an estimated radius from the star of 13 au, assuming blackbody emission from the grains.

5.43 HD 170773

HD 170773 is an F5 star at a distance of 37 pc with an estimated age of 200 Myr (Rhee et al. 2007) but which could be as young as 150 Myr and as old as 300 Myr (Zuckerman & Song 2004). The SONS survey 850 μm image shows a resolved structure, well-centred on the stellar position but extending to the south-east (Fig. A11c). The peak flux is 16.5 ± 1.8 mJy/beam, whilst the integrated flux, measured in an aperture of 40″ in diameter, is 26.0 ± 2.3 mJy. Assuming the structure represents a disc about the star the deconvolved radius is 6.8″ (∼250 au) at a PA of 140° (roughly aligned in a south-east direction; see Table 4), compared to a radius of 73 au obtained assuming pure blackbody emission from the dust grains. The 850 μm peak flux also agrees well with a previous photometry using LABOCA on APEX at 870 μm of 18 ± 5.4 mJy/beam (Liseau et al. 2010).

Herschel/PACS observations reveal a disc of radius 5.9″ (∼217 au) over the observed wavelength range of 70 to 160 μm (Moór et al. 2015), inclined at 31° to the plane of the sky and at a PA of 118° (Moór et al. 2015). These are in reasonably good agreement with the SCUBA-2 results. Modelling of the *Herschel*/PACS results suggested inner and outer radii for the disc of 81 and 265 au, respectively (Moór et al. 2015). The far-IR SED is well-characterised by measurements from *Spitzer*/MIPS (Chen et al. 2014) and *Herschel* PACS and SPIRE (Pawellek et al. 2014; Moór et al. 2015). The fit to the SED gives a single component disc with a dust temperature of 46 K, a β value of 0.5 to 1.4, and an estimated dust mass of 0.19 $M_\oplus$.

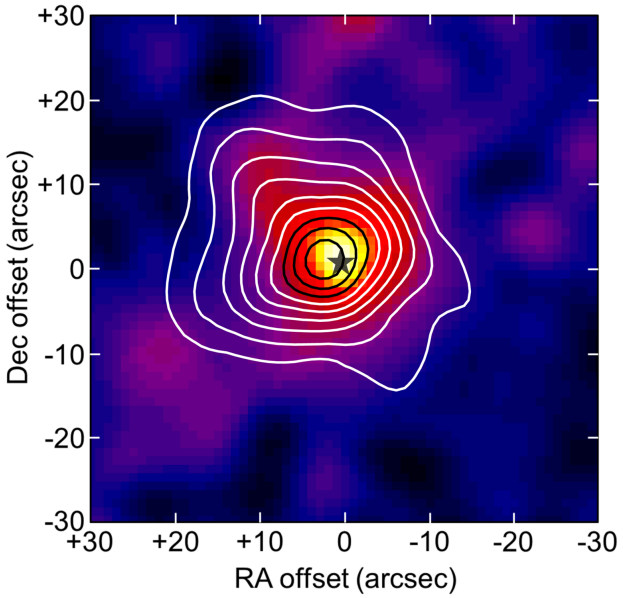

Figure 22. The 450 μm S/N image from observations of Vega (α Lyr; HD 172167) with contours from the 850 μm image overlaid. The contours are scaled from −3 σ to the maximum S/N in the image. The contours start at −3 σ (dashed white) and then solid colours from 4 σ to the maximum in 1.5σ steps. The star symbol represents the position of the star with respect to the disc.

5.44 Vega (HD 172167, α Lyr)

Vega (HD 172167) is a luminous A0 star at a distance of 7.7 pc with an estimated age of 700 Myr with a range extending from 625 Myr to 850 Myr (Monnier et al. 2012). The SONS image at 850 μm reveals a well-resolved, largely circularly-symmetric, smooth structure, with the peak in emission offset from the proper motion-corrected stellar position by only 2″ (Fig. A11d). The peak flux is 13.7 ± 0.8 mJy/beam, whilst the integrated flux, measured within a 50″ diameter aperture, is 34.4 ± 1.4 mJy. Both of these flux measurements are approximately 25% lower than the original SCUBA measurements (Holland et al. 1998), and just outside the threshold of the estimated measurement errors. Emission was also detected with high S/N at 450 μm with an integrated flux density of 229 ± 14 mJy (Fig. 22). Interpreting the structure as a disc about the star, gives deconvolved fitted radii, based on the measured 450 μm and 850 μm images, of 9.5 and 17.5″ (∼73 and 135 au), respectively.

The original SCUBA 850 μm result suggested a more clumpy structure than seen in the new SONS images, with the main peak being offset from the star by ∼6″ (Holland et al. 1998). With approximately 13 years separating the observations it is unlikely that there would be any significant change to the physical structure of the disc that might affect the offset. Both the SONS 450 μm and 850 μm images appear to be slightly elongated in the north-east direction, and it is possible that this extension is caused by another source. Given the proper motion of the star over the period between the SCUBA and SCUBA-2 observations (+2, +3.6″ in RA and dec, respectively) a possible scenario is that the north-east "clump", seen in the original SCUBA 850 μm image, is

a background object (see Section 6.5). There are, however, issues with this explanation in terms of the relative brightness of the peaks, and it is perhaps more plausible that the difference is due to a combination of statistical errors and pointing shifts from the two datasets (see Section 6.4 for a further discussion of offsets).

The Vega debris disc has been extremely well-studied in the near-IR to millimetre region since the original discovery of its large infrared excess by *IRAS* (Aumann et al. 1984). Interferometric observations at 1.3 mm detected dust peaks offset from the star by 8–14″ that were speculated to be part of a ring of emission at a radius of 60–95 au (Koerner, Sargent & Ostroff 2001; Wilner et al. 2002). Multi-band imaging using *Spitzer*/MIPS in the mid-far IR revealed a resolved, smooth disc, devoid of any clumpiness (Su et al. 2005). The disc also appeared to be much larger than originally thought, with measurements at 160 μm suggesting a radius as large as 800 au. Further observations with the CSO at 350/450 μm appeared to show a ring-like morphology with inhomogeneous azimuthal structure, having inner and outer radii of 6.9 and 13.9″ (∼53 and ∼107 au), respectively (Marsh et al. 2006). These observations tended to support a hypothesis that the disc changes from a smooth, axisymmetric structure in the infrared to a more clumpy structure in the millimetre, perhaps with an intermediate structural state governed by a grain population of around 1 mm in size at short submillimetre wavelengths. Theories to explain such a structure included a collision between two massive planetesimals (statistically unlikely) or that the clumps (dominated by grains of 1 mm and larger) are trapped in resonance with a Neptune-mass planet, whilst smaller grains are perturbed by radiation pressure and have a more uniform distribution in the disc (Wilner et al. 2002; Wyatt 2006; Marsh et al. 2006).

Herschel observations with PACS and SPIRE brought into question the clumpy nature of the disc at submillimetre wavelengths. All images between 70 and 500 μm show a well-resolved, but largely smooth disc, leading to the conclusion that the disc is steady-state in nature (Sibthorpe et al. 2010). The star-subtracted *Herschel* images at 70 and 160 μm show that the peak surface brightness of the disc occurs at a radius of ∼11″ (∼85 au) from the star. Furthermore, observations from SMA, CARMA and GBT at wavelengths of 870 μm, 1.3 mm and 3 mm, respectively, do not reveal any clumpy structure on the size-scale expected from previous observations (Hughes et al. 2012). Analysis of these more recent interferometric results, in particular, demonstrate that the observations are consistent with a smooth disc having an inner radius of between 20 and 100 au and a broad width estimated at >50 au.

Modelling of the well-sampled SED of Vega suggests a two component fit to the overall IR excess. The fit to the warmer, inner component is consistent with the analysis of *Spitzer*/IRS and 24 μm, and MSX mid-infrared photometry, carried out by Su et al. (2013), in which the existence of a warm, unresolved "asteroid belt" at a radius of ∼14 au was postulated. The colder component is modelled as a disc/belt with a dust temperature 46 K, and a β value in the range of 1.2 to 1.6, with an estimated dust mass of 0.011 $M_\oplus$ derived from the 850 μm flux. The derived dust temperature for the cold disc is also in good agreement with previous estimates (Su et al. 2005). The relatively high β range means that the equivalent disc radius, assuming blackbody emission, is 260 au, this being significantly lower than the values measured from the images. Since the measured disc radius at 450 μm is also less than that at 850 μm by almost a factor of two, one possibility to explain this discrepancy is a lack of sensitivity in the SONS observations to low-level, extended emission, i.e., the overall emission extends well beyond the lowest contours of the current maps, possibly to several hundred au. This is further discussed in Section 6.2.

The overall conclusion, supported by the new SONS images, is that the Vega debris disc is largely smooth and circularly symmetric at infrared to millimetre wavelengths. Vega is, however, certainly a complex system, most likely containing an inner "asteroid belt" analogue at a radius of <14 au, in addition to a smooth, wide outer disc, perhaps containing another belt at 30 to 100 au, as well as a diffuse halo extending to many hundreds of au.

5.45 HD 181327

HD 181327 is an F5 star and a member of the β Pictoris moving group, at a distance of 52 pc with an estimated age of 23 Myr ± 3 Myr (Mamajek & Bell 2014). At 850 μm the SONS image shows a bright, unresolved peak, well-centred on the stellar position with a flux density of 23.6 ± 3.4 mJy (Fig. A12a). The relatively high noise level is due to the short integration time (1 hr) and the low declination of the source. Interpreted as a disc about the star, the upper limit to the radius from the 850 μm image is 390 au. The LABOCA camera on APEX measured a peak flux of 24.2 mJy/beam at 870 μm (Nilsson et al. 2009), consistent with the 850 μm SONS result. The integrated flux from the LABOCA measurement, however, is far higher at 51.7 ± 6.2 mJy, which suggests the disc is well resolved. This is contrary to the result from the SONS 850 μm image.

The debris disc around HD 181327 has been well-studied in the infrared through to the millimetre. The disc was first resolved by *HST*/NICMOS and modelling revealed a face-on ring peaking in intensity at a radius of 1.7″ (∼86 au) with a width of 0.7″ (∼36 au), inclined at 32° to the plane of the sky and at a PA of 107° (Schneider et al. 2006; Stark et al. 2014). More recently, the disc has been resolved using ALMA at 1.3 mm revealing a circular ring with the emission radially confined between 1.0 and 2.4″ (∼50 – 125 au) with a peak intensity occurring at a radius of 1.7″ (∼86 au) from the star at a PA of 99° (Marino et al. 2016). The ALMA observations also detected ^{12}CO(2–1) emission around an F star for the first time.

Both the *HST*/NICMOS and ALMA results suggest the existence of one or more compact, background objects that could have contaminated the LABOCA photometry, leading to an artificially high flux estimate for the disc. There are also some low-level ($< 3\sigma$) features in the vicinity of the disc in the SONS 850 μm image, which could provide extra evidence to support this hypothesis. For the modelling of the SED it is therefore assumed that the peak flux value from LABOCA of 24.2 mJy/beam at 870 μm is more representative of a true disc flux (although the SED in Fig. A11a shows the integrated flux measurement this is not used in the fit). The SED is modelled as a two component disc with

the warmer element having a dust temperature of 95 K and located at a radius of 16 au from the star (assuming the grains behave like perfect blackbodies). Photometry from *Spitzer*/MIPS at 24, 70 and 160 μm (Chen et al. 2008, 2014), and *Herschel*/PACS observations (archival data) help constrain the mid-far IR part of the SED, in addition to a 7 mm photometric point from the VLA MacGregor et al. (2016a). Fitting the SED submillimetre points using the SONS result at 850 μm suggests a cold disc component with a dust temperature of 63 K, a β value tightly constrained between 0.4 and 0.6, and an estimated dust mass of 0.25 $M_\oplus$. The total flux measured of 7.9 ± 0.2 mJy, measured by ALMA at 1.3 mm, is also consistent with the fit to the SED (Marino et al. 2016).

5.46 HD 182681

HD 182681 is a luminous B8 star at a distance of 70 pc with an estimated age of 145 Myr (Chen et al. 2014), but is sometimes referred to as a pre-main-sequence star with an age as young as 19 Myr, but also as old as 208 Myr (Moór et al. 2015). The 850 μm image shows a unresolved disc, just offset from the stellar position, with a flux density of 6.8 ± 1.2 mJy (Fig. A12b). There is a second source offset by 19″ to the south-east, which is likely to be a background object, although there is a low-level (<3σ significance) ridge running approximately north-west to south-east. Assuming only the central peak is part of a disc structure, the upper limit to the disc radius from the 850 μm image is 525 au.

The disc was resolved by *Herschel*/PACS with the 160 μm image indicating a disc of radius 3.3″ (∼230 au), inclined at 67° to the line-of-sight and at a PA of 56° (Moór et al. 2015). Modelling of the PACS images suggests a structure where the flux density peaks at 159 au, with inner and outer radii of 52 au and 263 au, respectively. The south-east peak is not visible in any of the *Herschel* images, including longer wavelength results from SPIRE at 350 μm and 450 μm. Photometry from *Herschel* also helps to constrain the mid-far IR part of the SED (Pawellek et al. 2014; Moór et al. 2015). Fitting the SED suggests a single-component disc with a dust temperature of 80 K, a β value in the range of 0.2 – 1.0, and an estimated dust mass of 0.104 $M_\oplus$.

5.47 HD 191089

HD 191089 is an F5 star and a member of the β Pictoris moving group. It lies at a distance of 52 pc with an estimated age of 23 Myr (Mamajek & Bell 2014). The SONS survey image at 850 μm reveals a compact, unresolved structure, with a flux density of 4.9 ± 0.9 mJy (Fig. A12c). The peak emission is offset from the star position by ∼6″, i.e., greater than the maximum offset of 3.5″, caused by statistical uncertainties and expected pointing errors (see Section 6.4 for a discussion of offsets). Based on other observations (see below) it is believed that the observed structure is indeed a disc associated with the star, but there exists the possibility that there could be some contamination from a background source to account for the offset (see Section 6.5). The upper limit to the disc radius from the observed 850 μm image is 395 au.

The disc has been resolved from observations made with the T-ReCS instrument on the Gemini South telescope at 18.3 μm, which show the structure extending to a maximum radius of 0.85″ (∼90 au) at position angle of 80° (Churcher et al. 2011). Modelling indicates that the emission arises from a dust belt with radius 28 au to 90 au from the star, inclined at 35° to edge on, and with a central cavity largely devoid of emission. The disc has also been imaged in scattered light using the *HST*/NICMOS, revealing a ring-like structure that peaks in scattered light at ∼73 au, consistent with the mid-IR image (Soummer et al. 2014). The far-IR part of the SED is well characterised by measurements from *Spitzer*/MIPS (Chen et al. 2014), the CSO SHARC-II instrument (Roccatagliata et al. 2009), and *Herschel* PACS and SPIRE (archival data). The fit to the SED gives a single component disc with a dust temperature of 89 K, a β value in the range 0.3 to 2.3, and an estimated dust mass of 0.037 $M_\oplus$.

5.48 AU Microscopii (HD 197481)

AU Mic (HD 197481) is a young M1 star and a member of the β Pictoris moving group, at a distance of 10 pc with an estimated age of 23 Myr (Mamajek & Bell 2014). The disc appears to be unresolved at 850 μm with a flux density of 12.9 ± 0.8 mJy (Fig. A12d), despite apparently showing a slight extension roughly in the north-west to south-east direction (Matthews et al. 2015). Indeed, this extension is confirmed with 450 μm observations that reveal a disc of deconvolved radius 7.1″ (∼70 au) at a PA of ∼127° (as shown in Fig. 23, with details of the disc size given in Table 4). The 450 μm integrated flux, measured within a 40″ diameter aperture centred on the star, is 57 ± 9 mJy, consistent with previous photometry using JCMT/SCUBA at 450 μm and 850 μm (Liu et al. 2004) and CSO/SHARC-II at 350 μm (Chen et al. 2005).

The far-IR excess from AU Mic was first detected by *IRAS* (Moshir et al. 1990), and since then it has been studied across the spectrum from the optical to millimetre, with much of the interest focusing on the fact that it was the first M star to show evidence of a debris disc. Scattered light images of the disc from *HST*/ACS, the second of which to be resolved at optical wavelengths, revealed an edge-on disc extending to a radius of 10″ (∼100 au) at a PA of 128° (Krist et al. 2005). The disc was also resolved from *Herschel*/PACS observations at 70 μm and 160 μm, confirming the wide edge-on belt extending roughly from 1″ to 4″ (∼9 au − 40 au) at a PA of 135° (Matthews et al. 2015), somewhat less in size than the SONS 450 μm image shows. The *HST* results, and those from *Herschel* at 70 μm, suggest the presence of an extra component of small grains (sometimes referred to as a "halo"), extending beyond the radius of the main AU Mic belt, possibly to a radius of 140 au (Matthews et al. 2015).

The disc was first resolved at millimetre wavelengths by the SMA, revealing the broad belt with the emission peaking at a radius of 3.5″ (∼35 au) at a PA of 130° (Wilner et al. 2012). Subsequent imaging with ALMA at 1.3 mm shows a 10:1 aspect ratio for the edge-on belt, extending from a radius of 0.9″(∼9 au) outwards to 4″ (∼40 au), at a PA of 128° (MacGregor et al. 2013) in agreement with the *Herschel* results. The ALMA image was modelled as a narrow "birth-ring" or "parent belt" of planetesimals at 40 au (MacGregor et al. 2013). The SED is well-characterised in the far-IR with

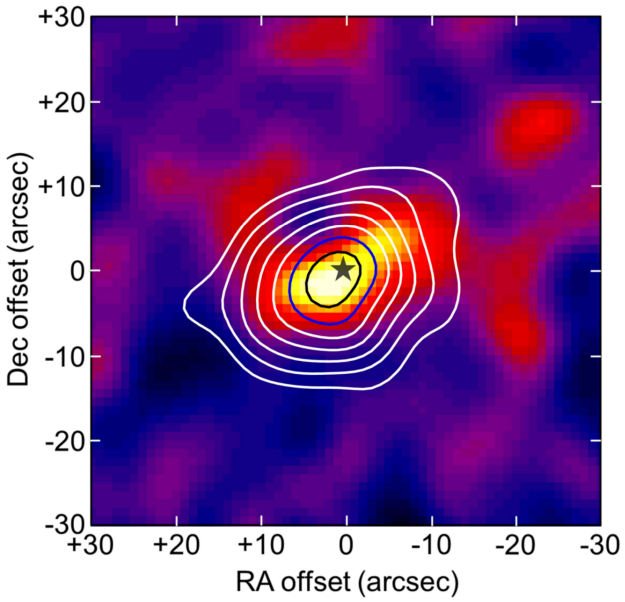

Figure 23. The 450 µm S/N image from observations of HD 197481 (AU Mic) with contours from the 850 µm image overlaid. The colours are scaled from -3σ to the maximum S/N in the image. The contours start at -3σ (dashed white) and then solid colours from 4σ to the maximum in 2σ steps. The star symbol represents the position of the star with respect to the disc.

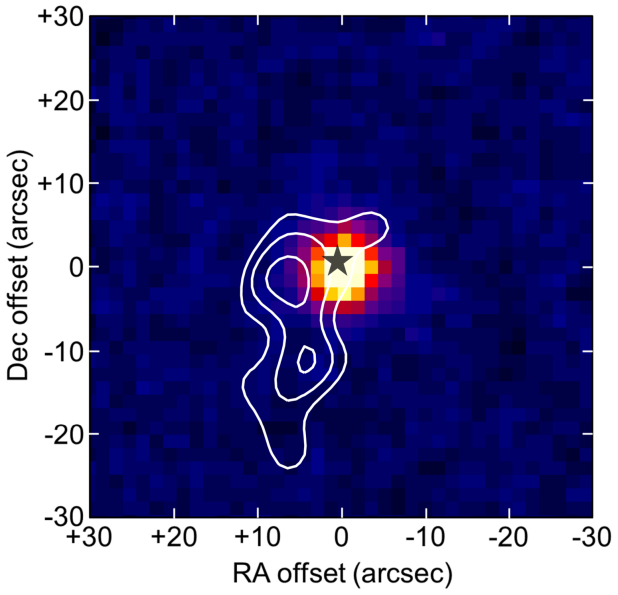

Figure 24. *Herschel*/PACS 100 µm image of HD 205674 with the SONS survey 850 µm contours overlaid. The contours start at 3σ and increase in 1σ steps. The *Herschel* image is taken from the *Herschel* Science Archive.

additional photometry from *Herschel*/SPIRE (Matthews et al. 2015), and is fit by an almost pure black body spectrum ($\beta = 0 - 0.3$; see Section 6.3 for further discussion) at a dust temperature of 50 K, and a estimated dust mass of $6{\times}10^{-3}$ $M_{\oplus}$. The radius of the disc determined from the fit to the SED, and assuming perfect blackbody emission from the dust grains, is 9 au, consistent with the inner edge estimates from ALMA imaging.

5.49 HD 205674

HD 205674 is an F0 star and possible member of the AB Doradus moving group lying at a distance of 52 pc with an estimated age of 130 Myr in a range of 110 Myr to 150 Myr (Barrado y Navascués et al. 2004). The image at 850 µm shows that the the emission is largely concentrated in two peaks running in a line from north to south (Fig. A13a). The image presented in this paper benefits from a considerable increase in integration time over that published in Panić et al. (2013), which clearly showed a peak to the south offset by 10″ from the star. The main dust peak has a flux of 4.0 ± 0.7 mJy/beam, and is offset by ∼6″ from the stellar position, greater than the maximum offset of 3.2″ expected due to statistical uncertainties and pointing errors (see Section 6.4). The total flux, including the second peak to the south, and measured in a 40″ diameter aperture centred between the two peaks, is 7.5 ± 1.1 mJy. Both the offset of the main peak from the star and the elongated structure are difficult to explain. The observed structure certainly hints at two distinct peaks, perhaps suggesting the peak to the south could be a background source.

Herschel/PACS imaging at 100 and 160 µm reveals an emission peak that is well-centred on the star position, and does not show any evidence of an extension or second source to the south (see Fig. 24). This strengthens the argument that the the peak seen to the south in the SONS 850 µm image is most likely a background source, although no such source has been identified from catalogues. Hence, in this paper the emission surrounding HD 205674 is interpreted as an offset disc, assuming the southern peak is a background source. The far-IR SED is well constrained by measurements from *Spitzer*/MIPS (Moór et al. 2011b) and archival data from *Herschel* PACS and SPIRE but the 850 µm SONS flux is the only other long wavelength photometric data. Fitting the SED suggests a disc with a dust temperature of 60 K, β in the range 0.1 to 1.1, and an estimated dust mass of 0.044 $M_{\oplus}$.

5.50 HD 206893

HD 206893 is an F5 star, lying at a distance of 38 pc with an age estimated to be 860 Myr (Pace 2013), but could be as young as 200 Myr (Zuckerman & Song 2004) or as old as 2.1 Gyr (David & Hillenbrand 2015). The SONS image at 850 µm shows a faint, unresolved peak of flux density 4.5 ± 1.1 mJy, offset from the stellar position by 4″ (Fig. A13b). Interpreting the peak as an unresolved disc associated with the star, gives an upper limit for the disc radius of 290 au.

Spitzer detected excess flux from the star at wavelengths between 3.6 µm and 160 µm (Moór et al. 2006). The disc has also been marginally resolved by *Herschel*/PACS observations at 70 µm, revealing a dust ring extending from 1.3 to 5.2″ (∼50 – 200 au) at a PA of 60° (Milli et al. 2017). The disc has also been imaged in scattered light extending to a radius of 4 – 5″ (∼150 – 190 au) at a very similar PA (Milli et al. 2017). Recently, a low-mass companion brown-

dwarf (mass in the range 24 to 73 M_{Jup}) was also detected using VLT/SPHERE at H-band, lying in an orbit of radius 10 au from HD 206893 (Milli et al. 2017). The detection of a low-mass companion inside a massive debris disc makes this system analogous to other young planetary systems, such as β Pictoris and HR 8799.

The SED is reasonably well-sampled in the near-far IR, but only has the SONS 850 μm photometric point at long wavelengths. The SED is modelled with a single-temperature modified blackbody deriving a dust temperature of 54 K, a β value only loosely constrained between values of 0.5 and 2.7, and an estimated dust mass of 0.030 $M_\oplus$ derived from the 850 μm flux.

5.51 HD 207129

HD 207129 is a Solar analogue (G2 star) at a distance of 16 pc with an estimated age of 3800 Myr but with large uncertainties spanning the range of 1300 Myr to 7400 Myr (Holmberg et al. 2007). The image at 850 μm shows emission in two 4 – 5σ peaks with the star equidistant between the two. The peak to the west has a flux of 7.0 ± 1.2 mJy/beam (Fig. A13c), whilst the integrated flux within a 40″ diameter aperture, covering both peaks, is 10.8 ± 1.8 mJy, indicating the disc is marginally resolved by the JCMT beam. The symmetric nature of the peaks about the star suggests a possible inclined toroidal geometry for the structure (perhaps similar to Fomalhaut, as described in Section 3.3). Interpreting the structure as a disc, extended in a roughly east-west direction, gives a deconvolved radius of 10″ (∼160 au) at a PA angle of ∼115°.

Being a relatively close solar analogue, HD 207129 has been well-studied at most wavelengths between the optical and millimetre. The debris disc was first discovered by *IRAS* (Walker & Wolstencroft 1988) with subsequent far-IR photometry from *ISO* (Jourdain de Muizon et al. 1999) and *Spitzer* (Krist et al. 2010). The disc is also well resolved in scattered light observations revealing a narrow ring of radius 10″ (∼160 au) at a PA of 127° (Krist et al. 2010). The HD 207129 disc has been resolved by *Herschel*/PACS as part of the DUNES key programme (Marshall et al. 2011; Löhne et al. 2012). Modelling of the 100 μm PACS image suggests a ring of radius 8.7″ (∼140 au), consistent with an interpretation of collisional dust being produced in an icy "exo-Kuiper" belt. The disc appears inclined at 53° from pole-on with a PA of 122°. The SCUBA-2 image at 850 μm is in good agreement with both the scattered light and the *Herschel* results. The SED is well-sampled by *Spitzer*/MIPS (Trilling et al. 2008; Tanner et al. 2009; Krist et al. 2010) and *Herschel* PACS and SPIRE (Marshall et al. 2011; Eiroa et al. 2013) in the far-IR. Fitting the SED suggests a disc with a single dust temperature of 46 K, a β value of 0.4 – 1.1, and an estimated dust mass of 0.015 $M_\oplus$.

5.52 HD 212695

HD 212695 is an old F5 star at a distance of 47 pc with an estimated age of 2300 Myr (Trilling et al. 2007). The 850 μm image shows unresolved emission, just offset from the star, with a flux density of 5.7 ± 1.1 mJy (Fig. A13d). Interpreting this structure as a disc about the star gives an upper limit to the disc radius from the 850 μm image of 350 au. The SED is not well-constrained in the far-IR, only having photometry from *Spitzer*/MIPS at 70 μm (Chen et al. 2014). A fit to this limited SED suggests the single-component disc is cold with a dust temperature of 35 K (but with errors of ± 19 K) and an estimated dust mass of 0.086 $M_\oplus$.

5.53 39 Pegasi (HD 213617)

39 Peg is a F1 star at a distance of 50 pc with an estimated age of 1200 +/- 300 Myr (Moór et al. 2011b). The SONS image at 850 μm shows a marginally-detected, unresolved peak of flux density 4.6 ± 1.3 mJy, offset from the stellar position by 4″ (Fig. A14a). Interpreting the peak as an unresolved disc associated with the star, gives an upper limit for the disc radius of 380 au.

Spitzer detected excess flux from the star at wavelengths up to 70 μm (Moór et al. 2011b), but the SONS 850 μm photometry is the only data at longer wavelengths. Modelling of the SED suggests a single component fit having a dust temperature of 59 K, a β value only loosely constrained between values of 0 and 2.1, and an estimated dust mass of 0.049 $M_\oplus$ derived from the 850 μm flux.

5.54 Fomalhaut (HD 216956, α PsA)

Fomalhaut (HD 216956) is a luminous A4 star at a distance of 7.7 pc with an estimated age of 440 Myr of (±40 Myr) (Mamajek & Bell 2014). The SCUBA-2 850 μm image shows the familiar double-lobed disc structure at a position angle of 160°, with the star positioned equidistant between the lobes (Fig. A14b). The two peaks have fluxes of 26.3 ± 1.0 mJy/beam (north-west) and 25.2 ± 1.0 mJy/beam (south-east), in good agreement with previous submillimetre results (Holland et al. 1998, 2003). The integrated flux within a 60″ diameter aperture is 91.2 ± 2.5 mJy[4], also in good agreement with the previous estimates (Section 3.3). As previously discussed in Section 4.3 the emission morphology is not well-represented by a Gaussian profile, and the resultant model-subtracted map shows a residual peak at the position. Nevertheless, for this paper such an approximation gives a reasonable estimation for the overall size of the structure. Interpreted as a disc/ring about the star, the deconvolved major and minor radii from the 2D Gaussian fitting are 19.7″ and 7.5″ (∼151 au and ∼57 au), respectively.

The IR excess from Fomalhaut was first discovered and resolved by *IRAS* (Gillet 1986; Backman & Paresce 1993). Further indication that the excess could be an extended disc structure came from point-by-point photometry using the JCMT (Zuckerman & Beckin 1993). In the late 1990's, the SCUBA camera (Holland et al. 1998) provided the first true image of the thermal emission from the Fomalhaut debris disc, resolving the double-lobed structure. The SCUBA image suggested a massive torus-like Kuiper Belt surrounds the star, with the possibility of one or more planets acting as shepherds to the disc structure. The first optical observations of the disc in scattered light revealed a narrow elliptical belt with semi-major and minor axes of 18.5″ and

[4] The calibration uncertainty at 850 μm adds an additional 7 per cent to this error estimate.

7.6″ (∼141 au and ∼58 au), respectively (Kalas et al. 2005), at a PA of 156° and with an estimated thickness of 15 au. Modelling of the geometry of the dust belt concluded that the observed features, such as the sharp inner edge and variation in the azimuthal brightness, were likely attributable to a planetary system.

The discovery of the first planet in the system, Fomalhaut b, was also made via *HST* observations with a location just inside the inner radius of the ring (Kalas et al. 2008), and subsequent observations have provided further insights on both the main belt structure and the possible planetary system (Kalas et al. 2013). However, the orbit of Fomalhaut b is not apsidally aligned with the dust ring, and so it may be the case that additional planets are responsible for shaping the dust morphology. It has also been suggested that Fomalhaut b is not actually a planet, but either a dust cloud (perhaps orbiting a planet) (Kennedy & Wyatt 2011) or the dusty aftermath of a collision between two Kuiper belt-like objects (Galicher et al. 2013).

Herschel observations provided high dynamic range images of the dust belt in the far-IR, as well as evidence that the system is remarkably active with dust grains being produced at a very high rate by a collisional cascade of planetesimals (Acke et al. 2012). Modelling of the 70 μm PACS image showed a ring with a mean radius of 18″ (∼138 au) at a PA of 157°, consistent with the submillimetre and optical images. Further constraints on the Fomalhaut planetary system have been obtained by high angular resolution observations with ALMA of the north-west side of the belt. Observations at 850 μm with ∼1.5″ resolution show a ring that peaks in surface brightness at a radius of 18.4″ (∼142 au), with a PA of 168°. The ring is inclined to the plane of the sky by 66° and has a width of ∼17 au (Boley et al. 2012). Moreover, the image showed that almost all of the emission is confined to the ring, with the flux estimates also agreeing with previous submillimetre measurements at 850 μm (for the half of the ring that was observed). More recent observations with ALMA on the entire ring at 1.3 mm, tightly constrain the radius to ∼136 au with a width of 13.5 au (White et al. 2016; MacGregor et al. 2017).

The Fomalhaut disc was also detected with high S/N at 450 μm, and Fig. 25 shows the 450 μm S/N image with the 850 μm contours overlaid. The general morphology is consistent with previous SCUBA observations, and there is even evidence of a slight flux excess to the east (e.g., a flux difference of 10 mJy compared to that at the equivalent radius from the star on the west side) as reported in the previous asymmetric description of the disc about the star (Holland et al. 2003). The striking difference here, however, is that the new image appears to show a brightness asymmetry between the north-west and south-east lobes at approximately the 3σ level. This asymmetry is also supported by CSO observations of the Fomalhaut disc (Marsh et al. 2005). The theory of "apocentre glow" predicts that a steady-state disc will show an over-density of dust at apocentre, due to the Keplerian orbital velocity in an eccentric disc being slower at apocentre rather than at pericentre (Pan et al. 2016). The most recent results from high resolution observations with ALMA provide conclusive evidence that the apocentre (north-west peak) has excess submillimetre/millimetre dust (MacGregor et al. 2017; Matrà et al. 2017). The SED in the far-IR and submillimetre is extremely well-sampled with a fit suggesting a dominant cold component disc with a dust temperature of 41 K, a β value well-constrained in the range of 1.0 to 1.3, and an estimated dust mass of 0.032 $M_\oplus$.

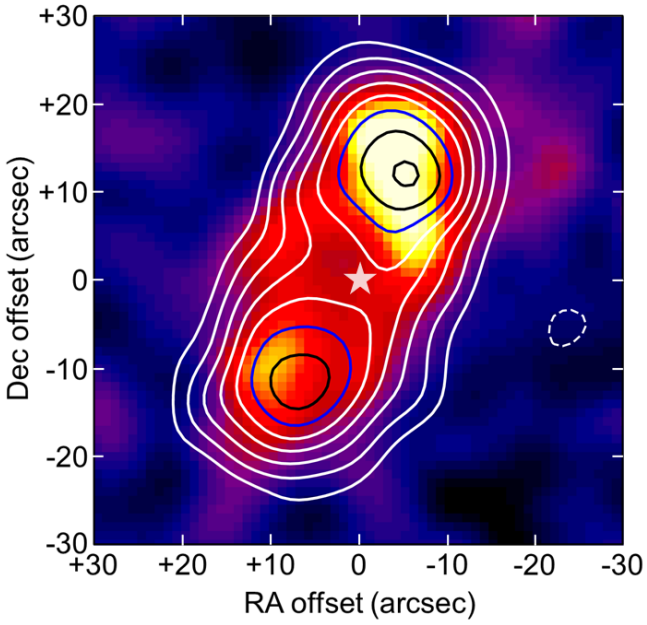

Figure 25. The 450 μm S/N image from observations of Fomalhaut (HD 216956) with contours from the 850 μm image overlaid. The colours are scaled from −3σ to the maximum S/N in the image. The contours start at −5σ (dashed white) and then solid colours from 5σ to the maximum in 5σ steps. The star symbol represents the position of the star with respect to the disc.

5.55 HR 8799 (HD 218396)

HR 8799 (HD 218395) is a young luminous A5 star in the Columba Moving Group (Doyon et al. 2010; Zuckerman et al. 2011), lying at a distance of 39 pc with an estimated age of 30 Myr (Torres et al. 2008; Marois et al. 2010). The SONS survey image at 850 μm reveals a significantly extended structure, with a peak flux of 10.9 ± 1.0 mJy/beam, well-centred on the stellar position (Fig. A14c). The integrated flux, measured in a 60″ diameter aperture, is 23.0 ± 2.0 mJy which takes in all the structure including the extension (possibly a separate background source) to the north-west (see discussion below). The peak flux is also consistent with the previous SCUBA flux estimate of 10.3 ± 1.8 mJy (Williams & Andrews 2006), which was measured in photometry mode and so not sensitive to any extended structure. Fitting the radial extent, but without including the north-west peak, gives a deconvolved disc radius of 10″ (∼395 au) at a PA of 71° (see Table 4).

The HR 8799 system also contains at least four known giant planets, all of which have orbital radii within ∼70 au of the star (Marois et al. 2008, 2010). The thermal emission from the debris disc was first detected by *IRAS* (Sadakane & Nishida 1986). The disc was first resolved by *Spitzer* at 24 μm and 70 μm and the results of SED modelling suggested there were three distinct components to the debris system (Su et al. 2009). The first is a warm (∼150 K) dust

cloud orbiting within planets "d" and "e" at a radius of <0.6″ (∼24 au) from the star. The second is a broad zone of cold (∼45 K) dust with a sharp inner edge and orbiting just outside the outermost planet ("planet b") at a radius of 2.3″ (∼90 au) but extending out to 7.7″ (∼300 au). The final component is a halo of small grains, perhaps originating in the cold belt, but extending from 7.7″ (∼300 au) to at least a radius of 25″ (∼1000 au), and suggesting dust grains are prevalent at very large radii from the host star (Su et al. 2009). Subsequent observations by *Herschel* also resolved the disc between wavelengths of 70 µm and 250 µm (Matthews et al. 2014) with deconvolved radii of 7.2″ and 7.7″ (∼284 au and 300 au) at a PA of 62°, based on the 70 to 160 µm PACS results. Modelling the images also supported the *Spitzer* findings that the disc consists of three distinct components: a warm inner asteroid belt analogue, a planetesimal belt extending from 100 au to 310 au and an outer halo reaching a radius of 1500 au from the star. Both the *Spitzer* and *Herschel* observations also show a compact source some 15″ to the north-west, coincident with the extension seen in the 850 µm image. It is therefore likely that this source is a separate background object.

The HR 8799 disc has also recently been observed with ALMA at 1.3 mm, resolving the planetesimal belt. The emission was modelled as a broad ring at a radius of between 3.7″ and 10.7″ (∼145 au and 429 au), with a PA of 51° (Booth et al. 2016). The outermost planet in the system ("planet b") was expected to be responsible for shaping the inner edge of the belt, but the size of the belt seems inconsistent with the planet's orbit. This inconsistency suggests that either the orbit has varied over time or there is another (smaller) planet further out from the star. The measured flux density of 2.8 mJy at 1.3 mm also seems inconsistent with the well-sampled SED, suggesting that the ALMA data is missing significant flux on a scale larger than its primary beam.

The SED in the far-IR is well-sampled, including the aforementioned photometry from *Spitzer* and *Herschel*. The disc is also detected with SCUBA-2 at 450 µm with a peak flux of 122 ± 22 mJy/beam (∼5 σ) and Fig. 26 shows the 450 µm image with the 850 µm contours overlaid. In common to the other (mainly shorter wavelength) observations from *Herschel*, there appears to be significant low-level extended emission seen to the south and south-west at 450 µm, outside of the reasonably compact central source. This wide extent is reflected in an integrated flux of 346 ± 34 mJy, measured in a 60″ diameter aperture centred on the star. This emission is likely due to a known dust cloud in the vicinity of HR 8799 (Matthews et al. 2014). Hence, taking this cloud into account, the peak flux value has been adopted as the photometric point at 450 µm. At 850 µm, the flux of the background source to the north-west (5.6 mJy) has been removed from the total flux estimate (revised value is 17.4 ± 1.5 mJy), and it has been assumed there is no contribution from the local dust cloud at this wavelength. Based on the modelling of the SED, there appears to be evidence of two components, and fitting to the near to mid-IR photometry suggests an inner disc of 190 K at a radius of 5 au from the star. The colder component, representative of the planetesimal disc, has a dust temperature of 43 K, a β value in the range 0.6 to 1.9, and an estimated dust mass of 0.156 $M_\oplus$.

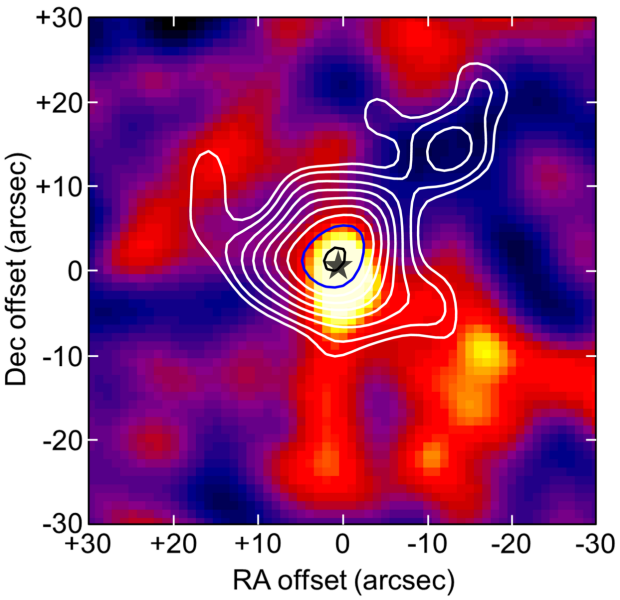

Figure 26. The 450 µm S/N image from observations of HR 8799 (HD 218396) with contours from the 850 µm image overlaid. The colours are scaled from −3σ to the maximum S/N in the image. The contours start at −3σ (dashed white) and then solid colours from 4σ to the maximum in 2σ steps. The star symbol represents the position of the star with respect to the disc.

Assuming the dust grains to be pure blackbodies implies that the disc would be at a radius of 80 au from the star.

6 DISCUSSION

6.1 Detection rate

The detection rate for discs at 850 µm (3σ+ peaks) within a half-beam diameter of the stellar position is 49 per cent (i.e., not including the five cases where the peak is significantly offset from the star that they are considered to be background objects, namely HD 17093, HD 22179, HD 128167, HD 141378 and HD 150378, and also Algol, where the emission is most likely related to the radio variability). Given that all the targets in the sample are known disc hosts, and assuming the fits to the photometric points in the SEDs are accurate, it is clear that the SONS observations do not go deep enough for the non-detected disc cases. Fig. 27 shows that the number of discs detected is largely uniform as a function of spectral type (stellar luminosity) which is to be expected from such a targeted survey. Table 5 summarises the sample numbers and detection rate by spectral type. Approximately 30 per cent of the targets that were detected at 850 µm also showed flux excesses at 450 µm, i.e., 14 out of the original list of 100 stars showed excess flux at the 5σ+ level within a 7″ radius of the stellar position. As discussed for individual targets (Section 5), the 450 µm photometry has been used to constrain further the fitting of the SED and in some cases offers improved angular resolution (∼7.5″, or ∼10″ with smoothing) for extended structures.

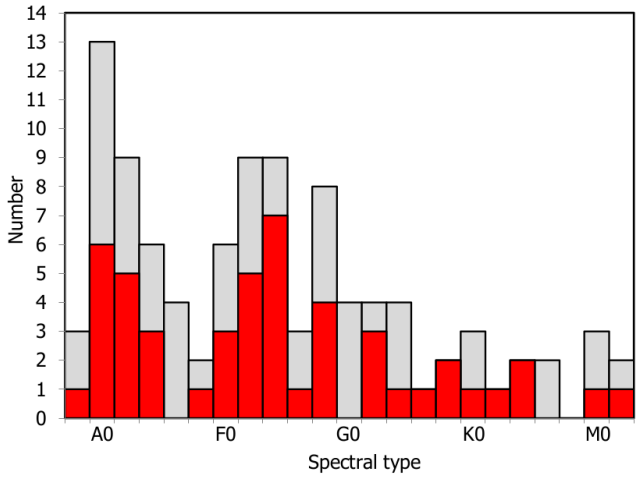

Figure 27. The number of discs detected at 850 µm (red bars) as a function of host star spectral type. The grey bars represent the non-detections within the survey.

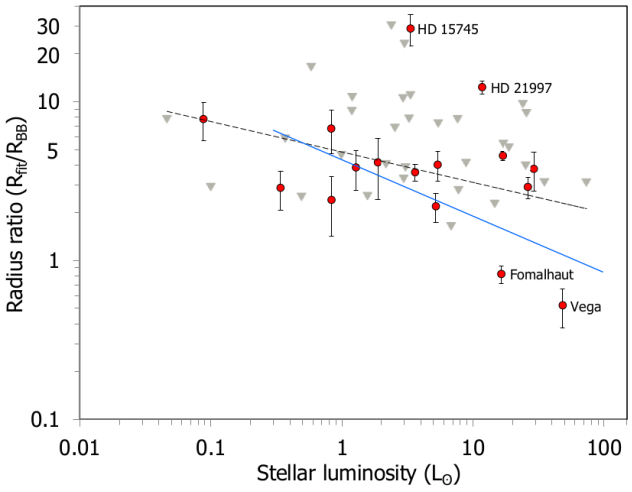

Figure 28. The ratio of the measured disc radius ($R_{\rm fit}$) to that derived from the SED (assuming the dust grains behave as perfect blackbodies; ($R_{\rm BB}$) plotted against stellar luminosity. The inverted triangles represent upper limits for the cases in which the disc is unresolved. The dashed line is a fit to the data points for which the disc is resolved (i.e. the upper limits are not included in the fit). The solid blue line is based on fitting the observed SED from *Herschel* observations assuming a dust composition dominated by ice and silicates (Pawellek & Krivov 2015).

Table 5. Summary of the sample numbers and detections (at 850 µm) by spectral type. The detections do not include the extreme offset cases (HD 17093, HD 22179, HD 128167, HD 141378 and HD150378), as well as Algol (HD 19356) where the emission is likely linked to radio variability i.e. not originating from a circumstellar disc. The errors in the detection fraction are derived assuming a binomial distribution according to $df = \sqrt{f(1-f)/N}$, where f is the detection fraction and N the number in the sample.

Spectral type	Number in sample	Number detected	Detection fraction (per cent)
B	3	1	33 ± 4.7
A	34	15	44 ± 5.0
F	35	20	57 ± 5.0
G	15	7	47 ± 5.0
K	8	4	50 ± 5.0
M	5	2	40 ± 4.9

6.2 Disc morphology and sizes

Within the sample, 16 discs have been spatially resolved, with deconvolved measured radii ranging from 40 au to 800 au (as shown in Table 3 and Table 4). If the disc is composed of small grains these will be hotter than their blackbody equivalent, and hence the disc size will be larger than that determined from the SED fit, according to equation 1 (see Section 4.3). Larger grains will behave more like blackbodies with the ratio of the measured (observed) radius ($R_{\rm fit}$) to that derived from the SED fit ($R_{\rm BB}$) approaching unity. Fig. 28 shows the ratio of $R_{\rm fit}/R_{\rm BB}$ plotted against stellar luminosity. It can be seen that the ratio is greater than unity in the vast majority of cases and typically less than 10. This behaviour implies the existence of planetesimals at larger radii than those derived by assuming a simple blackbody fit to the SED.

The general trend is for the discs around lower luminosity stars to be larger than expected based on their blackbody dust grain properties. The ratio is seen to decline as $\propto L_*^{-0.2}$, as shown in Fig. 28. A number of papers have compared the disc sizes resolved by, for example, *Herschel*, relative to the expectation from blackbody emission, and found that, although the ratio was typically less than 4, there was clear evidence of a decline with increasing stellar luminosity (Booth et al. 2013; Morales et al. 2013; Pawellek et al. 2014; Pawellek & Krivov 2015). This decline was interpreted as being consistent with the expectation from blowout, where higher luminosity stars have removed the smallest grains via radiation pressure, leaving relatively large, blackbody-like dust grains, whilst stars of lower luminosity should have super-heated grains. For comparison, Fig. 28 also shows the ratio based on fitting the observed SED from *Herschel* observations, assuming a model in which the dust composition mixture is dominated by ice and silicates (Pawellek & Krivov 2015). The SONS results support a similar behaviour, although with a larger scatter than seen in the *Herschel* data and a lower number of resolved sources. Some of the difference between the SCUBA-2 and *Herschel* results is to be expected due to the different methods used to measure the resolved disc sizes. The *Herschel* papers listed above all fit narrow rings to the data, whilst in this paper 2D Gaussians are adopted. In cases where the disc is wide, a Gaussian fit will tend to give a radius closer to the outer radius, whereas a narrow ring fit will give a radius close to that dominating the emission and hence closer to the equivalent blackbody radius.

There are two prominent (high) outliers in the plot with ratios above a value of 10 (namely HD 15745 and HD 21997). As discussed in Section 5.12, the disc around HD 15745 appears to be extended at 850 µm, but shows no such morphology at far-IR wavelengths (appearing unresolved in *Herschel*/PACS 100 µm and 160 µm observations). The scattered light image (Kalas et al. 2007b; Schneider et al. 2014) seems to suggest that the disc does extend to a radius close to that seen in the SCUBA-2 image (∼500 au), although the scattered light disc has a PA of ∼22.5°, com-

pared to the ∼164° from the SONS 850 µm image. It is unclear what could cause such a discrepancy, although it has been hypothesised that it may be related to interstellar winds (Schneider et al. 2016). HD 21997 is only marginally resolved based on an extended 3σ contour to the south (Section 5.15). Nonetheless, a previous multi-wavelength analysis does suggest the possibility of a disc extending to at least 490 au (Moór et al. 2013), and it is likely that the radius ratio is so high because the disc is very wide and the SED is dominated by warmer grains at the inner edge (∼50 au).

Vega, on the other hand, has a low ratio of 0.52 based on the fitted 850 µm image (or 0.28 based on the 450 µm image), meaning that the observed disc is significantly smaller than that implied assuming the dust grains are radiating as pure blackbodies. As discussed in Section 5.44, one possibility is that there is undetected, low-level emission in the SONS images, extending well beyond the lowest contours of the map, resulting in an underestimate for the measured radius of the disc. It is already known that the disc radius could extend to many hundreds of au (Su et al. 2005), and so it is possible that the far-IR emission (which sets the temperature) is dominated by halo grains at a radius significantly larger than the main belt (peaking around 200 − 300 au). This would, however, mean that the halo properties for Vega are different than those around other stars (e.g., AU Mic) in that such grains would have to be cooler than their blackbody equivalents. This remains an unexplained issue.

In summary, the median $R_{\rm fit}$ to $R_{\rm BB}$ ratio for all the targets is 3.8 (or 3.6 if the high and low outliers are excluded). The greater than unity ratio in the vast majority of cases implies the existence of planetesimals at larger radii than those derived from a blackbody fit. There are several anomalies that still need to be explained, including both high ratio outliers such as HD 15745 and targets, such as Vega, that have a low ratio.

After the gas dissipates from a circumstellar disc, planetesimals need to be stirred to initiate a collisional cascade. Moór et al. (2015) investigate stirring in a number of massive discs (many of which are also in this survey). Fig. 29 shows a tentative decline in the measured radius of the resolved discs in the SONS sample as a function of the host star age. The red and blue lines represent "self-stirring" models[5] computed for the host stars with masses of 1 $M_\odot$ (red) and 2 $M_\odot$ (blue) and for three different scaling factors, x_m, adapted from Moór et al. (2015), and where x_m is the ratio of the assumed mass of the initial protostellar disc to the minimum mass Solar nebula. The results are also in agreement with Moór et al. (2015) in that that self-stirring can explain large discs but only around old systems. For young stars with discs extending out to radii of greater than ∼100 au, planet stirring is currently the only explanation for the detection of dust at such large distances from the star. In this survey such an explanation would apply to the discs detected around 49 Cet, HD 15745, HD 21997, 44 Ser, γ Oph, HD 170773 and HR 8799.

[5] To achieve "self-stirring" requires the formation of Pluto-sized planetesimals.

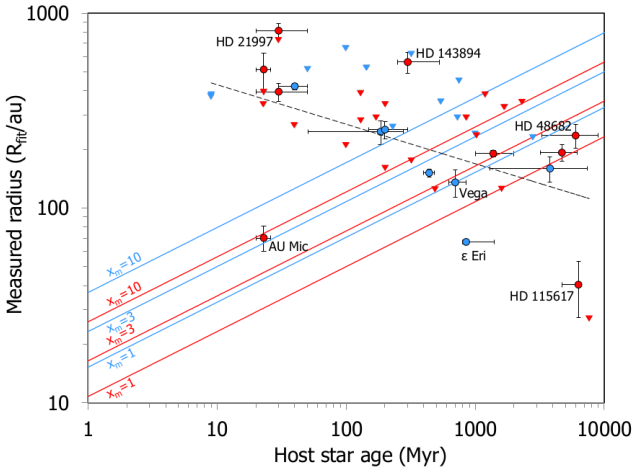

Figure 29. The measured radius as a function of host star age for the 16 targets in the SONS survey for which the disc radius was resolved, as represented by the red and blue circles (with error bars). The inverted triangles are upper limits to the radius for the cases in which the disc is unresolved. For both the circles and triangles, red symbols represent stars in the mass range of 0.3 − 1.5 $M_\odot$, whilst blue covers the 1.5 − 3.3 $M_\odot$ range. The red and blue lines represent self-stirring models computed for the host stars with masses of 1 $M_\odot$ (red) and 2 $M_\odot$ (blue) and for three different scaling factors, x_m, adapted from Moór et al. (2015). The dashed line is a fit to the resolved disc data points, and tentatively indicates a decline in disc radius as a function of stellar age $\propto t^{-0.2}$, where t is the host star age.

6.3 Spectral slopes and grain properties

There are many instances where the absence of photometric data beyond 160 µm means that the critical wavelength (λ_0) and the dust emissivity index (β) are degenerate and independent constraints are not possible. The 850 µm (and 450 µm, when available) data greatly improve this situation for the majority of the targets in the SONS survey. Fig. 30 shows a combined contour plot of the 3σ constraints on β against λ_0 for all the detections in the survey, using the SED modelling described in Section 4.2. The plot highlights that whilst there are plenty of systems in which λ_0 could be quite long (and hence β quite high), where there are constraints they tend to be around $\lambda_0 \sim 100 - 300$ µm and $\beta \sim 0.5 - 1.0$. Since it is unlikely that λ_0 will be much greater than 300 µm, this assumption means that there are reasonable constraints on β being less than 1.5. The spectral index (defined as α, where $\alpha = 2 + \beta$) of grains in the interstellar medium typically has a value of $\alpha = 4$ (i.e., $\beta = 2$) whilst debris discs tend to have shallower spectral indices (smaller β), as shown by the majority of discs having $\alpha < 4$ ($\beta < 2$) in Fig. 31. There are a few cases for which the spectral index could approach 4 or more, based on the range of β values derived from the SED modelling. Such a steep spectrum, if confirmed, could signify a disc dominated by small grains, most likely not greater than 10 µm in size (Ertel et al. 2012; Booth et al. 2013).

It is clear that there is a paucity of data between 160 µm and 850 µm for all but the brightest discs. For example, the *Herschel*/SPIRE data at 250 µm, 350 µm and 500 µm reach the background confusion limit too quickly for fainter disc candidates to be confirmed, and so the SCUBA-2 450 µm

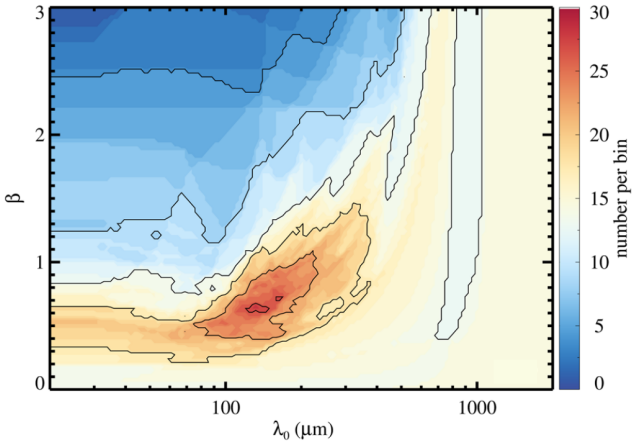

Figure 30. The 3σ constraints of dust emissivity (β) plotted against critical wavelength (λ_0) for all the detections in the SONS survey. The contours are at levels of 5, 10, 15, 20, 25 and 30.

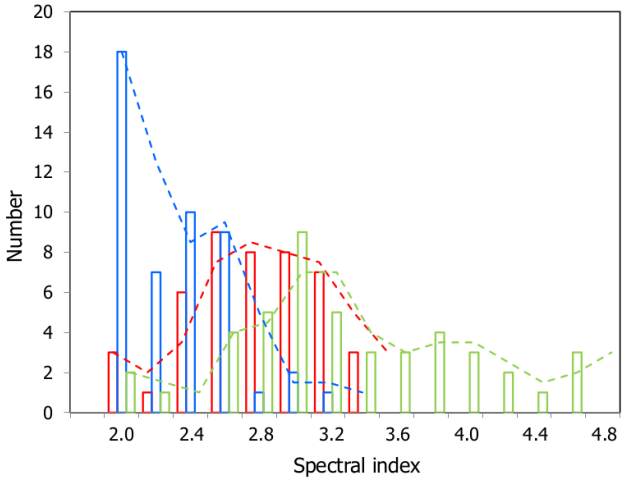

Figure 31. Histogram of the spectral indices derived from the SED modelling. The three coloured bars represent the range of α ($\alpha = 2 + \beta$) based on the derived β values (blue the minimum value, red the median and green the maximum of the range).

data potentially become critical in sampling this important region of the SED for debris discs. In addition, the fact that the 450 μm and 850 μm data are obtained simultaneously with SCUBA-2 means that systematic biases in flux calibration *should* impact both wavelengths in the same way. This inherent behaviour would suggest that any high spectral indices derived directly from the ratio of 450 μm to 850 μm fluxes would appear to be genuine, but defy interpretation in terms of our understanding of the dust size distribution for discs. From the SONS survey, there is only one example in which the spectral index, derived directly from the 450:850 flux ratio, is 4 or higher, namely HD 76582. This source has a spectral index of 4.3 ± 1.5, with the estimated error representing a significant uncertainty in the value derived. There are also examples from *Herschel* observations where a steep spectrum is observed beyond 70 μm (Ertel et al. 2012). Further data are needed to confirm disc signatures and to improve the S/N of (at least) some of the 450 μm detections to make any definitive conclusions.

The use of the modified blackbody is a simplified way of taking into account the absorption and emission efficiencies of the grains in the disc (Backman & Paresce 1993). The radiative efficiency of individual grains depends on a variety of different properties including the molecular composition, molecular structure, size and porosity (e.g. Draine 2006). Even if it is assumed that the composition and structure of particles is the same throughout the disc, there will be a distribution of particle sizes, and, potentially, grains at a wide variety of distances from the star. Hence, the shape of the SED for the disc as a whole will depend on the summation of the emission from particles at a range of temperatures (Backman & Paresce 1993; Gáspár et al. 2012). Resolved images can help break this degeneracy. For example, the low β value for AU Mic is largely due to the main belt being wide, extending from ∼8 au to 40 au, with a halo of small grains beyond this radius (Matthews et al. 2015; Schüppler et al. 2015). This means there are grains at a wide range of temperatures contributing to the SED fit, resulting in a shallow spectral slope that masks any size distribution effects. Conversely, if it is known that the ring is narrow then the spectral slope is likely to be largely due to the size distribution (Draine 2006). For a small sample of discs, MacGregor et al. (2016a) found values of β between roughly 0.4 and 1.1, and showed how these suggest size distributions with power law indices around 3.4, slightly less than the canonical Dohnanyi et al. (1969) value of 3.5, and considerably less than the values predicted by Gáspár et al. (2012) and Pan & Schlichting (2012), taking into account more complicated physical processes. The authors propose that a wavy size distribution is a possible cause of these lower β values. The SONS survey larger sample backs up the results of MacGregor et al. (2016a) as most discs have β values in the $0.4 - 1.1$ range.

6.4 Flux peak offsets

As discussed in Section 5 a significant number of detections show emission offset from the star, at a distance not explainable by positional errors. The statistical uncertainty in a position is commonly expressed by $0.6\,\theta\,(\mathrm{S/N})^{-1}$ (Ivison et al. 2007), where θ is the FWHM of the telescope beam, and S/N is the peak signal-to-noise ratio, under the assumption of Gaussian noise properties in the maps. In addition, there is also a potential error associated with the telescope pointing accuracy, which being uncorrelated, is added in quadrature with the positional error. In the case where a target is observed over multiple nights, leading to several hours of integration time, it is possible that cumulative pointing errors may conspire to create an artificial offset between the star and the disc. No correlation, however, has been found between the magnitude of the offset and the total number of observations.

As an example, taking the RMS pointing accuracy of the telescope as 2″ in azimuth and elevation[6], then at 850 μm the overall positional uncertainty for a peak detected at 4σ should be no greater than 3.5″ for the effective FWHM beam size of 15″ (after smoothing). Fig. 32 shows the measured

[6] See: http://www.eaobservatory.org/jcmt/about-jcmt/

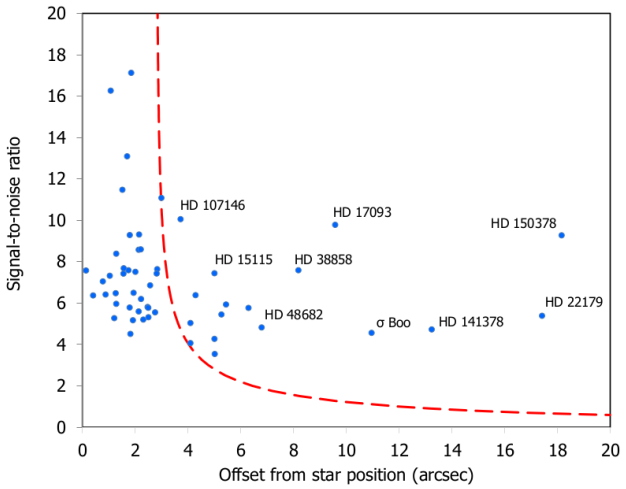

Figure 32. The offset of the flux peak from the star position as a function of S/N at 850 µm measured from the SONS survey images. The red curve represents the expected positional offset based on the statistical uncertainties and RMS telescope pointing errors of 2″ in both azimuth and elevation. The peaks detected in the vicinity of HD 22179, HD 17093, σ Boo, HD 141378 and HD 150378, are all believed to be background objects.

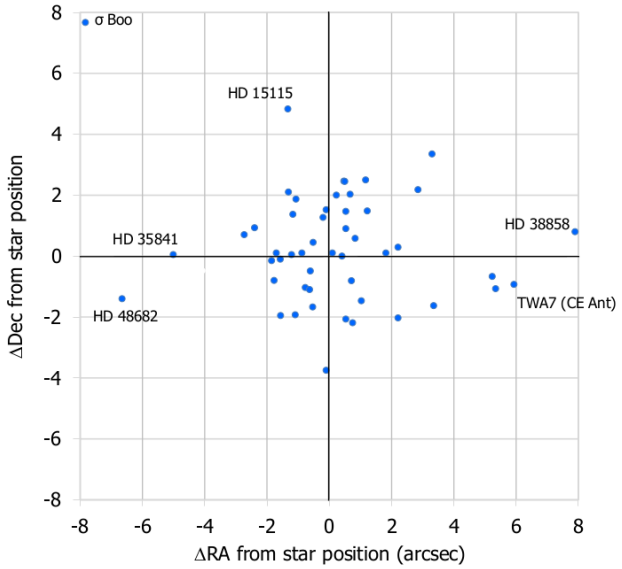

Figure 33. Correlation between the measured difference in RA and dec of the flux peak from the stellar position for the SONS survey sample. The names of some of the stars that show a significant offset in RA or dec are also given. Three of the extreme offset cases (as indicated in Fig. 32, namely HD 17093, HD 22179 and HD 150378) are not shown.

offset of the flux peak from the stellar position as a function of the peak S/N of the detection[7]. Also plotted (red line) is the expected positional offset based purely on the statistical uncertainties and a RMS telescope pointing error of 2″ in both azimuth and elevation. As can be seen the majority of the points lie to the left of the curve, suggesting that the pointing accuracy of the telescope is routinely better than 2″ in both axes (which based on the pointings in this survey, taken prior to target observations, seems to be the case). In some of the more extreme cases (i.e., HD 17093, HD 22179, σ Boo, and HD 150378), where the offset is ∼10″ or more, it is very unlikely that the detected peak is associated with the star (as discussed for individual cases in Section 5). In total, 12 out of 49 peaks fall strictly outside the expected positional error (not including the five extreme cases) based on the statistical and nominal telescope pointing uncertainties.

Why there are so many "offset" disc cases remains a mystery. Fig. 33 shows the measured difference in RA and dec of the flux peak from the stellar position (ensuring corrections are made for the proper motion of the star). It is interesting to note that there is a slight tendency for the offsets to occur predominantly in RA, i.e., in an east-west direction in the images. Periodic tracking errors from the telescope are ruled out as the the JCMT is an Alt-Az mounted telescope, and indeed, rebinning a selection of the offset case datasets in an Azimuth-Elevation coordinate frame showed no indication of any preferential positional shift. Some of these cases have speculative (i.e., unproven) explanations, usually citing the possible presence of a background source as in the case of several of the more extreme offset cases shown (see Section 6.5). The association of an offset peak with a putative disc about the star can also have a physical explanation. For instance, such emission might indicate a perturbed disc that could have detectable volatiles. Within the SONS survey sample there are a few examples of systems containing molecular CO gas, including the young (<50 Myr) A-stars HD 21997 and 49 Ceti (Zuckerman et al. 1995; Moór et al. 2011a). No CO, however, has been detected around HD 38858, the most extreme offset disc in the sample that is not believed to be a background object based on current understanding (Kennedy et al. 2015).

6.5 Background contamination

At the sensitivity levels achieved within the SONS survey (e.g., an average 1σ noise level of 1.2 mJy/beam at 850 µm in the central 3 arcmin^2 region), images will have some level of "contamination" by high redshift galaxies (submillimetre galaxies; SMGs). Indeed, SMG occurrence is a growing issue in terms of the interpretation of debris discs as surveys go deeper. There are a number of examples in the SONS survey where asymmetric features or close-by peaks could be due to background galaxies. An example is the disc around q^1 Eri (Fig. A2a) as already discussed in Section 5.5. In this case, 870 µm observations with APEX/LABOCA (Liseau et al. 2010) showed evidence of the east-west extension, which was very clearly seen by SCUBA-2, and identified as an isolated point-source at shorter wavelengths by *Herschel* (Liseau et al. 2010).

It is possible to estimate the chances of a background galaxy lying, say, within a half-beam distance from the star of interest. Assuming an average detection threshold of 4 mJy (3σ) at 850 µm, the source count number is ∼1400 per sq. degree (e.g., Blain et al. 1999). This surface density

[7] For HD 207129 and Fomalhaut the offset is measured from the geometric centre between the two peaks, i.e., it is assumed that the emission is distributed in a ring about the star. Likewise, for ϵ Eri the offset is measured from the geometric centre of the dust ring.

corresponds to ∼2.1 sources in the 3 arcmin^2 central area of a SONS field. Alternatively, simply counting the number of 3.5σ peaks in the same area (avoiding the central region of radius 15″, i.e., a distance of ∼2 beam radii from the star), gives an average of 2.3 peaks per field, in good agreement with the galaxy count models. Therefore, the probability of a background galaxy lying within a half-beam distance of any star is crudely estimated to be around 5 per cent. This expectation means that 2–3 fields within the SONS sample could have a background galaxy within a half-beam distance of the star. Based on the discussion outlined for individual targets in Section 5, there are potentially as many as nine out of the 49 cases (ignoring the five extreme offsets and Algol) for which the interpretation of a disc structure could be influenced by a background object. The stars for which the observed structure (or part thereof) is believed to be a background object, supported by multi-wavelength imaging, are q^1 Eri, ϵ Eri, HD 107146 and σ Boo, whilst those which require further investigation are HD 38858, HD 92945, HD 104860, HD 127821, and HD 205674.

Finally, the SONS survey amounts to 100 fields of ∼10 arcmin^2, equating to ∼3 deg^2 of total area. Even though the use of the DAISY mode means that the noise increases almost linearly with radius outside the central 3 arcmin^2 region (estimated maximum 1 σ noise level of 2 mJy/beam at the edge of the field; Holland et al. 2013), this performance still represents a significant depth and area to carry out an unbiased survey count of SMGs. Such a study is planned in the future.

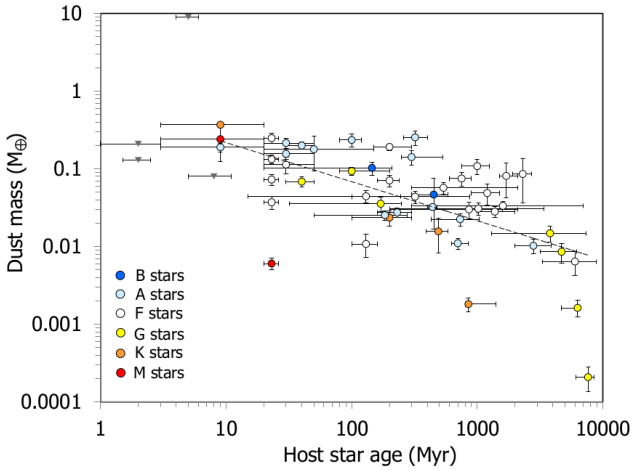

Figure 34. The derived dust mass variation with host star age for the SONS survey sample. The circular symbols represent the dust mass estimates for the debris discs in the SONS sample (all the stars have estimated ages of > 9 Myr). A fit to the SONS results (shown by the dashed line) suggests a decline in dust mass according to $0.8t^{-0.5}$, where t is the host star age. The inverted grey triangles represent the approximate 3 σ mass sensitivity levels from recent published surveys of circumstellar discs within clusters/associations: Upper Scorpius around 8 ± 3 Myr (Barenfeld et al. 2016), λ Orionis around 5 ± 2 Myr (Ansdell et al. 2015), Lupus 2 ± 1 Myr (Ansdell et al. 2016) and Chamaeleon I around 2 ± 0.5 Myr (Pascucci et al. 2016). Although these targets are mainly classified as pre-main sequence protoplanetary discs, it should be noted that some debris disc candidates are also contained in the Upper Scorpius sample.

6.6 Disc mass evolution

In describing how a disc evolves the key parameters to investigate are how the fractional luminosity (f) and the dust mass (M_d) vary with stellar age. Understanding how stellar ages are derived and the accuracy (and consistency) of the results is fundamental in this regard (Zuckerman & Song 2004). Different diagnostics can give conflicting results (Moór et al. 2006) and so conclusions about disc evolution depend on stellar ages being determined in a consistent manner. The values adopted in this paper, and referenced for individual stars in Section 5, have been deliberately conservative in terms of the quoted uncertainties in stellar age. For the cases in which no age uncertainty is available, a value of ±25 per cent has been adopted.

Emission from debris discs is expected to diminish over time as the reservoir of large planetesimal bodies is depleted and the collisional timescales increase (Wyatt 2008). Fig. 34 shows how the dust mass, calculated from the 850 μm flux and the dust temperature derived from the SED fit, varies with stellar age for the SONS survey sample (circular symbols). The largest measured dust masses within the sample over the range 10 to 10000 Myr are around 0.4 M$_\oplus$, whilst the smallest are around the two old G-stars, namely HD 115617 and τ Cet, with a minimum value of 2 $\times 10^{-4}$ M$_\oplus$) for the latter. Although there is considerable scatter (as shown by the errors), the general trend is for a decline in dust mass as the star gets older according to $\sim t^{-0.5}$, where t is the host star age. This trend is less steep than expected from a condition of steady-state collisional evolution in which $M_d \propto t^{-1}$ (Wyatt 2008). As discussed in Panić et al. (2013), there is, however, a degree of uncertainty in this interpretation due to observational bias. As shown in Fig. 35, the younger stars in the sample tend to be more distant, meaning that the mass sensitivity for these targets is lower than for older, but closer stars (around which low-mass discs are easier to detect). This effect can certainly be seen in Fig. 34 for a few very old stars with derived masses lower than 0.01 M$_\oplus$, but not around younger stars since such stars are more distant. Hence, it is likely that at least some of the variation seen in the dust mass with stellar age plot is due to an observational bias, and not a true indication of disc mass evolution.

In more general terms, the mass in millimetre-sized grains within circumstellar discs has previously been shown to apparently decline sharply in the period around 10 Myr (generally considered to be the "transitional phase" between protoplanetary and debris discs, Wyatt 2008), experiencing a drop of at least two orders of magnitude to the level shown for the youngest stars (e.g. Panić et al. 2013). It is suggested that this age may represent a period of rapid accretion of material onto planetesimals, potentially one of the final phases in the evolution of a transition disk to a debris disc (Wyatt et al. 2015).

Until the recent advent of interferometers the mass sensitivity of single-dish telescopes in the submillimetre was rather limited for protoplanetary discs since they tend to be more distant (e.g., 2 kpc for Taurus) than the debris discs chosen in most surveys (e.g., for SONS, the criterion was a distance of <100 pc). The new surveys with SMA and

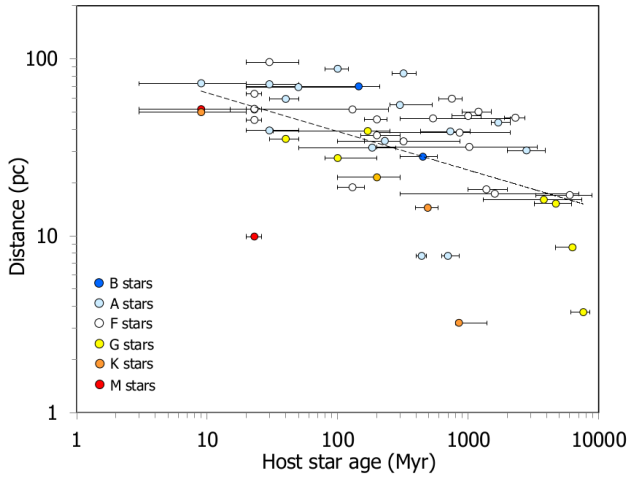

Figure 35. Distance of the star plotted against host star age for the SONS survey sample. The dashed trend line ($\propto t^{-0.2}$) illustrates the bias of younger stars being more distant within the survey sample.

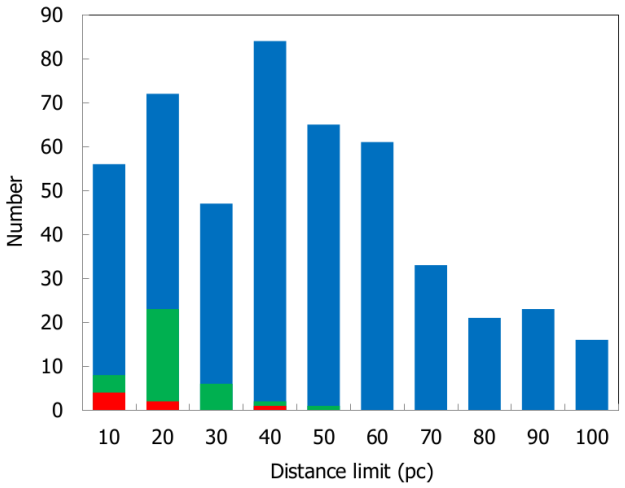

Figure 36. Histogram of the known planet hosts (blue bars) in distance bins of 10 pc from the Sun (Han et al. 2014) (i.e. the distance bin labelled "10" contains stars up to 10 pc distance from the Sun). The green and red bars represent the stars that have both known planets and detected debris discs based on recent *Herschel* surveys (Marshall et al. 2014a; Moro-Martín et al. 2015) and the SONS survey, respectively.

ALMA have shown mass sensitivities to levels as low as, for example, $\sim$0.1 $M_\oplus$ for the Upper Scorpius OB association (Barenfeld et al. 2016). Fig. 34 also shows the 3σ mass sensitivity from a number of recent such surveys of early circumstellar disc candidates (denoted by the inverted grey triangles in the plot). The improved mass sensitivity now suggests the decline in mass is not as steep as previously suggested i.e., the concept that protoplanetary discs suddenly dissipate at $\sim$10 Myr is no longer strongly supported by the data. Given that there also debris discs in the recent interferometer surveys of young associations, it is likely that some such discs form at a much earlier stage than previously believed (<10 Myr), and therefore co-exist with protoplantary discs within star-forming regions. Finally, the significant fraction of the mass is expected to be contained in larger (km-sized) planetesimals, particularly for debris discs, and so the total mass of the disc may be considerably higher than the estimates presented in this paper.

Future surveys might target younger stars, allowing us to quantify how disc properties, such as the size distribution and mass, vary with age, at stages when the evolution of these properties is most rapid. At such ages, the discs may not yet have reached equilibrium following the dispersal of the protoplanetary disc, a point that would be evidenced in a difference in the properties derived for the youngest discs in this sample. For example, ALMA observations of the young disc HD 21997 have shown that whilst the dust emission is consistent with a debris disc (i.e., the fractional luminosity is too low for a protoplanetary disc), it also hosts a CO disc (Greaves et al. 2016), with well-defined Keplerian rotation that may be primordial (Kóspál et al. 2013). It is not unequivocal that systems do take on "debris-like" dust properties before the primordial gas is dispersed, and it is clear from the most recent surveys that there is a less significant change in the bulk of the millimetre-sized grains over a short period of time around the 10 Myr mark than previously hypothesised (Panić et al. 2013).

6.7 Planet hosts

As outlined in Section 2 the targets in the SONS survey are selected on detectability at 850 µm and distance, and hence do not represent a comprehensive exoplanet sample (i.e. it is a reasonably unbiased sample with respect to known disc-planet occurrences). There are, however, ten known planet hosts in the sample (as summarised in Table 6 and including the τ Ceti planetary system and planet "b" around ϵ Eridani, which remain controversial) with seven having a detected debris disc based on the observations carried out in this survey. A Fisher exact probability test (Fisher 1922), carried out on the planet/disc data within the survey, suggests the likelihood of the planet-hosting stars having a higher disc frequency than the rest of the sample is only 7.7 per cent. Three other planet hosts were not detected within the SONS survey, HD 82943 (Kennedy et al. 2013), GJ 581 (Lestrade et al. 2012), and HD 113337 (Su et al. 2013), all of which have known debris discs from *Herschel* observations, but were too faint to be detected at 850 µm based on the current observations. The majority of stars with known planets and a debris disc are naturally chosen to be close to the Sun, as shown in Fig. 36 for both SONS and recent *Herschel* surveys (Marshall et al. 2014a; Moro-Martín et al. 2015). It is also the case that the few directly-imaged exoplanets (i.e. HD 216956 and HR 8799) are also found in debris systems. Indeed, with the exception of these systems, the planets discovered tend to be on orbits of just a few astronomical units and so will have little influence on discs with size-scales of 50 au or more (see Table 6).

Other work has derived detection rates for disc systems around planet-hosting stars of 20 − 30 per cent, based on more targeted surveys of planet hosting stars using *Spitzer* and *Herschel* surveys (Trilling et al. 2008; Eiroa et al. 2013; Marshall et al. 2014a). Further studies identified possible trends between low-mass planets and the presence of cool dust (Wyatt et al. 2012). Since debris discs and planets form

Table 6. A summary of the information on the planet hosts in the SONS survey sample.

HD number	Other names	Planet name	Orbit semi-major axis (au)	Eccentricity	$Msini$ (M_{Jup})
10647	q[1] Eri	HD 10647 b	2.022 ± 0.082	0.16 ± 0.20	0.93 ± 0.24
10700	τ Cet	τ Cet b	0.105 ± 0.005	0.16 ± 0.22	0.006 ± 0.002
		τ Cet c	0.195 ± 0.011	0.03 ± 0.28	0.010 ± 0.005
		τ Cet d	0.374 ± 0.02	0.08 ± 0.26	0.011 ± 0.005
		τ Cet e	0.552 ± 0.03	0.05 ± 0.22	0.014 ± 0.007
		τ Cet f	1.35 ± 0.09	0.03 ± 0.26	0.021 ± 0.011
22049	ϵ Eri	ϵ Eri b	3.38 ± 0.32	0.25 ± 0.23	1.05 ± 0.19
38858		HD 38858 b	1.038 ± 0.019	0.27 ± 0.17	0.096 ± 0.012
82943		HD 82943 c	0.742 ± 0.013	0.43 ± 0.03	1.590 ± 0.103
		HD 82943 b	1.185 ± 0.022	0.20 ± 0.07	1.589 ± 0.097
113337		HD 113337 b	1.033 ± 0.035	0.46 ± 0.04	2.83 ± 0.24
115617	61 Vir	61 Vir b	0.050 ± 0.001	0.12 ± 0.11	0.016 ± 0.002
		61 Vir c	0.217 ± 0.004	0.14 ± 0.06	0.033 ± 0.004
		61 Vir d	0.475 ± 0.008	0.35 ± 0.09	0.072 ± 0.009
	GJ 581	GJ581 e	0.028 ± 0.001	0.03 ± 0.01	0.006 ± 0.001
		GJ581 b	0.041 ± 0.001	0.03 ± 0.01	0.050 ± 0.002
		GJ581 c	0.073 ± 0.002	0.07 ± 0.06	0.017 ± 0.001
216956	Fomalhaut	Fomalhaut b	115	0.12 ± 0.01	<0.5[1]
218396	HR 8799	HR 8799 e	14.5 ± 0.5	0	7 ± 3[1]
		HR 8799 d	24 ± 0	0.1	7 ± 3[1]
		HR 8799 c	38 ± 0	0	7 ± 3[1]
		HR 8799 b	68 ± 0	0	5 ± 2[1]

[1]The mass is not $Msini$ in this case, but model estimates based on their photometry.

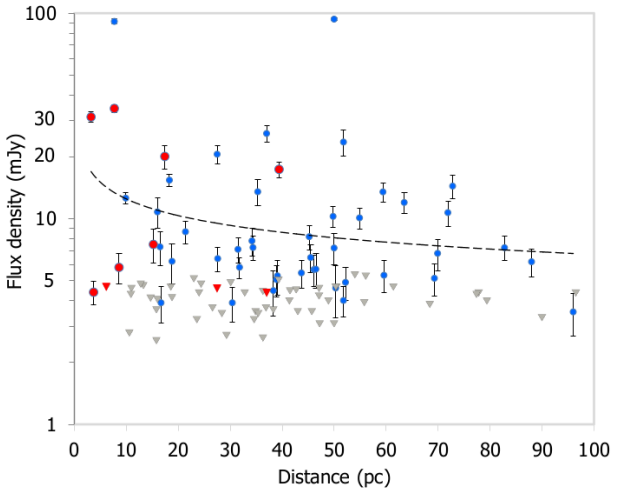

Figure 37. The measured 850 µm flux density against distance for the detected discs in the SONS survey. The blue circles represent disc detections, whilst the inverted triangles are the 3σ upper flux limits. The red filled circles and triangles indicate the known planet hosts in the sample. The dashed curve is a fit to the detected discs only as a function of distance.

and evolve together, the amount of solids present largely determines the outcome of each, implying that discs around planet hosting stars will be brighter than those around stars with no planets (Wyatt, Clarke & Greaves 2007). Fig. 37 shows the measured 850 µm flux density for all the detected SONS targets as a function of stellar distance. Based on the small number of planet hosts in this sample, there is no obvious evidence to support this hypothesis. A more recent study of 204 FGK stars also did not find any compelling evidence that debris discs are more common (or, indeed, more dusty) around stars harbouring planets (Moro-Martín et al. 2015). In the current era of planet hunting, dynamical studies of debris discs can provide a unique avenue for the detection of sub-Jupiter mass planets at large orbital radii (e.g., see Fig. 11 in Wyatt 2008).

7 CONCLUSIONS

The SONS survey has detected 850 µm emission from the vicinity of 55 stars in a sample of 100 targets. At least five of these detections are believed to be background sources, and one is thought to be due to radio emission variability rather than emission from a disc. The remainder trace dust grains up to a few millimetres in size and, by inference, the distribution of planetesimals around the host stars. The legacy of the survey is a catalogue of fluxes and images, and better characterisation of the detected discs via modelling of their SEDs to derive dust temperatures and masses. Key results from the SONS survey include:

1. The number of detected discs at 850 µm from single-dish telescope observations has doubled from 24 known pre-SONS (mainly from JCMT, CSO and APEX) to 49;
2. Approximately one-third (16 out of 49 detected discs) have been spatially resolved by the 850 µm beam of the JCMT, allowing a measurement of the disc size;
3. From the observed radial profiles, the discs are around 1 – 10 × the size of the Edgeworth-Kuiper belt in our own Solar System (assumed diameter of 100 au);
4. The majority of the measured 850 µm disc radii are substantially larger than expected based on the blackbody fit to the SED, implying the existence of planetesimals at large radii from the host stars;

5. The ratio of the observed (measured) disc radius to that derived from the blackbody fit also declines with stellar luminosity according to $L_*^{-0.2}$. This trend is consistent with the higher luminosity stars having removed the smallest grains, leaving behind relatively large (blackbody-like) dust grains;
6. The dust spectral index (α) is constrained to be between values of 2.5 and 3.5 for the vast majority of the discs in the SONS survey sample, less than the typical value of 4 found in the interstellar medium;
7. As surveys go deeper in terms of sensitivity, interpretation of disc structures becomes more difficult due to the inevitable contamination by background (notably high redshift) galaxies. There are a number of examples within SONS for which the presence of a background galaxy could help to explain the observed disc morphology;
8. The fractional dust luminosity covers the wide range of 10^{-1} to 10^{-5} compared to a value of $\sim 10^{-7}$ for the Edgeworth-Kuiper belt. All of the discs in the survey have f-values of less than the 10^{-2} threshold usually adopted for debris discs, with the exception of HD 98800 ($f \sim 0.1$) and is usually classified as a protoplanetary rather than a debris disc;
9. The most massive discs are around $0.5\,M_\oplus$ whilst the least massive are in the $10^{-2} M_\oplus$ range (with one exception, a tiny $2 \times 10^{-4}\,M_\oplus$). The least massive range of $10^{-2} M_\oplus$ is a similar level to the Edgeworth-Kuiper belt;
10. The amount of dust appears to decline roughly as $t^{-0.5}$, where t is the host star age, consistent with theories of steady state collisional evolution models (with the caveat that at least some of this variation may be due to an observational bias);
11. Although the SONS survey does not represent a planet-host sample, a disc detection around many of the nearest stars means that such systems will become key planet-search targets for the future.

Just as diverse outcomes of planetary system architectures are now recognised (e.g., via Kepler; Batalha 2014), so have recent debris disc surveys (including SONS) revealed a large diversity in disc geometries. The observed diversity in exo-planetary system architectures implies that the debris material should be distributed in different ways. Establishing how varied debris discs are is thus a key piece of information that will help link the formation and evolution of planetary systems with the evolution of planetary building blocks (planetesimals). Building such empirical bridges between discs and planets brings us closer to unravelling the physical processes that led to the formation of planetary systems. Surveys such as SONS, via the study of the location, mass, morphology, and dust properties of these discs, highlight the submillimetre as an important waveband to address these questions. One of the key legacy goals of the SONS survey was indeed to lay the foundation for future, high angular resolution studies with existing and new facilities such as SMA, ALMA, and *JWST*, with a view, for example, to studying belts of planetesimals in fine detail.

ACKNOWLEDGEMENTS

During the period of these observations the James Clerk Maxwell Telescope was operated by the Joint Astronomy Centre on behalf of the Science and Technology Facilities Council of the United Kingdom, the National Research Council of Canada and the Netherlands Organisation for Pure Research. Additional funds for the construction of SCUBA-2 were provided by the Canada Foundation for Innovation. MCW acknowledges the support of the European Union through ERC grant number 279973. GMK is supported by the Royal Society as a Royal Society University Research Fellow. MB acknowledges support from a FONDECYT Postdoctoral Fellowship, project no. 3140479 and the Deutsche Forschungsgemeinschaft through project Kr 2164/15-1. JPM is supported by a UNSW Vice Chancellor's postdoctoral research fellowship. The work of OP is supported by the Royal Society through a Royal Society Dorothy Hodgkin fellowship. GJW gratefully acknowledges support from the Leverhulme Trust. This research has made use of the Exoplanet Orbit Database, the Exoplanet Data Explorer at exoplanets.org and the SIMBAD database operated at CDS, Strasbourg, France. The Starlink software (Currie et al. 2014) is currently supported by the East Asian Observatory. This research used the facilities of the Canadian Astronomy Data Centre operated by the National Research Council of Canada with the support of the Canadian Space Agency.

REFERENCES

Acke B. et al., 2010, A&A, 540, A125
Andrews S. et al., 2010, ApJ, 710, 462
Ansdell M., Williams J. P., Cieza L. A., 2015, ApJ, 806, 221A
Ansdell M. et al., 2016, ApJ, 828, 46
Ardila D. R. et al., 2004, ApJ, 617, L147
Aumann H. H. et al., 1984, ApJ, 278, L23
Aumann H. H., 2004, PASP, 97, 885A
Backman D., Paresce F., 1993, in Levy E. H., Lunine J. I., eds., Protostar and Planets III, University of Arizona Press, Tucson, p. 1253
Backman D. et al., 2016, ApJ, 690, 1522
Barenfeld S. A., Carpenter J. M., Ricci L., Isella A., 2016, ApJ, 827, 142
Batalha N., 2014, PNAS, 111, 35, 12647
Barrado y Navascués D., Stauffer J. R., Jayawardhana R., 2004, ApJ, 614, 386
Barrado y Navascués D., 2006, A&A, 459, 511B
Barry D. C., 1988, ApJ, 334, 436
Beichman C. et al., 2006, ApJ, 652, 1674
Benedict G. F. et al., 2006, AJ, 132, 2206
Béthermin M. et al., 2012, A&A, 542, 58
Bintley D. et al., 2014, in Holland W. S., Zmuidzinas J., eds., Proc SPIE Conf. Ser. Vol. 9153, Millimeter, Submillimeter and Far-Infrared Detectors and Instrumentation for Astronomy VII, SPIE, Bellingham, p.3
Blain A. W., Smail I., Ivison R. J., Kneib J.-P., 1999, ApJ, 512, L87
Boley A. C. et al., 2012, ApJ, 750, L21
Bonfanti A., Ortolani S., Piotto G., Nascimbeni V., 2012, A&A, 575, A18
Bonsor A. et al., 2013, MNRAS, 431, 3025
Booth M. et al., 2009, MNRAS, 399, 385
Booth M. et al., 2013, MNRAS, 428, 1263
Booth M. et al., 2016, MNRAS, 460, L10

Booth M. et al., 2017, MNRAS, in press (arXiv:1705.01560v1)
Bryden G. et al., 2000, ApJ, 705, 1126
Burns J. A., Lamy P. L., Soter S., 1979, Icarus, 40, 1
Butler R. P. et al., 2006, ApJ, 646, 505
Carpenter J. et al., 2005, AJ, 129, 1049C
Carpenter J. et al., 2009, ApJS, 181, 197
Chapin E. L. et al., 2013, MNRAS, 430, 2545
Chavez-Dagostino M. et al., 2016, MNRAS, 462, 2285
Chen C. H. et al., 2005, ApJ, 634, 1372
Chen C. H. et al., 2008, ApJ, 689, 589
Chen C. H. et al., 2014, ApJS, 211, 25C
Choquet E. et al., 2016, ApJ, 817, 2C
Choquet E. et al., 2017, ApJ, 834, 12C
Chrysostomou A., 2010, Highlights Astron., 15, 797
Cieza L. A. et al., 2013, ApJ, 762, 100
Corder S. et al., 2009, ApJ, 660, L65
Churcher L., Wyatt M. C., Smith R., 2011, MNRAS, 410, 2
Cultri R. M. et al., 2003, 2MASS All Sky Catalog of point sources, NASA/IPAC Infrared Science Archive
Currie M. J., Berry D. S., 2013, Starlink User Note 95, KAPPA Kernel Application Package, Joint Astronomy Centre, Hilo, Hawaii
Currie M. J. et al., 2014, in Manset N., Forshay P., eds., ASP Conf. Ser, Vol 485, Astronomical Data Analysis Software and Systems XXIII, Astron. Soc. Pac., San Francisco, p. 391
David T. J., Hillenbrand L. A., 2015, ApJ, 804, 146
Dempsey J. T. et al., 2013, MNRAS, 430, 2534
Dent W. R. F., Walker H. J., Holland W. S., Greaves J. S., 2000, MNRAS, 314, 702
Dent W. R. F. et al., 2013, PASP, 125, 477
Dent W. R. F. et al., 2014, Science, 343, 1490
Deschamps R. et al., 2015, A&A, 577, A55
Desidera S. et al., 2011, A&A, 529, 54
Di Folco E. et al., 2004, A&A, 426, 601
Dohnanyi S. et al., 1969, JGR, 74, 2531
Doyon R. et al., 2010, in Boccaletti A., ed., Proc. Conf. In the Spirit of Lyoy 2010: Direct Detection of Exoplanets and Circumstellar Disks, Univ. Paris Diderot, p. 42
Draine B. T., 2006, ApJ, 636, 1114D
Ducourant C. et al., 2014, A&A, 563, A121
Duchêne G. et al., 2014, ApJ, 784, 148
Dulk G. A., 1985, AR&A, 23, 169
Eiroa C. et al., 2013, A&A, 555, A11
Ertel S. et al., 2012, A&A, 541, 148
Farihi J., 2016, A&A, 541, 148
Fisher R. A., 1922, J. Royal Statistical Society, 85, 87
Fujiwara H. et al., 2012, ApJ, 759, 18
Fujiwara H. et al., 2013, A&A, 550, A45
Galicher R. et al., 2013, ApJ, 769, 42
Gáspár A. et al., 2012, ApJ, 754, 74G
Gibb A. G., Jenness T., Economu F., 2013, Starlink User Note 265, PICARD - A Pipeline for Combining and Analyzing Reduced Data, Joint Astronomy Centre, Hilo, Hawaii
Gillet F. C. et al., 1986, in Israel F., ed., Light on dark matter: Proceedings of the First Infra-Red Astronomical Satellite conference, D. Reidel Publishing Co., p. 61
Golimowski D. A. et al., 2011, AJ, 142, 30
Greaves J. S. et al., 1998, ApJ, 506, L133
Greaves J. S. et al., 2004, MNRAS, 351, L54
Greaves J. S. et al., 2005, ApJ, 619, L187
Greaves J. S., Hales A. S., Mason B. S., Matthews B. C., 2012, MNRAS, 423, L70
Greaves J. S. et al., 2016, ApJ, 791, L11
Greaves J. S. et al., 2016, MNRAS, 461, 3910
Habing S. et al., 2001, A&A, 365, 545
Han E. et al., 2013, PASP, 126, 827
Hatzes A. P. et al., 2000, ApJ, 544, L145
Heap S. et al., 2000, ApJ, 539, 435
Hillenbrand L. A. et al., 2008, ApJ, 677, 630
Hines D. C. et al., 2008, ApJ, 662, 1067
Holland W. S. et al., 1998, Nature, 392, 788
Holland W. S. et al., 1999, MNRAS, 303, 659
Holland W. S. et al., 2003, ApJ, 582, 1141
Holland W. S. et al., 2013, MNRAS, 430, 2513
Holmberg J., Nordström B., Anderson J., 2007, A&A, 475, 519
Holmberg J., Nordström B., Anderson J., 2009, A&A, 501, 941
Howard A. W., J., Fulton B. J., 2016, PASP, 128, 4401
Hughes A. M. et al., 2011, ApJ, 740, 38
Hughes A. M. et al., 2012, ApJ, 750, 82H
Hughes A. M. et al., 2017, ApJ, 839, 86
Ishihara D. et al., 2010, A&A, 514, 1I
Ivison R. J. et al., 2007, MNRAS, 380, 199
Jayawardhana R. et al., 1998, ApJ, 503, L79
Jenness T., Ecomomou F., 2015, Astron. Comput., 9, 40
Jenness T. et al., 2015, Astron. Comput., 12, 146
Jones J. et al., 2015, ApJ, 813, 58J
Jourdain de Muizon M. et al., 1999, A&A, 350, 875
Kalas P., Graham J. R., Clampin M. C., 2005, Nature, 435, 1067
Kalas P. et al., 2007, ApJ, 661L, 85
Kalas P., Duchene G., Fitzgerald M., Haghighipour P., Graham J. R., 2007, ApJ, 671, L161
Kalas P. et al., 2008, Sci, 322, 1345
Kalas P. et al., 2013, ApJ, 775, 56
Kennedy G. M., Wyatt M. C., 2011, MNRAS, 412, 2137
Kennedy G. M. et al., 2012, MNRAS, 426, 2115
Kennedy G. M. et al., 2013, MNRAS, 436, 898
Kennedy G. M., Wyatt M. C., 2014, MNRAS, 444, 3164
Kennedy G. M. et al., 2015, MNRAS, 449, 3121
Krivov A. V., 2015, RAA, 10, 383
Koerner D. W., Ressler M. E., Werner M. W., Backman D. E., 1998, ApJ, 503, L83
Koerner D. W. et al., 2000, ApJ, 533, L37
Koerner D. W., Sargent A. I., Ostroff N. A., 2001, ApJ, 560, L181
Koerner D. W. et al., 2010, ApJ, 710, 26
Kóspál Á. et al., 2009, ApJ, 700, L73
Kóspál Á. et al., 2013, ApJ, 776, 77
Krist J. E., Ardila D. R., Golimowski D. A., 2005, AJ, 129, 1008
Krist J. E. et al., 2010, ApJ, 140, 1051
Krist J. E. Stapelfeldt K. R., Bryden G., Plavchan P., 2012, AJ, 144, 45
Lagrange A. M., Backman D. E., Artymowicz P., 2000, in Mannings V., Boss A. P., Russell S. S., eds., Protostar and Planets IV, University of Arizona Press, Tucson, p. 639
Lawler S. M. et al., 2014, MNRAS, 444, 2665
Lebouteiller V. et al., 2011, ApJS, 196, 8L
Lee N., Williams J. P., Cieza L. A., 2011, ApJ, 736, 135
Lestrade J.-F., Mutel R. L., Preston R. A., Phillips R. B., 1988, ApJ, 328, 232
Lestrade J.-F. et al., 2012, A&A, 548, A86
Lestrade J.-F., Thilliez E., 2015, A&A, 576, A72
Liseau R. et al., 2008, A&A, 480, L47
Liseau R. et al., 2010, A&A, 518, L132
Liu M. C. et al., 2004, ApJ, 608, 526
Löhne T. et al., 2012, A&A, 537, A110
Low F. et al., 2005, ApJ, 631, 1170
MacGregor M. A. et al., 2013, ApJ, 762, L21
MacGregor M. A. et al., 2015, ApJ, 811, 47
MacGregor M. A. et al., 2016a, ApJ, 823, 79M
MacGregor M. A. et al., 2016b, ApJ, 828, 113M
MacGregor M. A. et al., 2017, ApJ, in press (arXiv:1705.05867v1)
Mamajek E. E., Hillenbrand, L. A., 2008, ApJ, 687, 1264
Mamajek E. E., Bell, C. P. M., 2014, MNRAS, 445, 2169
Marino S. et al., 2016, MNRAS, 460, 2933
Marino S. et al., 2017, MNRAS, 465, 2595
Marino S. et al., 2017, MNRAS, in prep.
Markwardt C. B., 2009, in Bohlender D. A., Durand D., Dowler

P., eds., ASP Conf. Ser. Vol. 411, Astronomical Data Analysis and Systems XVIII, Astron. Soc. Pac., San Francisco, p. 251
Marois C. et al., 2008, Science, 322, 1348
Marois C. et al., 2010, Nature, 468, 1080
Marsh K. A. et al., 2005, ApJ, 620, L47
Marsh K. A. et al., 2006, ApJ, 646, L77
Marshall J. P. et al., 2011, A&A, 529, A117
Marshall J. P. et al., 2014a, A&A, 565, 15N
Marshall J. P. et al., 2014b, A&A, 570, A114
Marshall J. P. et al., 2016, MNRAS, 459, 2893
Matrà L. et al., 2017, ApJ, in press (arXiv:1705.05868v1)
Matthews B. C. et al., 2007, PASP, 119, 855
Matthews B. C., Kalas P. G., Wyatt M. C., 2007, ApJ, 663, 1103
Matthews B. C. et al., 2014, in Beuther H., Klessen R. J., Dullemond C. P. Henning T., eds., Protostar and Planets VI, University of Arizona Press, Tucson, p. 521
Matthews B. C. et al., 2015, ApJ, 811, 100
Melis C. et al., 2010, ApJ, 717, L57
Miller B. A. et al., 2006, ApJ, 656, 1075
Milli J. et al., 2017, A&A, 597, L2
Monnier J. D. et al., 2012, ApJ, 761, L3
Montesinos B., Eiroa C., Mora A., Merín B., 2009, A&A, 495, 901
Montesinos B. et al., 2016, A&A, 593, A51
Moòr A. et al., 2006, ApJ, 644, 525
Moòr A. et al., 2011a, ApJ, 740, L7
Moòr A. et al., 2011b, ApJS, 193, 4
Moòr A. et al., 2013, ApJ, 777, L25
Moòr A. et al., 2015, MNRAS, 447, 577
Morales F. et al., 2011, ApJ, 730, 29
Morales F., Bryden G., Werner M. W., Stapelfeldt K. R., 2013, ApJ, 776, 111
Morales F., Bryden G., Werner M. W., Stapelfeldt K. R., 2016, ApJ, 831, 97
Moro-Martín A. et al., 2015, ApJ, 801, 143
Moshir M. et al., 1990, IRAS Faint Source Catalogue, version 2
Mouillet D., Lagrange A.-M., Beuzit J.-L., Renaud N., 1997, A&A 324, 1083
Najita J., Williams, J. P., 2005, ApJ, 635, 625
Nilsson R. et al., 2009, A&A, 508, 1057
Nilsson R. et al., 2010, A&A, 518, A40
Olofsson J. et al., 2016, A&A, 591, 108
Pace G. 2015, A&A, 551, L8
Pagano M., Truitt A., Young P. A., Shim S.-H., 2015, ApJ, 803, 90
Pan M., Schlichting H. E., 2012, ApJ, 747, 113P
Pan M., Nesvold E. R., Kuchner M. J., 2016, ApJ, 832, 81P
Panić O. et al., 2013, MNRAS, 435, 1037
Pascucci I. et al., 2016, ApJ, 831, 128
Pawellek N. et al., 2014, ApJ, 792, 65
Pawellek N., Krivov A. V., 2015, MNRAS, 454, 3207P
Perryman M. A. C. et al., 1997, A&A, 323, L49
Phillips N., 2011, Ph.D Thesis, University of Edinburgh
Plavchan P. et al., 2009, ApJ, 698, 1068
Pollack J. B. et al., 1994, ApJ, 421, 615
Quillen A. C., Thorndike S., 2002, ApJ, 578, L149
Reffert S., Quirrenbach A., 2011, A&A, 527, A140
Rhee J. et al., 2005, ApJ, 620, 1010
Rhee J. et al., 2007, ApJ, 660, 1556
Ricarte A. et al., 2015, ApJ, 744, 80
Ricci L. et al., 2015a, ApJ, 798, 124
Ricci L. et al., 2015b, ApJ, 813, 138
Richards M. T., Waltman E. B., Ghigo F. D., Richards D. P., 2003, ApJS, 147, 327
Riviere-Marichalar P., 2013, A&A, 555, A67
Roberge A. et al., 2013, ApJ, 771, 69
Roccatagliata V. et al., 2009, ApJ, 497, 409
Rodriguez D. R., Zuckerman B., 2012, ApJ, 745, 147R
Roseboom I. G. et al., 2013, MNRAS, 436, 430
Sadakane K., Nishida M., 1986, PASP, 98, 685
Schneider G. et al., 1999, ApJ, 513, L127
Schneider G. et al., 2006, ApJ, 650, 414
Schneider G. et al., 2009, AJ, 137, 53S
Schneider G. et al., 2014, AJ, 148, 59S
Schneider G. et al., 2016, AJ, 152, 64
Schütz O. et al., 2004, A&A, 414, L9
Schüppler Ch. et al., 2015, A&A, 581, A97
Sheret I., Dent W. R. F., Wyatt M. C., 2004, MNRAS, 348, 1282
Sibthorpe B. et al., 2010, A&A, 518, L130
Silverstone M. D., 2000, Ph.D. thesis, UCLA
Söderhjelm S., 1980, A&A, 89, 100
Song I., Caillault J.-P., Barrado y Navascués D., Stauffer J. R., 2001, ApJ, 546, 352
Song I., Zuckerman B., Bessell M. S., 2004, ApJ, 614, 125S
Soummer R. et al., 2014, ApJ, 786, L23
Stapelfeldt K. et al., 2007, in Kalas P., eds, the Spirit of Bernard Lyot: the Direct Detection of Planets and Circumstellar Discs in the 21st Century, University of California, Berkeley, CA, USA, 47
Stark C. C. et al., 2014, ApJ, 789, 58
Steele A. et al., 2016, ApJ, 816, 27
Stencel R. E., Backman D. E., 1991, ApJS, 75, 905
Su K. et al., 2005, ApJ, 628, 487S
Su K. et al., 2006, ApJ, 653, 675
Su K. et al., 2008, ApJ, 679, L125
Su K. et al., 2009, ApJ, 705, 314
Su K. et al., 2013, ApJ, 763, 118S
Sylvester R. J., Skinner C. J., Barlow M. J., Mannings V., 1996, MNRAS, 279, 915
Takeda G. et al., 2007, ApJS, 168, 297
Tanner A., et al., 2009, ApJ, 704, 109
Thebault P., Haghighipour N., 2016, arXiv:1406.1357v4
Thureau N. D. et al., 2014, MNRAS, 445, 2558
Torres G., Stefanik R. P., Latham D. W., Mazeh T., 1995, ApJ, 452, 870
Torres C. A. O., Quast G. R., Melo C. H. F., Sterzik M. F., 2008, in Reipurth, B., ed., Handbook of Star Forming Regions, Volume II: The Southern Sky, ASP Monograph Publications, Vol.5, p.757
Trilling D. et al., 2007, ApJ, 658, 1289
Trilling D. et al., 2008, ApJ, 674, 1086
Tuomi M. et al., 2013, A&A, 551, A79
van Leeuwen F., ed., 2007, Astrophysics and Space Science Library, Vol. 350, Hipparchos, the New Reduction of the Raw Data
Vican L., 2012, AJ, 143, 135
Vican L. et al., 2016, ApJ, 833, 263
Wahhaj Z., Koerner D. W., Sargent A. I., 2007, ApJ, 661, 368
Walker H. J., Butner H. M., 1995, Ap&SS, 224, 389W
Walker H. J., Wolstencroft R. D., 1988, PASP, 100, 1509
Wenger M. et al., 2000, A&AS, 143, 9
White J. A. et al., 2016, arXiv:1612.016481v1
Williams J. P. et al., 2004, ApJ, 604, 414
Williams J. P., Andrews S. M., 2006, ApJ, 653, 1480
Wilner D. J. et al., 2012, ApJ, 749, L27
Wilner D. J., Holman M. J., Kuchner M., Ho P. T. P., 2002, ApJ, 569, L115
Wright E. L. et al., 2010, AJ, 140, 1868
Wyatt M. C., Dermott S. F., Telesco C. M., 2000, in Garzon F. et al., eds., Disks, Planetesimals and Planets, ASP Conf. Ser., 219, 289
Wyatt M. C., Dent W. R. F., 2002, MNRAS, 334, 589
Wyatt M. C., 2003, ApJ, 598, 1321
Wyatt M. C. et al., 2005, A&A, 433, 1007
Wyatt M. C., 2006, ApJ, 639, 1153
Wyatt M. C., Clarke C. J., Greaves J. S., 2007, MNRAS, 380, 1737

Wyatt M. C. et al., 2007, ApJ, 663, 365
Wyatt M. C., 2008, ARA&A, 46, 339
Wyatt M. C. et al., 2012, MNRAS, 424, 1206
Wyatt M. C., Panić O., Kennedy G. M., Matrà L., 2015, Ap&SS, 357, 103
Zechmeister M. et al., 2011, A&A, 552, A78
Zorec J., Royer F., 2012, A&A, 537, A120
Zuckerman B., Becklin E. E., 1993, ApJ, 414, 793
Zuckerman B., Forveille T., Kastner J. H., 1995, Nature, 373, 494
Zuckerman B., Song I., 2004, ApJ, 603, 738
Zuckerman B., Rhee J. H., Song I., Bessell M. S., 2011, ApJ, 732, 61
Zuckerman B., Song I., 2012, ApJ, 758, 77

List of affiliations

[1]UK Astronomy Technology Centre, Royal Observatory, Blackford Hill, Edinburgh, EH9 3HJ, UK
[2]Institute for Astronomy, University of Edinburgh, Royal Observatory, Blackford Hill, Edinburgh, EH9 3HJ, UK
[3]National Research Council of Canada Herzberg Astronomy & Astrophysics Programs, 5071 West Saanich Road, Victoria, BC, V9E 2E7, Canada
[4]Department of Physics & Astronomy, University of Victoria, 3800 Finnerty Road, Victoria, BC, V8P 5C2, Canada
[5]Institute of Astronomy, University of Cambridge, Madingley Road, Cambridge, CB3 0HA, UK
[6]School of Physics and Astronomy, University of St. Andrews, North Haugh, St. Andrews, Fife, KY16 9SS, UK
[7]Instituto de Astrofisica, Pontificia Universidad Catolica de Chile, Vicua Mackenna 4860, 7820436, Macul, Santiago, Chile
[8]Astrophysikalisches Institut and Universität-Sternwarte, Friedrich-Schiller-Universität Jena, Schillergässchen 2-3, 07745 Jena, Germany
[9]Centre de recherche en astrophysique du Québec and Department de Physique, Université de Montreal, Montreal, QC, H3C 3J7, Canada
[10]Jet Propulsion Laboratory, California Institute of Technology, 4800 Oak Grove Drive, Pasadena, CA 91109, USA
[11]Department of Physics and Astronomy, James Madison University, MSC 4502-901 Carrier Drive, Harrisonburg, VA 22807, USA
[12]Space Telescope Science Institute, 3700 San Martin Drive, Baltimore, MD 21218, USA
[13]Centre for Astrophysics Research, Science and Technology Research Institute, University of Hertfordshire, College Lane, Hatfield, Herts, AL10 9AB, UK
[14]Joint ALMA Observatory, Alonso de Cordova 3107, Vitacura 763-0355, Santiago, Chile
[15]Astronomy Department, University of California, Berkely, CA, 94720-3411, USA
[16]Univ. Grenoble Alpes/CNRS, IPAG, F-38000 Grenoble, France
[17]Department of Physics & Astronomy, University of British Columbia, 6224 Agricultural Road, Vancouver BC V6T 1Z1, Canada
[18]JointAstronomy Centre, 660 N. A'ohōkū Place, University Park, Hilo, HI 96720, USA
[19]European Southern Observatory, Karl-Schwarzschild-Str. 2, D-85738 Garching, Germany
[20]Observatoire de Paris, PSL Research University, CNRS, Sorbonne Universités, UPMC, 61 Av. de l'Observatoire, F-75014 Paris, France
[21]School of Physics, UNSW Australia, High Street, Kensington, NSW 2052, Australia
[22]Australian Centre for Astrobiology, UNSW Australia, High Street, Kensington, NSW 2052, Australia
[23]Computational Engineering and Science Research Centre, Uuniversity of Southern Queensland, Toowoomba, QLD 4350, Australia
[24]Center for Astrophysical Sciences, John Hopkins University, Baltimore, MD 21218, USA
[25]School of Physical Sciences, The Open University, Milton Keynes, MK7 6AA, UK
[26]SRON Netherlands Institute for Space Research, NL-9747 AD Groningen, The Netherlands
[27]Department of Physics & Astronomy, University of California, Los Angeles, 90095, USA
[28]Jeremiah Horrocks Institute, University of Central Lancashire, Preston, Lancashire, PR1 2HE, UK
[29]Leiden Observatory, Leiden University, PO Box 9512, NL-2300 RA Leiden, The Netherlands
[30]RAL Space, The Rutherford Appleton Laboratory, Chilton, Didcot, OX11 0NL, UK
[31]Harvard-Smithsonian Center for Astrophysics, 60 Garden Street, Cambridge, MA, 02138, USA

APPENDIX A: THE SONS SURVEY IMAGES AND SPECTRAL ENERGY DISTRIBUTIONS

This Appendix presents the 850 μm S/N images from the SONS survey and spectral energy distributions together with model fits to the stellar photosphere and infrared to millimetre thermal (disc) excess. Unless otherwise stated the colours are scaled from -3σ to the maximum S/N in the images. Similarly the contours start at -3σ (dashed white) and then solid colours from 3σ to the maximum in 1σ steps. The white bar represents the spatial scale corresponding to the FWHM beam in astronomical units at the star. The "star symbol" represents the position of the star with respect to the disc, taking into account any proper motion corrections if required.

For the spectral energy distributions, the black symbols represent measured fluxes whilst the brown symbols are stellar photosphere-subtracted values (i.e. disc fluxes from the infrared to millimetre excess). Small green dots are the star-subtracted *Spitzer*/IRS spectrum (if it exists). The grey and black inverted triangles represent the 3σ upper flux limits (again, star-subtracted). Photometry from the SONS survey are highlighted by the blue circles.

This paper has been typeset from a TEX/LATEX file prepared by the author.

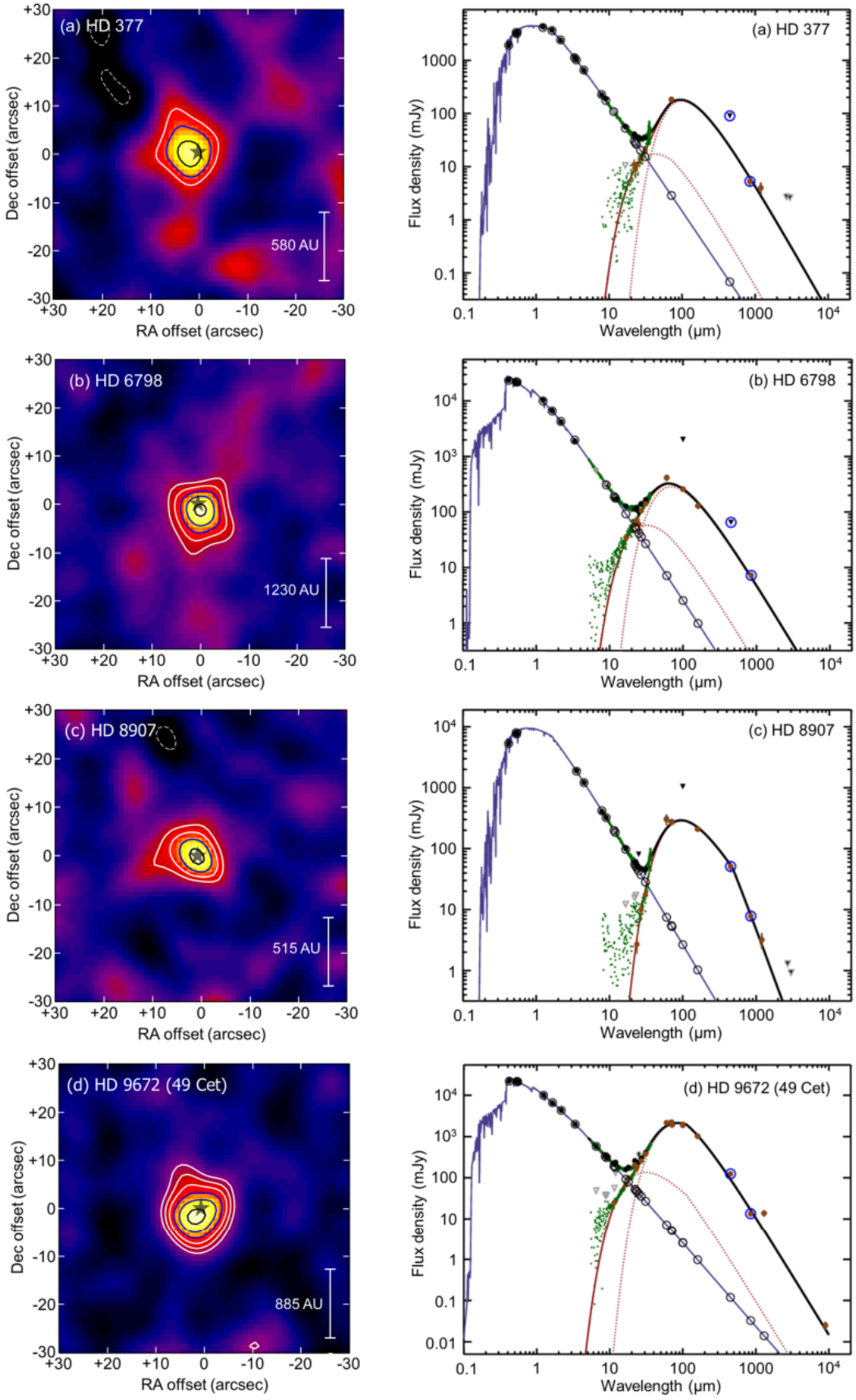

Figure A1. 850 μm S/N images and spectral energy distributions for the targets (a) HD 377, (b) HD 6798, (c) HD 8907 and (d) HD 9672 (49 Cet).

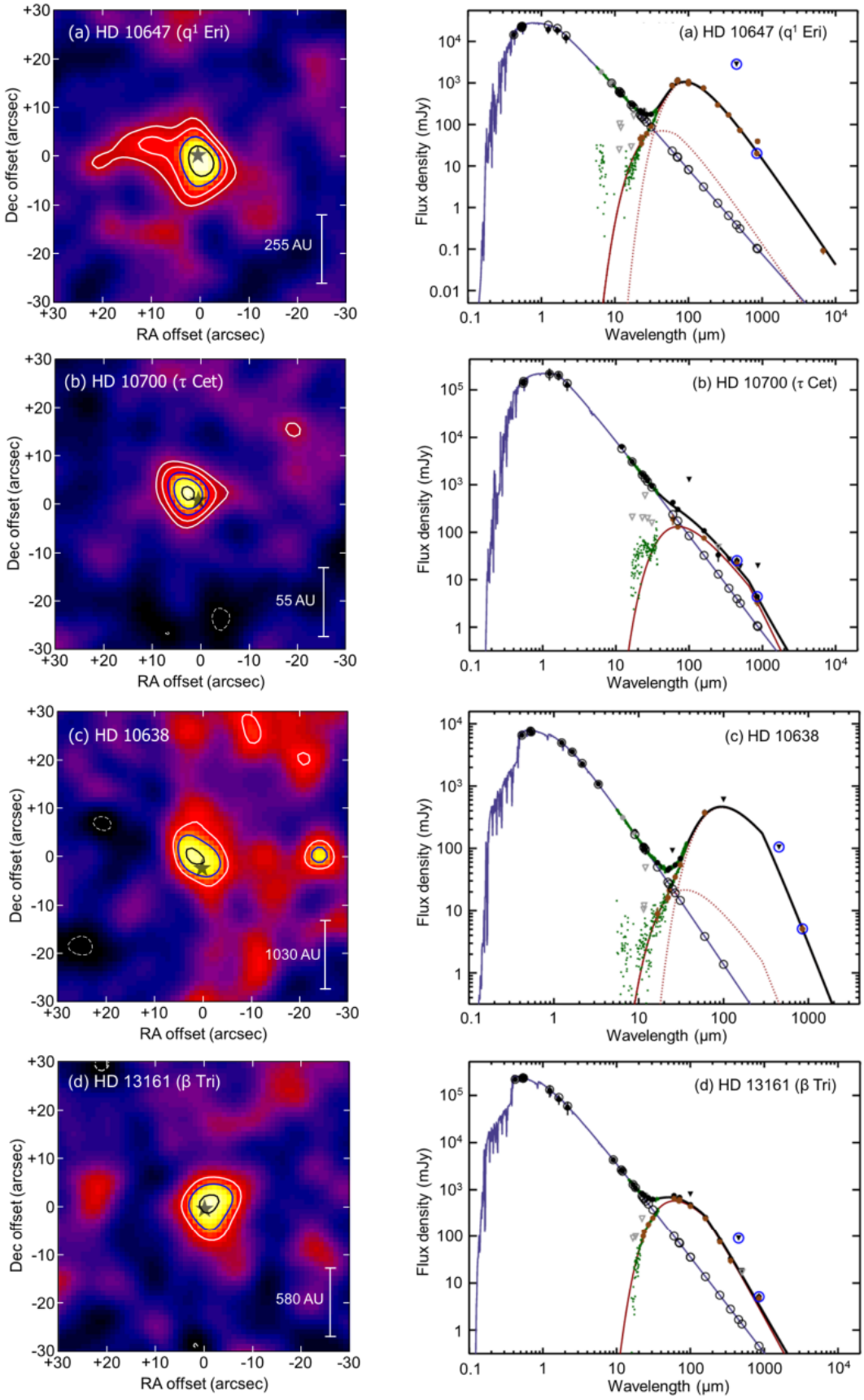

Figure A2. As for Figure A1 for the targets (a) HD 10647 (q^1 Eri), (b) HD 10700 (τ Cet), (c) HD 10638 and (d) HD 13161 (β Tri).

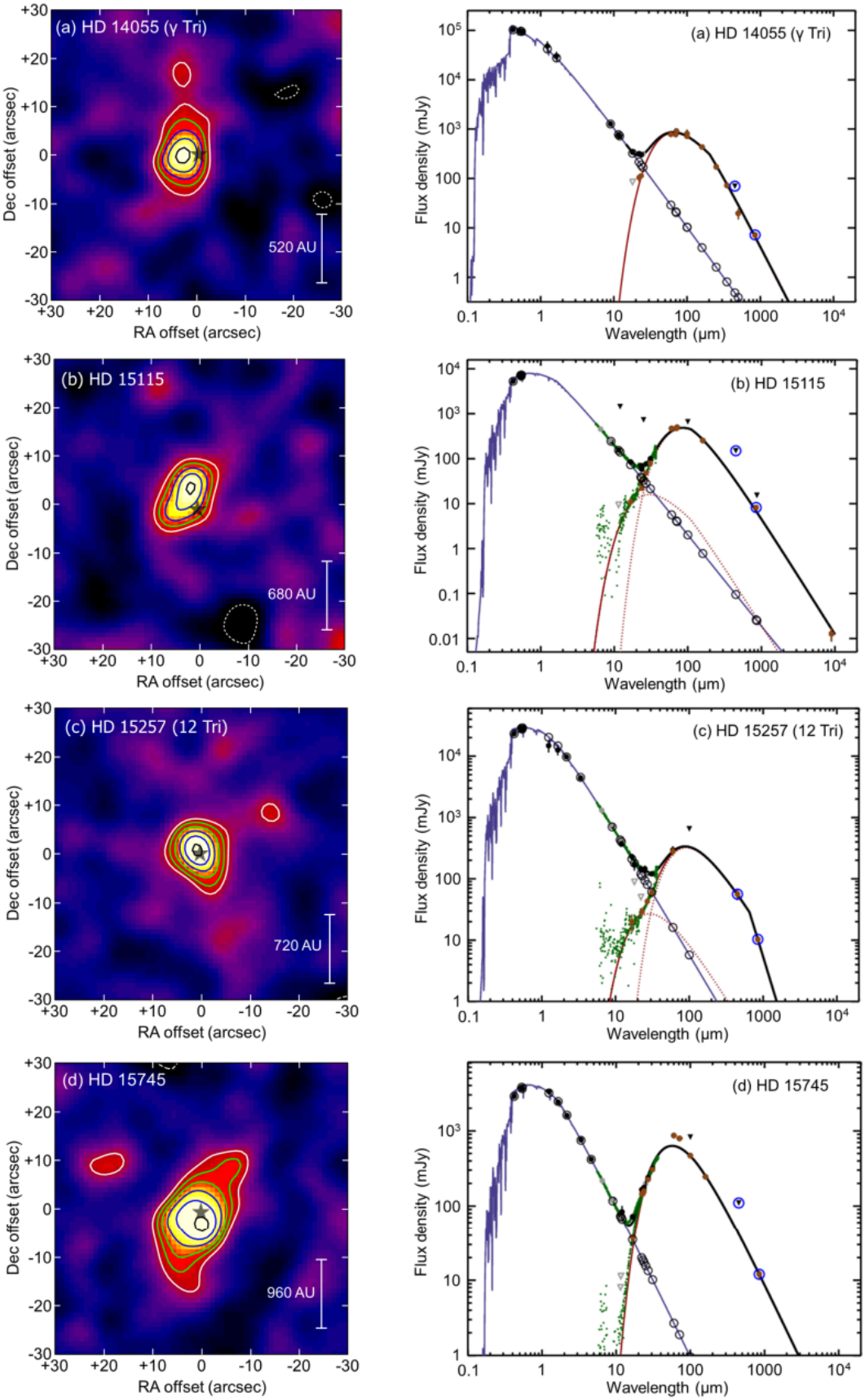

Figure A3. As for Figure A1 for the targets (a) HD 14055 (γ Tri), (b) HD 15115, (c) HD 15257 (12 Tri) and (d) HD 15745.

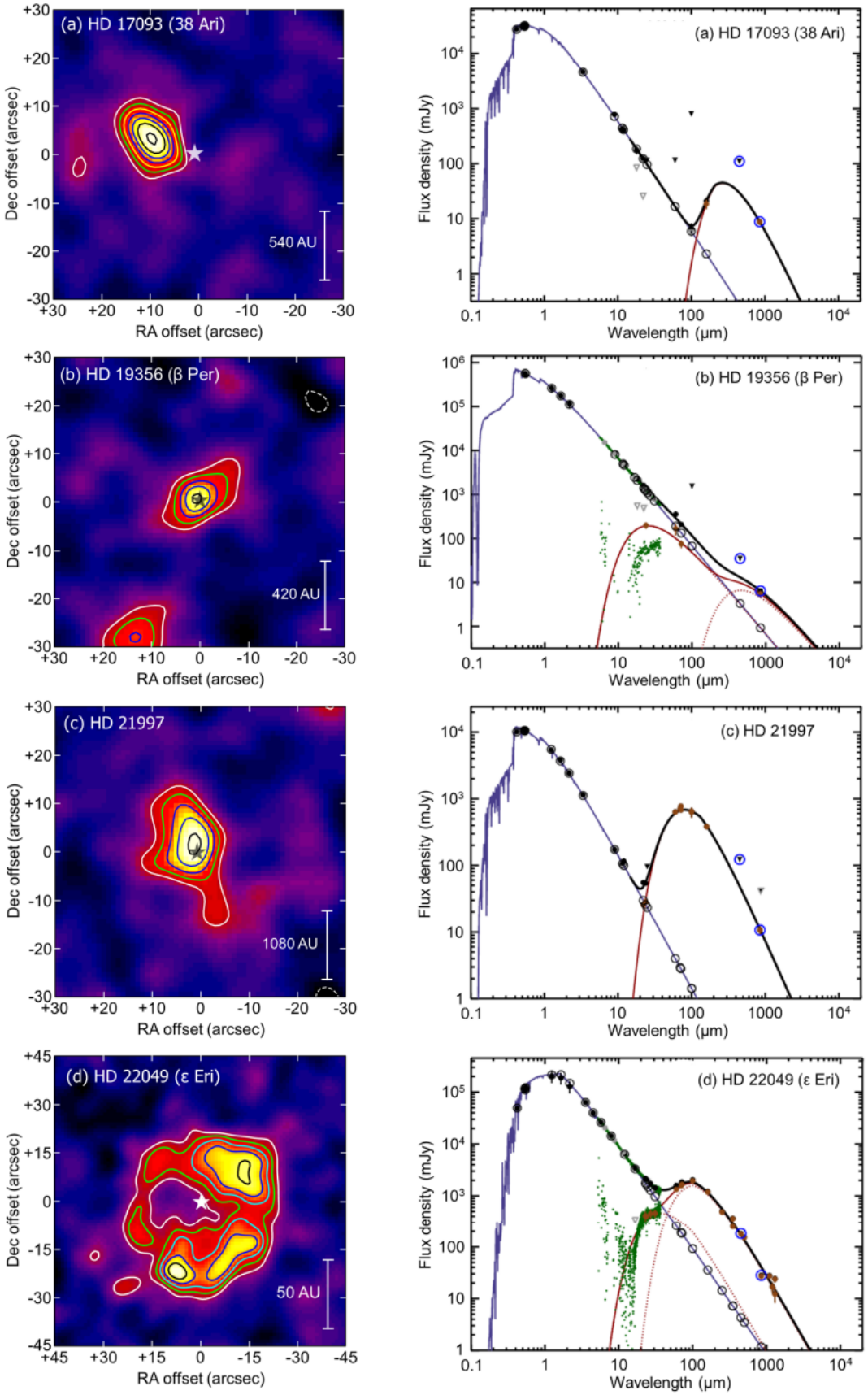

Figure A4. As for Figure A1 for the targets (a) HD 17093 (38 Ari), (b) HD 19536 (β Per), (c) HD 21997 and (d) HD 22049 (ϵ Eri).

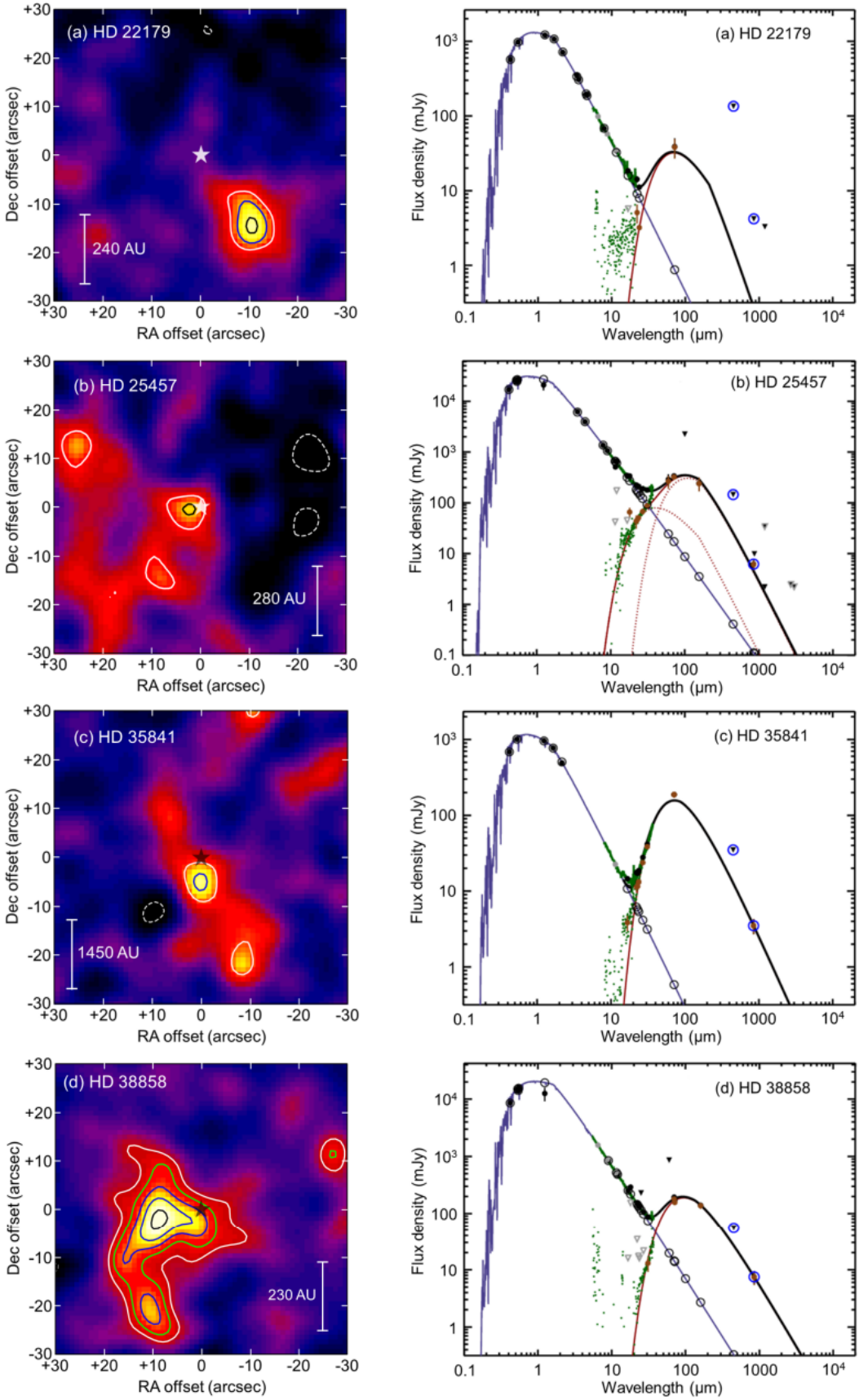

Figure A5. As for Figure A1 for the targets (a) HD 22179, (b) HD 25457, (c) HD 35841 and (d) HD 38858.

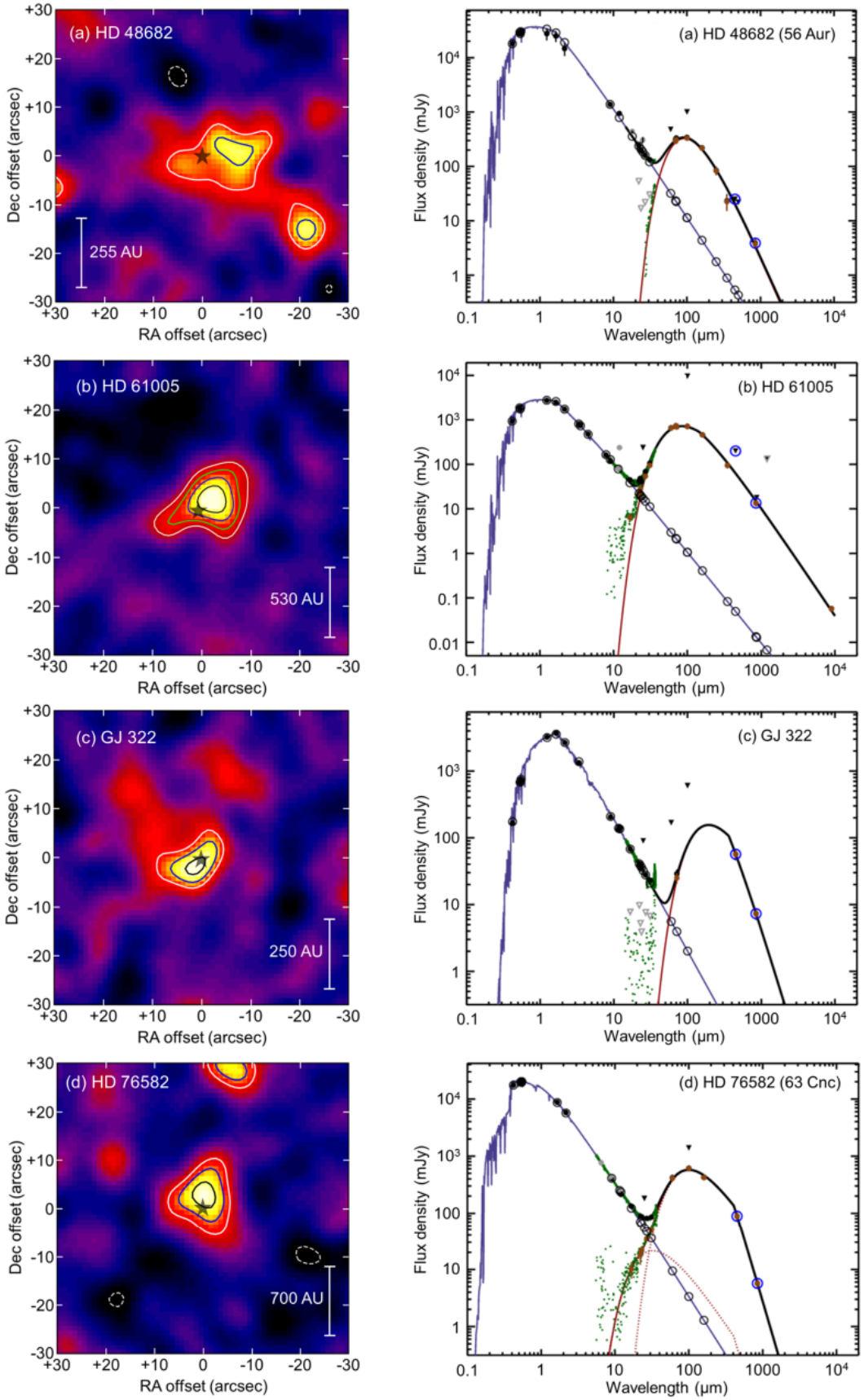

Figure A6. As for Figure A1 for the targets (a) HD 48682, (b) HD 61005, (c) GJ 322 and (d) HD 76582 (63 Cnc).

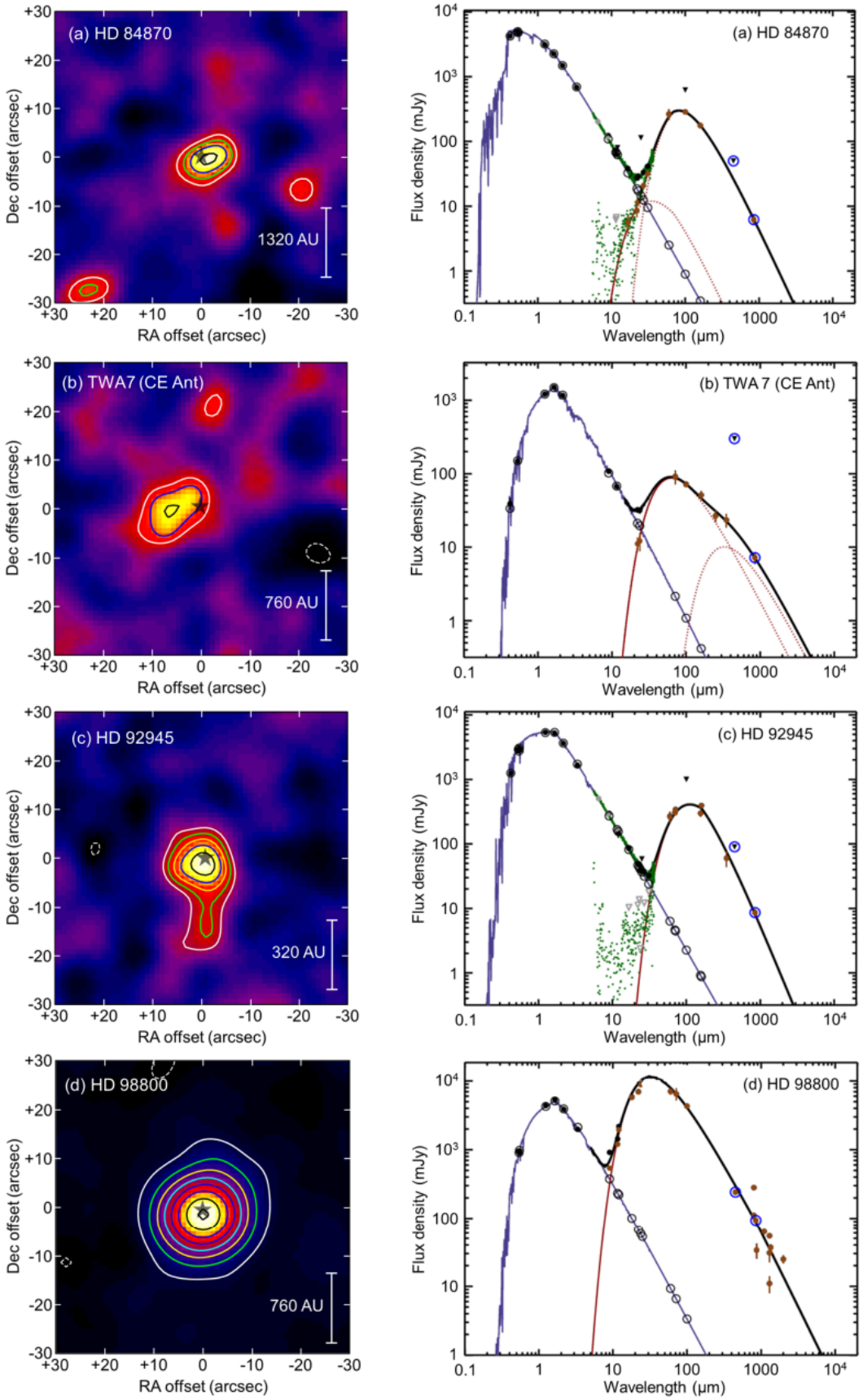

Figure A7. As for Figure A1 for the targets (a) HD 84870, (b) TWA7 (CE Ant), (c) 92945 and (d) HD 98800. The contours for HD 98800 are -4σ (dashed) and then solid contours starting at 4σ and increasing in 8σ steps.

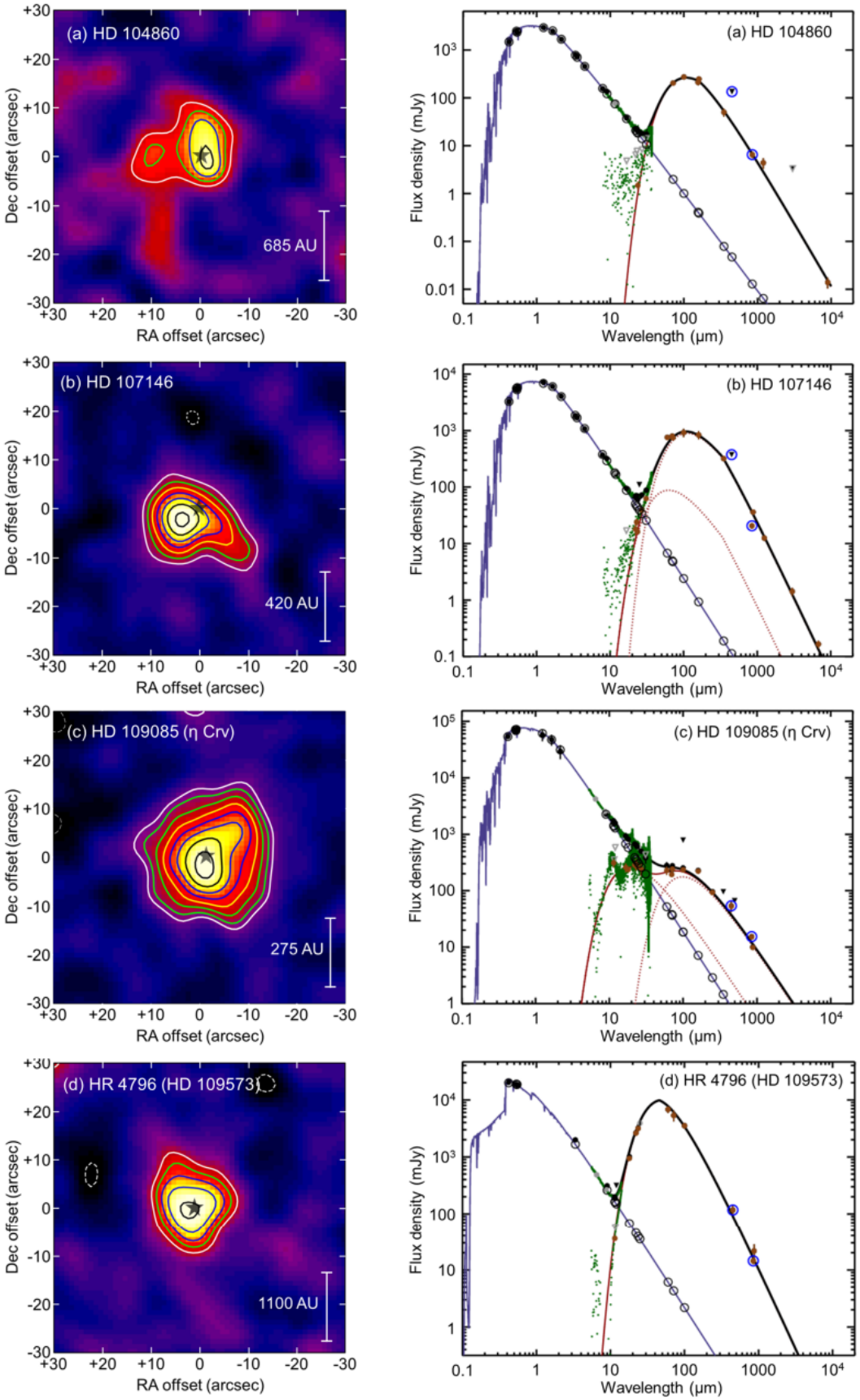

Figure A8. As for Figure A1 for the targets (a) HD 104860, (b) HD 107146, (c) HD 109085 (η Crv) and (d) HR 4796 (HD 109573).

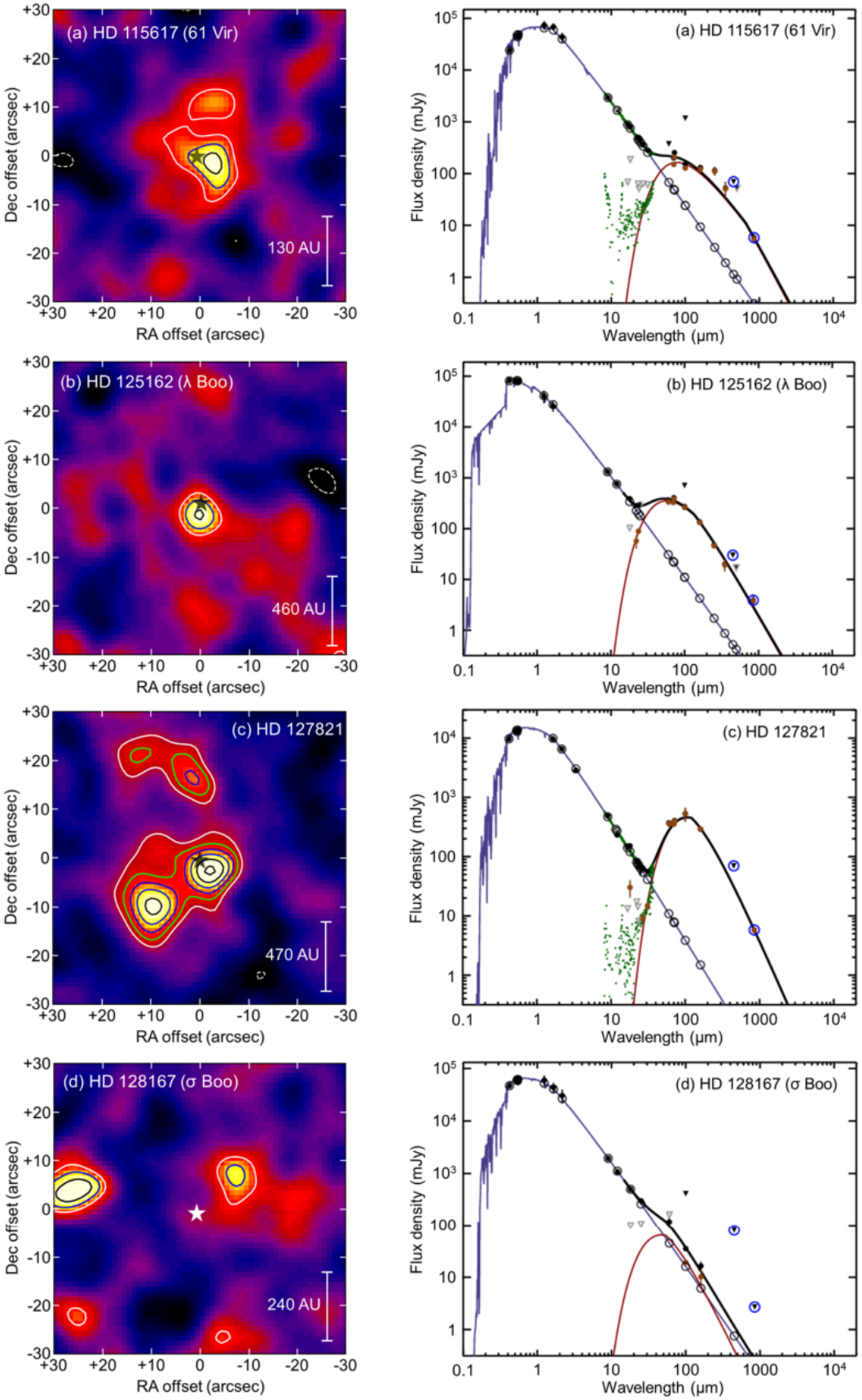

Figure A9. As for Figure A1 for the targets (a) HD 115617 (61 Vir), (b) HD 125162 (λ Boo), (c) HD 127821 and (d) HD 128167 (σ Boo).

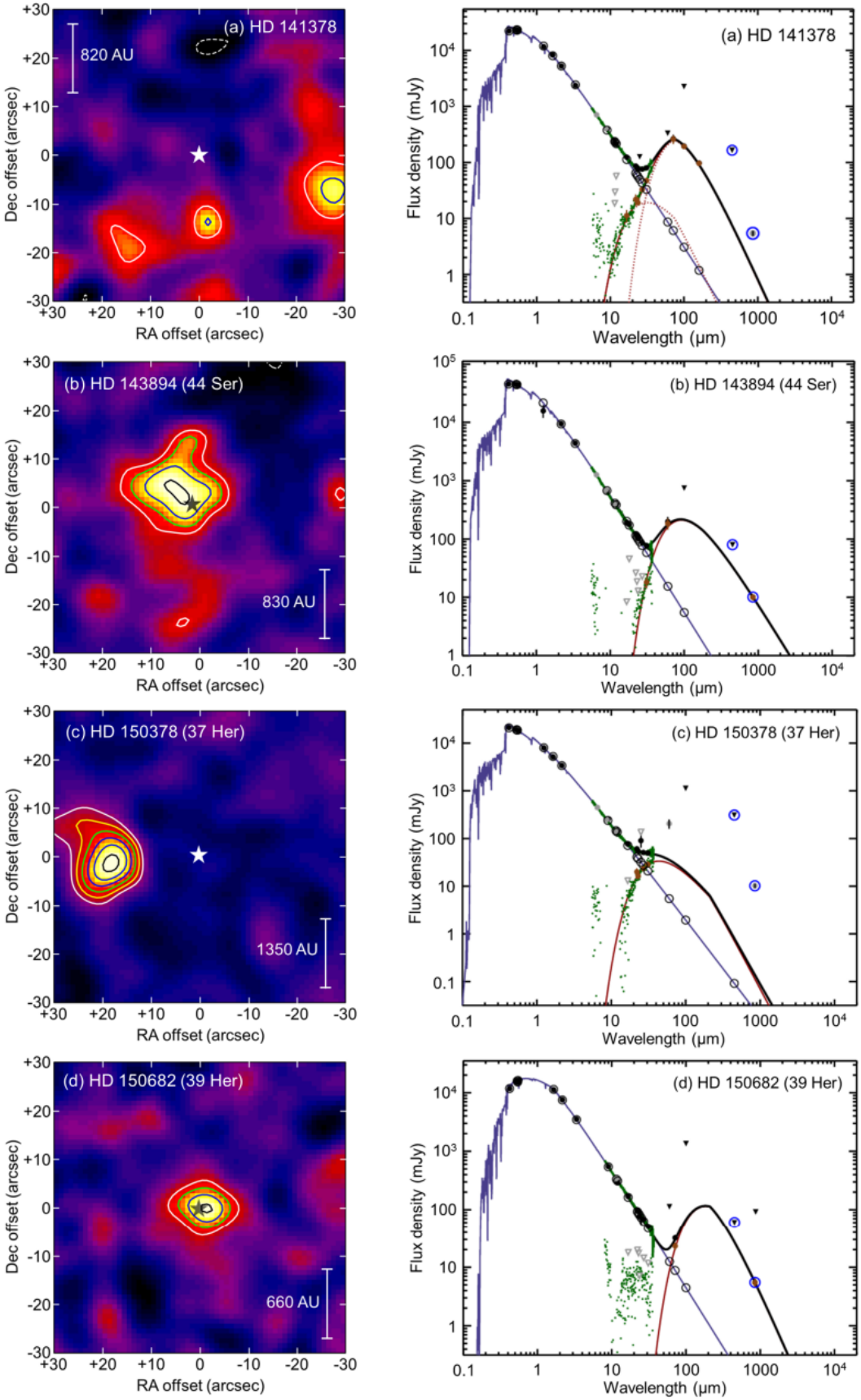

Figure A10. As for Figure A1 for the targets (a) HD 141378, (b) HD 143894 (44 Ser), (c) HD 150378 (37 Her) and (d) HD 150682 (39 Her).

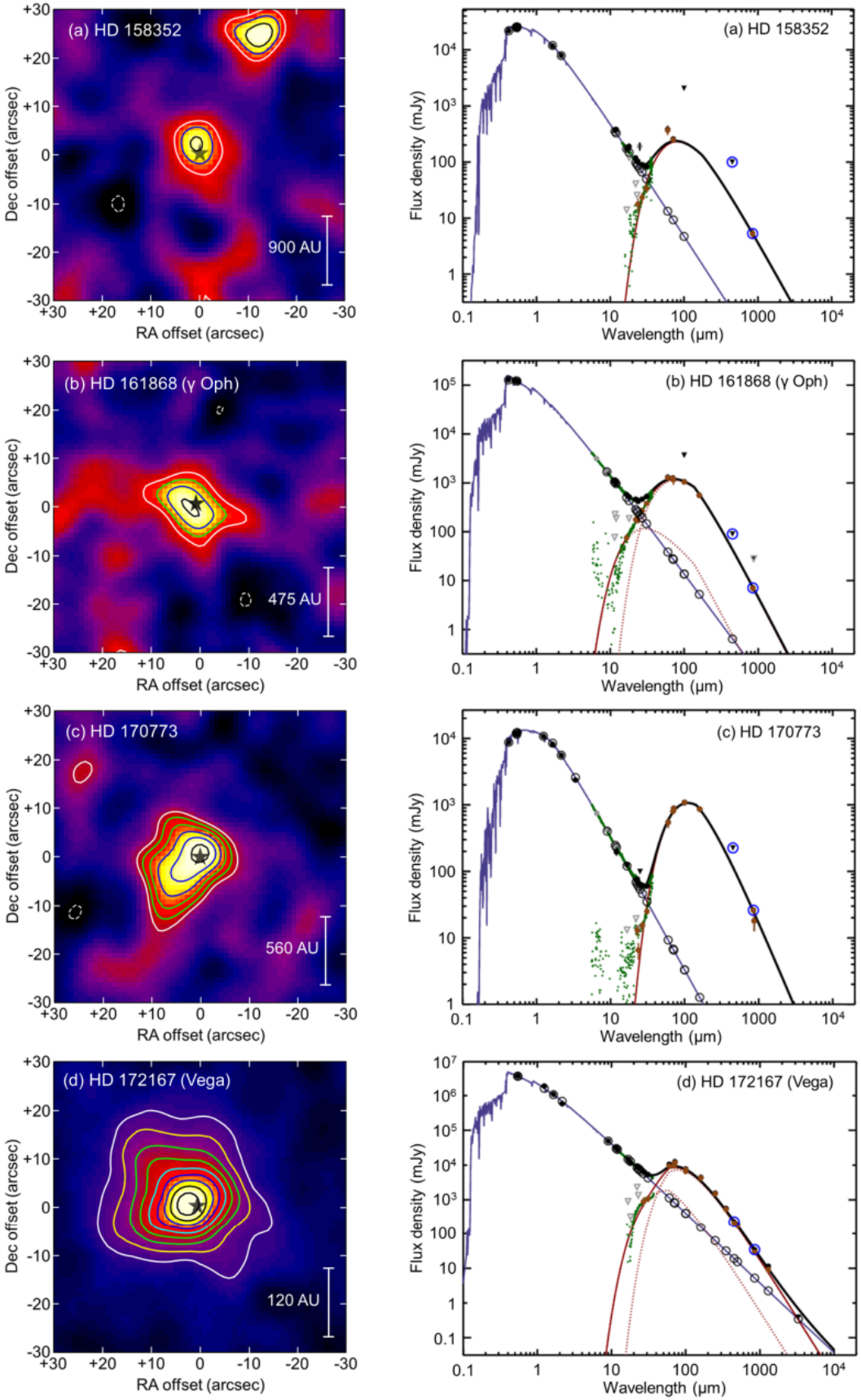

Figure A11. As for Figure A1 for the targets (a) HD 158352, (b) HD 161868 (γ Oph), (c) HD 170773 and (d) HD 192167 (Vega).

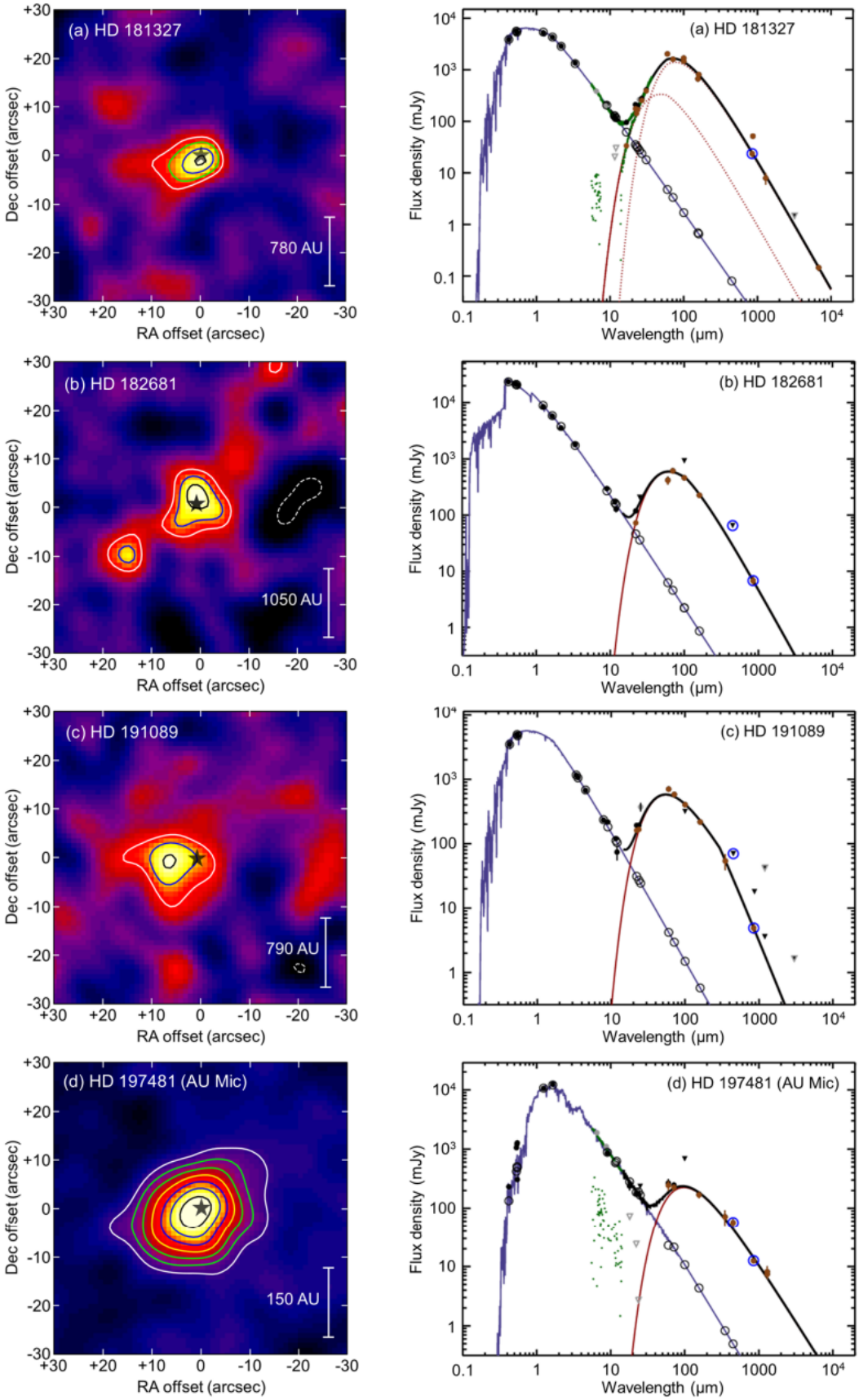

Figure A12. As for Figure A1 for the targets (a) HD 181327, (b) HD 182681, (c) HD 191089 and (d) HD 197481 (AU Mic). The contours for the HD 197481 are -3σ (dashed) and then from $+4\sigma$ in 2σ steps.

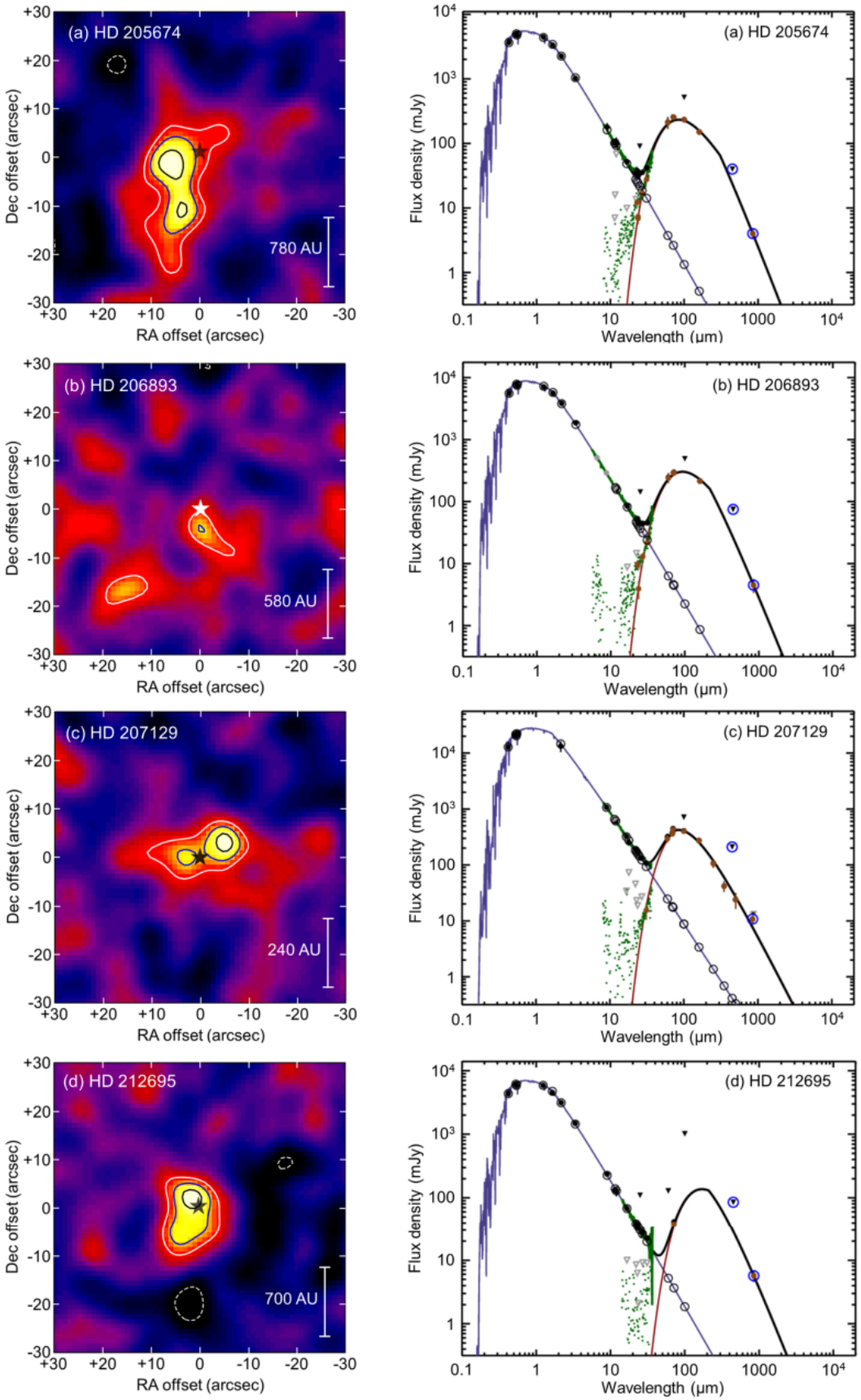

Figure A13. As for Figure A1 for the targets (a) HD 205674, (b) HD 206893, (c) HD 207129 and (d) HD 212695.

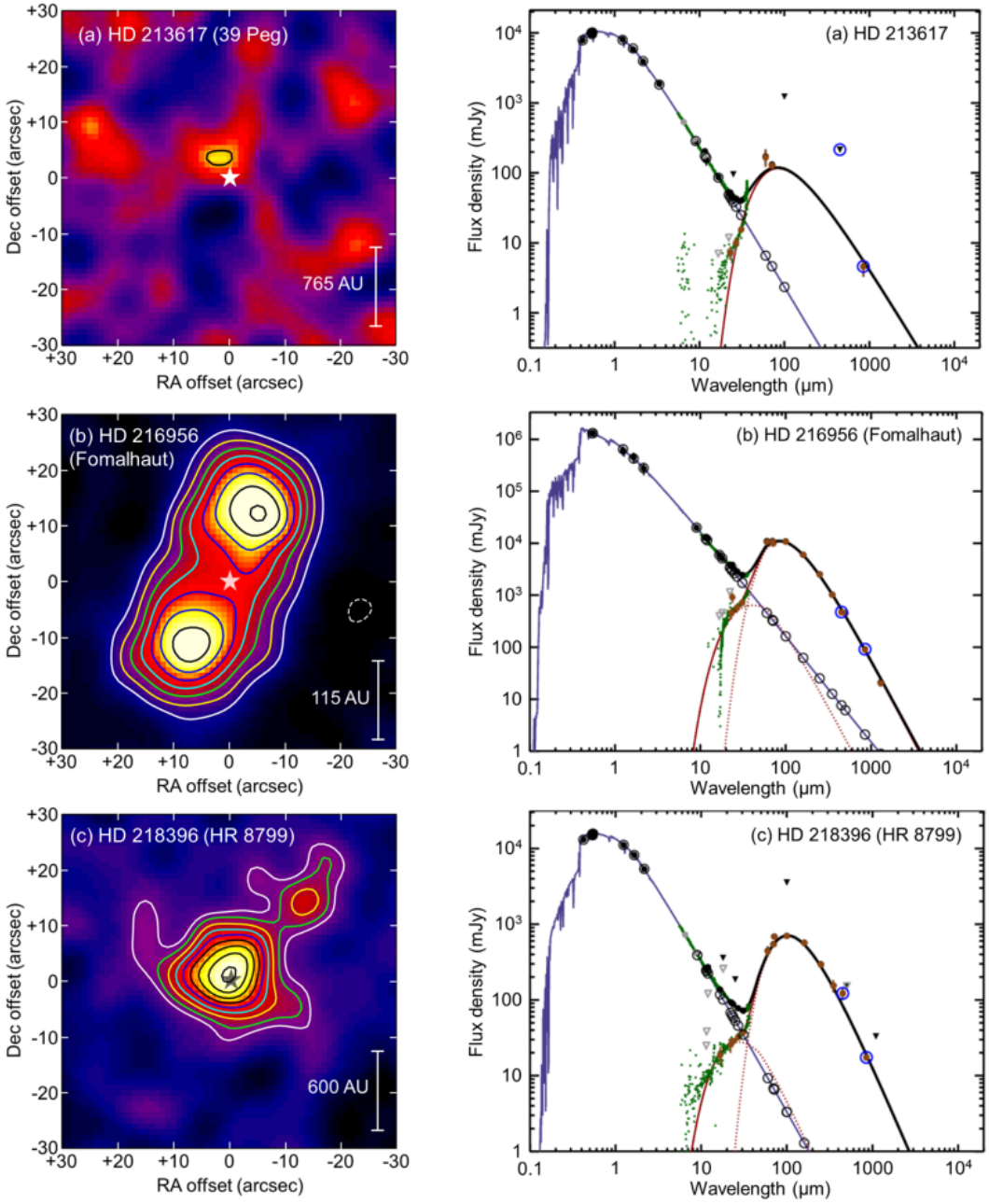

Figure A14. As for Figure A1 for the targets (a) HD 213617, (b) HD 216956 (Fomalhaut), and (c) HD218396 (HR 8799). The contours for the HD 216396 are -5σ (dashed) and then from $+5\sigma$ in 3σ steps.